大阪公立大学
Osaka Metropolitan University
学術情報リポジトリ

Pathological Studies on the Biliary Fibrosis with Special Reference to Macrophage Properties in Relation to Myofibroblast Development

メタデータ	言語: eng 出版者: 公開日: 2012-11-28 キーワード (Ja): キーワード (En): 作成者: Golbar, Hossain Md. メールアドレス: 所属:
URL	https://doi.org/10.24729/00000575

大阪府立大学博士（獣医学）学位論文

Pathological Studies on the Biliary Fibrosis with Special Reference to Macrophage Properties in Relation to Myofibroblast Development

（胆管線維症に関する病理学的研究：特に筋線維芽細胞形成との関連におけるマクロファージの特性について）

Hossain Md. Golbar

2012 年

Contents

Preface

Cirrhosis is an international public health burden owing to impact of significant morbidity and mortality across the globe. Parenchymal injury induced by ischemia, viruses, chemicals and malnutrition is the key initial starting point of hepatic fibrosis. Injured hepatocytes secrete cytokines, which can recruit inflammatory cells into injured sites. Infiltrating cells, in turn, orchestrate a series of remodeling events that culminate in fibrosis (Heymann et al. 2009). However, hepatic fibrosis can progress towards cirrhosis, an end stage condition, depending on degrees of injury or type of injurious agents. Biliary fibrosis, a subtype of hepatic fibrosis, is developed in humans due to cholangiocyte injury caused mainly by enteric bacterial infection and autoimmunity (Harada et al. 2011). Because of the complex pathologic process, no accepted therapy for fibrotic diseases is currently available (Ryu and Daniels 2010). Animal models for biliary fibrosis represent a series of events of fibrogenesis in the Glisson's sheath and may serve as a useful tool to clarify the underlying mechanisms, as well as to assess efficacy of anti-fibrotic agents.

Basically, fibrosis is evoked through the activities of a number of cell types including inflammatory cells, vascular cells, and mesenchymal cells. Among them, macrophages are heterogeneous cells of mononuclear phagocytic system and display a wide range of patho-biological properties. Ontogenetically, they could be divided into exudative macrophages, resident macrophages and dendritic cells. Exudate macrophages are in the monocytic lineage of monocytes, promonoblasts, monoblasts, and macrophage-colony forming unit (M-CFU) originating from hematopoietic stem cells of the bone marrow. Resident macrophages such as microglia, Kupffer cells, and alveolar macrophages also develop from hematopoietic stem cells; however, the precursors migrate from the bone marrow into connective tissues during ontogeny, and then differentiate into resident macrophages. Dendritic cells are composed of the interstitial dendritic cells, the interdigitating follicular cells of spleen and lymph nodes, and the Langerhans cells of the epidermis; the differentiation pathway is distinct from those of exudate or resident

macrophages. Based on activating agents and mirroring the Th1 and Th2 lymphocyte phenotypes, macrophages are also classified into M1 macrophages (classically activated macrophages) and M2 macrophages (alternatively activated macrophages). M1 macrophages infiltrate the wound at the early stage of tissue injury, play roles in removal of tissue debris and necrotic cells by phagocytosis, attract more inflammatory cells by producing proinflammatory cytokines and aggravate the situation. On the other hand, M2 macrophages attenuate inflammation by secretion of anti-inflammatory cytokines. However, macrophages can change phenotypes (M1 to M2 or vice versa) depending on microenvironmental conditions (Bouhlel et al. 2007, Sporrer et al. 2009). The phenotypical changes of macrophages remain to be investigated.

In 1980s, studies on liver fibrosis originally proposed that hepatocytes are responsible for the production of extracellular matrix proteins in liver fibrosis (Diegelmann et al. 1983). It was subsequently shown that hepatic stellate cells (HSCs), the liver specific pericytes located along the sinusoid, are a major source (Friedman et al. 1985, Maher et al. 1988). In a normal liver, HSCs are referred to as ‘quiescent’ and function to store much of the body’s vitamin A (Burt 1999). Myofibroblasts are regarded as the cells with a central role in liver fibrogenesis and as the main cellular source of extracellular matrix components (Parola et al. 2008). Despite some debate on the precise origin, myofibroblasts can derive from quiescent HSCs and portal fibroblasts (Wallace et al. 2008). Myofibroblasts have been also considered to be developed from hepatocytes and cholangiocytes (Robertson et al. 2007, Zeisberg et al. 2007, Rygiel et al. 2008) via epithelial-mesenchymal transition, from endothelial cells via endothelial-mesenchymal transition (Piera-Velazquez et al. 2011), or from circulating fibroblasts called fibrocytes (Forbes et al. 2004, Kisseleva et al. 2006). Besides the origin, however, cellular properties of myofibroblasts in biliary fibrosis remain to be determined. Therefore, understanding the properties of macrophages and myofibroblasts in biliary fibrosis may provide a new avenue in exploring agents for type specific therapeutic interventions of this intractable disease.

Mesenchymal cells express various intermediate filament proteins, which comprise about forty individual proteins that are divided into six main classes (I-VI) based on molecular structures (Lendahl et al. 1990, Steinert and Liem 1990). Classes I and II comprise basic and acidic keratins of epithelial cells; class III proteins include desmin, glial fibrillary acidic protein (GFAP), peripherin and vimentin; class IV consists of neurofilaments and α-internexin; class V are nuclear lamins; class VI includes nestin. Changes in the spatial and temporal expression of these proteins regulate tissue remodeling and fibrosis in different pathological conditions, playing important roles in cell proliferation, migration and survival (Coulombe and Wong 2004, Michalczyk and Ziman 2005). Myofibroblasts in fibrotic lesions express variously the class III proteins. Insight into the function and regulation of intermediate filament proteins may help modulate fibrotic process, particularly in relation to development of myofibroblasts.

The fibrogenic mechanism is the result of the interplay of several pro- and anti-fibrotic/inflammatory cytokines (Pinzani and Rombouts 2004). Transforming growth factor-β (TGF-β) is a profibrogenic factor and considered the master cytokine in the pathogenesis of liver fibrosis (Gressner and Gressner 2008). In mammals, three isoforms termed TGF-β1, 2 and 3 have been identified. Among the three isoforms, the subtype TGF-β1 has been implicated particularly in the pathogenesis of liver fibrosis not only by inducing production of extracellular matrices (ECMs) but also inhibiting the ECM degradation by downregulating matrix-degrading enzymes and promoting expression of matrix metalloproteinase (MMP) inhibitors (Verrecchia et al. 2001, Liu et al. 2006, Patil et al. 2011). Activated macrophages and mesenchymal cells, including HSCs, which are also one of the most important targets of TGF-β1, have been identified as the principal source of this cytokine (Knittel et al. 1996, Gressner and Gressner 2008). Besides, hepatocytes in chronic liver disease can produce TGF-β1 (Dooley et al. 2008, Nitta et al. 2008, Turato et al. 2010). Once activated, tissue macrophages and recruited macrophages become the major source of TGF-β1 in damaged tissues (Bataller and Brenner 2005, Strieter et al. 2007). Activated myofibroblasts may themselves secrete TGF-β1 that can maintain self-

activation by autocrine fashion (Bataller and Brenner 2005). The roles of TGF-β1 in biliary fibrosis remain to be clarified.

In this thesis, a series of studies were conducted to explore underling mechanisms of biliary fibrosis, with particular reference to macrophages in relation to myofibroblast differentiation. In chapter 1, to know the properties of macrophages existing in normal liver and to establish baseline data, immunohistochemical analyses was performed for macrophages and mesenchymal cell populations as well as bile duct epithelial cells in the developing livers. Macrophages have been demonstrated to implicate in the modulation of fibrotic process in experimental settings (Wynn and Barron 2010). However, their roles in spontaneous biliary cirrhosis have not been adequately entertained. To understand the macrophages that take part in spontaneous fibrogenesis, in chapter 2, *Fasciola*-infected cattle livers involving biliary cirrhosis were investigated by immunohistochemistry with a panel of antibodies for macrophages. In humans, the elucidation of early events in the induction of biliary cirrhosis have been hampered by the cryptic onset of the disease, and the practical limitations in accessing liver; additionally, the suitable animal models have not yet been established. In chapter 3, an attempt was undertaken to develop an acute animal model of biliary fibrosis in rats with α-naphthylisothiocyanate (ANIT) and to analyze the early events using the obtained lesions. Additionally, it is not well understood the reasons why biliary regeneration fails to keep pace with cholangiocyte loss during progressive biliary injury. Therefore, in chapter 3, the author also made an attempt to investigate the expression of nestin, an intermediate filament protein of class VI known to influence cell proliferation, migration and survival, in acute ANIT-induced biliary lesions. ANIT-induced biliary fibrosis in the acute animal model represented simply the early events. It is equally important to know what is actually happening during the entire course of fibrogenesis in the Glisson's sheath. Therefore, in chapter 4, the author established a slowly progressive biliary fibrosis model induced in rats by repeated administrations of ANIT, and the obtained lesions were analyzed in detail. In both the acute and chronic models, the author paid attention on the roles of macrophages in relation to myofibroblast

development. Because the expressions of colony stimulating factor-1 (CSF-1), monocyte chemoattractant protein-1 (MCP-1) and TGF-β1 are reported to be related to the growth and differentiation of macrophages (Rathinam et al. 2011), their infiltration in injured tissue (Seki et al. 2009) and induction of myofibroblasts (Inagaki and Okazaki 2007), the author investigated their expressions at mRNA levels by real-time RT-PCR method in chapters 3 and 4. Finally, to more clarify the characteristics of macrophages and myofibroblasts in the biliary fibrosis, based on the data obtained in chapters 3 and 4, comparisons were made in their properties between the acute and chronic models in chapter 5.

In conclusion, the present studies demonstrate that heterogenous macrophage populations showing differences in immunophenotypes, tissue distribution and functions participate in hepatogenesis and spontaneous/experimental biliary fibrosis, and that their appearances are closely related with homeostasis in normal liver and myofibroblast differentiation in biliary fibrosis. The findings of these studies may offer new insight on the pathogenesis of biliary fibrosis and would be helpful in formulating therapeutic strategies. Additionally, the animal models of biliary fibrosis introduced in this study may be used to test efficacy of newly designed anti-fibrotic drugs.

Chapter 1

Immunohistochemical Analyses of the Kinetics and Distribution of Macrophages, Hepatic Stellate Cells and Bile Duct Epithelial Cells in the Developing Rat Liver

Introduction

Immunohistochemical staining has opened new vistas in identification of cell phenotypes, cell receptors, cytokines and chemokines, as well as functional cell changes such as enzyme induction (Hall and Rojko 1996). The approach has been widely used to investigate tissue modeling in developing organs, and to characterize spontaneous lesions and the pathogenesis of chemically-induced toxicopathological lesions.

The liver is comprised of parenchymal hepatocytes and non-parenchymal cells; the non-parenchymal cells include endothelial cells, Kupffer cells, pit cells (liver-associated natural killer cells), hepatic stellate cells (HSCs) (Ito cells or perisinusoidal cells) and cholangiocytes (Bouwens 1988). The relationship between these parenchymal and non-parenchymal hepatic cells is important for maintenance of homeostasis. To analyze the temporal tissue modeling of rat livers, the author used immunohistochemistry with different antibodies against macrophages, HSCs and cholangiocytes. Macrophages are divided mainly into three types: exudative macrophages, resident macrophages (histiocytes, Kupffer cells) and cells differentiating into dendritic cells. These macrophages differ in ontogeny, morphology, immunophenotypes, and tissue distribution (Dijkstra et al. 1985, Damoiseaux et al. 1994, Takahashi et al. 1996, Valledor et al. 1998). Macrophages reveal heterogenous functions such as phagocytosis, antigen presentation and production of cytokines, depending on microenvironmental conditions (Takahashi et al. 1996, Yamate et al. 2000). Along with the storage of vitamin-A in the form of retinyl esters, HSCs are capable of becoming myofibroblastic cells producing collagens in response to injury, indicating that HSCs play important roles in hepatic fibrogenesis (Maher et al. 1988, Milani et al. 1990). Cholangiocytes form bile ducts excreting bile and bile plugs are developed in jaundice (Greve 1992). In hepatotoxicity, macrophages, HSCs and cholangiocytes participate in complex lesion development. The present study was carried out to establish the kinetics and distribution of these hepatic non-parenchymal cells in rat hepatogenesis.

To identify macrophages including Kupffer cells, the author used ED1, ED2, OX6 and SRA-E5 antibodies. ED1 recognizes CD68 located on lysosomal membranes, particularly phagosomes, and thus, the expression level implies enhanced phagocytosis (Dijkstra et al. 1985, Damoiseaux et al. 1994, Suda et al. 1998, Haralanova-Ileava et al. 2005). CD163, recognized by ED2, is in the macrophage scavenger receptor (SR) family, and its increased expression may be related to production of proinflammatory factors; ED2 labels resident macrophages (Kupffer cells) in normal tissues (Polfliet et al. 2006). OX6 labels the major histocompatibility complex class II (MHC class II) molecule (rat Ia) on mature dendritic cells and activated macrophages (Yamashiro et al. 1994, Ide et al. 2005). SRA-E5 antibody was generated by immunizing SR-A knockout mice with recombinant human type I SR-A protein (CD204). CD204 expression is related to lipid metabolism in macrophages via scavenger receptor (Greaves et al. 1998). HSCs are mesenchymal cells, which are considered to show various cytoskeletal proteins such as vimentin, desmin, α-smooth muscle actin (α-SMA) and glial fibrillary acidic protein (GFAP) depending on microenvironmental conditions (Tsutsumi et al. 1987, Sappino et al. 1990); the author used a panel of antibodies to these cytoskeletal proteins for characterizing HSCs. To identify cholangiocytes, the author used two cytokeratin antibodies: CK19 and AE1/AE3.

Materials and Methods

Animals and diet

Four-week-old male F344 rats and pregnant F344 rats were purchased from Charles River Japan (CRJ, Hino, Shiga, Japan). These animals were housed in an animal room at a controlled temperature of 21 ± 3˚C and with a 12-hour light-dark cycle; they were provided a standard diet for rats (MF, Oriental Yeast Co. Ltd., Tokyo, Japan) and tap water *ad libitum*. Livers collected from rats at weeks 5, 10, 15 and 35 were considered adult livers.

Fetal livers were taken from the pregnant rats on gestational (fetus) days 18 and 20. After delivery, liver tissues were also obtained from neonates on days 1, 4, 8, 15, and 21. At each examination point, three rats were euthanized by exsanguinations under ether anesthesia. Animal housing and sampling conformed to the institutional guidelines of animal care of Osaka Prefecture University.

At necropsy, liver tissues were fixed in 10% neutral buffered formalin, Zamboni's (0.21% picric acid and 2% paraformaldehyde in 130 mM phosphate buffer, pH 7.4) (Ide et al. 2003) and periodate-lysine-paraformaldehyde (PLP) solutions. A part of liver samples were also immersed in RNAlater^{TM} (Qiagen GmbH, Hilden, Germany) and stored at −80˚C until extraction of mRNA.

Histology and immunohistochemistry

Formalin-fixed, deparaffinized sections of 4 μm in thickness were stained with hematoxylin and eosin (HE) for morphological observations. Deparaffinized tissue sections also were immunolabeled with mouse monoclonal primary antibodies for AE1/AE3, CK19 (clone b170), vimentin (clone V9), desmin (clone D33), α-SMA (clone 1A4), ED1 (CD68), ED2 (CD163), OX6 (MHC class II), and SRA-E5 (CD204), as well as rabbit

polyclonal antibody for GFAP; the information of these antibodies used are shown in Table 1. Before treatment with 3% H_2O_2 in distilled water for 10 minutes to quench endogenous peroxidase, and then with 5% skimmed milk in phosphate buffered saline (PBS) for 30 minutes to inhibit non-specific reactions, the sections were pretreated as follows: 1) microwave for 5 minutes in 0.01 M citrate buffer (pH 6.0) for vimentin, desmin and SRA-E5: 2) 0.1% trypsin in PBS at 37˚C for 20 minutes for AE1/AE3 and CK19: 3) 10 μg/ml proteinase K in Tris buffered saline (pH7.5) for 10 minutes for α-SMA, ED1, ED2 and OX6. The sections were then incubated overnight with each primary antibody at 4˚C followed by treatment with horseradish peroxidase-conjugated secondary antibody (Histofine Simple Stain MAX-PO, Nichirei, Tokyo, Japan) for 30 minutes. Signals were visualized with 3, 3'-diaminobezidine tetrahydrochloride (DAB Substrate Kit, Vector Laboratories, Inc., Burlingame, CA, USA). Non-immunized mouse or rabbit IgG, which was used instead of primary antibodies, served as negative control. Sections were counterstained lightly with hematoxylin.

The immunopositive cells were counted using ImageJ software version 1.44 (NIH, Bethesda, MD, USA) at a magnification of ×400 in five randomly selected fields (0.2 mm^2) at periportal and perivenular areas of liver lobules of neonates on days 4, 8, 15 and 21, and adulthood (Ide et al. 2003). For fetuses on days 18 and 20 and neonates on day 1, the immunopositive cells were counted without distinguishing areas, because periportal and perivenular areas in early hepatogenesis were indistinguishable; therefore, total cell count at periportal and perivenular areas were divided by two to obtain average values for neonates on days 4, 8, 15 and 21, and adulthood.

RNA extraction and real-time reverse transcriptase polymerase chain reaction (RT-PCR)

Total RNA was extracted from liver tissues by using an SV total RNA isolation system kit® (Promega Corporation, Madison, WI, USA), and then reverse transcribed to cDNA with the superscript II transcriptase system® (Invitrogen, Carlsbad, CA, USA) (Ide et al. 2003). The cDNA was amplified in duplicate with the SYBR® Green Real-time PCR Master Mix (Toyobo Co. Ltd, Osaka, Japan) using the LineGene system (Bioflux, Tokyo, Japan) and each of the specific primers for rat colony stimulating factor-1 (CSF-1) and ribosomal protein S18 (Rps18) (an internal control gene). The following conditions were used for amplification: after 1 minute of denaturation at 95˚C, forty cycles of 15 seconds of denaturation at 95˚C, 15 seconds of annealing at 60˚C and 20 seconds of extension at 72˚C. The oligonucleotide sequences used for PCR are shown in Table 2. The PCR products were electrophoresed in 2% agarose gel and stained with ethidium bromide.

Statistical evaluation

Data were represented as the mean ± standard deviation (SD), and statistical analysis was performed using student's *t*-test. A P value < 0.05 was considered significant. Data obtained at weeks 5, 10, 15 and 35 showed no significant differences from each age; therefore, data obtained from these samples were evaluated together as adult samples.

Results

Histology

In HE-stained sections on fetus days 18 and 20, and neonate day 1, erythroblasts were distributed diffusely among hepatocytes (Fig. 1A-C), indicating hepatic hematopoiesis; the structures of hepatic lobules were indistinct, although there were some veins resembling central veins. On neonate day 4, erythroblasts formed clusters consisting of several cells and distinct hepatic lobules including central veins and Glisson's sheath began to form. In the Glisson's sheath cholangiocytes were organizing into bile ducts. On neonate day 8, erythroblasts were infrequently observed. On neonate day 15, histological structures of liver lobules were without erythroblasts and similar to those of adulthood (Fig. 1D).

Macrophages

The kinetics of macrophages reacting to ED1, ED2, OX6 and SRA-E5 in developing liver is shown in Fig. 2. The ED1-positive macrophages were greatest as early as fetal day 18; among macrophages positive to these antibodies, the number of ED1-positive cells was greatest on fetal day 18. As compared with the number on fetal day 18, the number of ED1-positive cells at other examination points (on fetal day 20 and neonatal days 1-21, and in adult livers) was significantly decreased (Fig. 2A). ED1-positive macrophages had a round to oval configuration with short cytoplasmic processes and a nucleus, and were distributed evenly throughout the hepatic parenchyma (Fig. 3A, B). On the other hand, ED2-, SRA-E5-, and OX6-positive cells were increased in number after birth (Fig. 2B-D). As compared with the number on fetal day 18, the ED2-positive cell number at subsequent examination points gradually increased until neonatal day 15, and the number slightly decreased on neonatal day 21 and at adult weeks. The ED2-positive cells appeared evenly scattered in the parenchyma, and occasional cells had cell

cytoplasmic processes (Fig. 3C, D). As compared with the number on fetal day 18, the SRA-E5-positive cell number was significantly increased on neonatal days 1-21 and at adult weeks; interestingly, the number was almost similar on neonatal days 4, 8, 15, and 21 and at adult weeks (Fig. 2C), indicating the consistent presence. The SRA-E5-positive cells were small round, oval or spindle in shape, and were distributed uniformly in the hepatic parenchyma (Fig. 3E, F). It was worthy to note that the distribution patterns of ED2- and SRA-E5-positive cells were similar to each other, although the number of SRA-E5-positive cells was greater than that of ED2-positive cells (Fig. 2B for ED2 and Fig. 2C for SRA-E5). OX6-positive macrophages were present in the Glisson's sheath and occasionally in perivenular areas (Fig. 3G, H). Therefore, on neonatal days 4 and 8 when distinct hepatic lobules began to be formed, the number of OX6-positive cells were quickly increased with a significant change as compared with the number on fetal day 18; the number was slightly decreased on neonatal days 15 and 21, but at adult weeks, OX6-positive cells recovered to levels on neonatal days 4 and 8 (Fig. 2D). OX6-positive cells showed elongated or dendrite configurations.

There were no significant differences in the number of cells reacting to ED1, ED2, SRA-E5 and OX6 between periportal and perivenular areas on neonate days 4-21, and at adult weeks.

Expression of CSF-1 mRNA

In preliminary analyses, the expression patterns of commonly used internal control genes such as β-actin, β-glucuronidase (Gusβ), 18s rRNA, β-2 microglobulin (β2M), and Rps18 were investigated using developing rat liver samples. Among them, the author found that Rps18 mRNA was expressed consistently; therefore, the author selected Rps18 as an internal control gene. Gene expression analysis showed a significantly increased expression of CSF-1 mRNA on neonatal day 15 compared to that on fetal day 18 (Fig. 4).

Additionally, the tendency of CSF-1 mRNA to increase was seen on neonatal day 21 and at adult weeks.

HSCs

Among mesenchymal HSCs reacting to vimentin, desmin, α-SMA and GFAP, vimentin expression was the most common (Fig. 5). A large number of cells reacting to vimentin were seen as early as fetal day 18; although there were a significant decreases (on neonatal days 1 and 21, and at adult weeks) or increases (on neonatal days 4-15), generally the number of vimentin-positive cells appeared to be maintained from fetuses to adulthood (Fig. 5A), indicating a consistent cytoskeletal vimentin for HSCs. Many desmin-positive cells were detected in parenchymal tissues as early as fetal day 18. The desmin-positive cell number was significantly decreased on fetal day 20, and neonatal days 1-21, as well as at adult weeks (Fig. 5B). Although the GFAP-positive cell number on fetal day 20 was significantly decreased, a large number of GFAP-positive cells were seen from fetal day 18 until neonatal day 4; however, the number was quickly decreased on subsequent examination days (on neonatal days 8-21, and at adult weeks) (Fig. 5C). α-SMA-positive HSCs were not detected at any examination point.

Histologically, vimentin (Fig. 6A)-, desmin (Fig. 6B)-, and GFAP (Fig. 6C)-positive cells were evenly distributed along the sinusoids in hepatic lobules.

Cholangiocytes

Cholangiocytes reactive to AE1/AE3 and CK19 were detected as early as fetal day 18 with a faint reaction (Fig. 7A); immunoreactivity for CK19 was greater than that for AE1/AE3. With age, cholangiocytes organized into bile ducts in the Glisson's sheath on neonatal day 8 (Fig. 7B) and onwards.

Discussion

Hepatic macrophages

In fetal rat liver, macrophages can be identified on fetus day 11 before the initiation of hepatic and bone marrow hematopoiesis (Naito et al. 1982, Sakamoto et al. 2007). Such macrophages, called primitive macrophages, appear in the yolk sac and differentiate into fetal macrophages (Takahashi et al. 1996, Naito et al. 1997, Watanabe et al. 2003). The primitive macrophages possess phagocytic and mitotic activities (Naito et al. 1982, Rees et al. 1988). The present study investigated the appearance of macrophages reacting to ED1, ED2, OX6 and SRA-E5 in developing rat liver from fetuses on day 18 to adulthood. Basically, it was found that macrophages reacting to ED1 were greatest as early as fetus day 18, and thereafter the number was gradually decreased until adulthood. On the contrary, the numbers of macrophages reacting to ED2, OX6 and SRA-E5 were gradually increased after birth. Similar tendency has been reported in rat developing livers by the immunohistochemistry with ED1 and SRA-E5 antibodies (Sakamoto et al. 2007). The increased expression of CD68 recognized by ED1 reflects phagocytic activity, because CD68 is located on membranes of phagosomes (Dijkstra et al. 1985, Damoiseaux et al. 1994, Suda et al. 1998). The tissue modeling is completed by proliferation, differentiation and apoptosis of constituting cells. Many ED1-positive cells seen in fetuses might be related to removal of apoptotic cells and cell debris in tissue modeling and hematopoiesis during hepatogenesis; with tissue modeling after birth, therefore, the ED1-positive cells might be decreased. Therefore, ED1-positive cells are regarded as primitive macrophages which develop in the yolk sac (Takahashi et al. 1996, Naito et al. 1997, Watanabe et al. 2003).

ED2 has been used to detect resident macrophages in normal tissues (Dijkstra et al. 1985, Ide et al. 2005). Interestingly, ED2-positive cells began to increase after birth, in contrast to ED1-positive cells showing decreased numbers after birth. ED2-positive cells were present along the sinusoids of the hepatic lobules. ED2-positive cells were considered

to be so-called Kupffer cells present in adult rat livers (Armbrust and Ramadori 1996), and the increased number after birth might be related to the completion of hepatic lobules consisting of hepatic cords, sinusoids and Disse's cavities. Recently, it has been reported that CD163 recognized by ED2 may be associated with the production of proinflammatory factors such as nitric oxide (NO) and tumor necrosis factor-α (TNF-α) (Polfliet et al. 2006). These factors are important in host defense mechanisms, and CD163, an endocytic receptor for hemoglobin-haptoglobin complexes, is presumed to play roles in clearance of toxic-free hemoglobin from circulation (Kristiansen et al. 2001, Madsen et al. 2004, Nielsen et al. 2006). Therefore, the increased number of ED2-positive cells (Kupffer cells) after birth suggests the commencement of hepatic functions.

The SRA-E5 expression is related to lipid metabolism through the scavenger receptors (Greaves et al. 1998). The liver is the most crucial organ for regulating lipid metabolism. Similar to ED2-positive cells, the increased number of SRA-E5-positive cells after birth might be in connection with commencement of liver functions during tissue modeling. The distribution of SRA-E5-positive cells was generally similar to that of ED2-positive cells, although the number of former was greater than that of the latter. SRA-E5 may label Kupffer cells during hepatogenesis.

OX6 recognizes MHC class II (Ia molecule), and its expression implies antigen-presentation capacity (Yamashiro et al. 1994, Ide et al. 2005). Dendritic cells are well known as professional antigen-presenting cells; they are present in the connective tissues (as interstitial dendritic cells), lymph nodes and spleen (as interdigitating and follicular dendritic cells) and epidermis (as Langerhans cells). It is interesting to note that OX6-positive cells appeared in limited areas of the liver such as the Glisson's sheath; therefore, the distribution of OX6-positive cells was clearly different from that of ED1-, ED2- and SRA-E5-positive cells which were seen in parenchyma of hepatic lobules (Tomokiyo et al. 2002, Polfliet et al. 2006). The Glisson's sheath consists of interlobular arterioles, interlobular veins, and interlobular bile ducts as well as supporting connective tissues.

OX6-positive cells seen in the Glisson's sheath may be regarded as interstitial dendritic cells. The number of OX6-positive cells was increased on neonate days 4 and 8, indicating that the appearance may be related to the establishment of the immune system after the formation of hepatic lobules.

The present study demonstrated that macrophages with different immunophenotypes appeared during hepatogenesis in the absence of overt inflammatory stimuli. These macrophages seem to participate in phagocytosis, hematopoiesis, lipid metabolism, or immune system function, leading to tissue modeling of liver and homeostasis (Naito et al. 1997). CSF-1, a multi-functional protein, is released by HSCs and stimulates proliferation, differentiation, and survival of mononuclear phagocytes (Wynn et al. 2001, Abboud et al. 2003). CSF-1 mRNA tended to increase in late stages of neonates (on days 15 and 21) and in adulthood. This finding might have been related to completion of hepatic lobules including ED2-, SRA-E5- and OX6-positive cells; these macrophage populations seem to be related to hepatic homeostasis, as mentioned above.

HSCs

In response to injury, reactive macrophages secrete growth factors; these factors incite the phenotypic modulation of HSCs into myofibroblasts capable of producing extracellular matrices (Sappino et al. 1990, Ng et al. 1998). Thus, there is a close relationship between the appearance of macrophages and myofibroblast development in hepatic fibrogenesis (Hines et al. 1993, Muchaneta-Kubara and el Nahas 1997, Yamate et al. 1999, Yamate et al. 2003). During hepatic fibrogenesis, HSCs show various cytoskeletal proteins such as vimentin, desmin, α-SMA and GFAP (Yamate et al. 2003, Ide et al. 2005); particularly, α-SMA expression is the most significant hallmark of developing myofibroblasts evolving from HSCs. In the present study, α-SMA-positive HSCs were not seen, indicating that α-SMA is not expressed in HSCs in rat hepatogenesis. On the other hand, vimentin was

constitutively expressed in HSCs during hepatogenesis. HSCs have a mesenchymal nature and vimentin is a basic cytoskeletal component of HSCs. Desmin is also expressed in HSCs after liver injury, and later HSCs express α-SMA leading to fibrosis (Hines et al. 1993). The increased number of HSCs expressing desmin was seen on fetal day 18, and on neonate days 8 and 15. Desmin-expressing HSCs may be related to early tissue modeling of hepatic lobules. Although GFAP is generally considered specific for astroglial cells, more interestingly, it was found that HSCs, particularly in early hepatogenesis from fetal day 18 to neonate day 4 are GFAP immunopositive. GFAP immunoreactivity has been reported in HSCs (Gard et al. 1985, Neubauer et al. 1996), and cultured HSCs immunopositive for GFAP changed their phenotype to cells expressing α-SMA (Akiyoshi and Terada 1999, Baba et al. 2004). Desmin- and GFAP-expressing HSCs are seen exclusively in early hepatogenesis. Taken together, HSCs can change their cytoskeletal phenotype under microenvironmental conditions evoked during hepatogenesis.

Cholangiocytes

There have been debates on the origin of cholangiocytes in hepatogenesis; some studies have indicated that hepatoblasts give rise to both hepatocytes and cholangiocytes (Shiojiri et al. 1991, Rogler 1997, Spagnoli et al. 1998). After liver injury in adulthood, so-called oval cells may differentiate into hepatocytes and cholangiocytes (Kon et al. 2009). Hepatoblasts in embryos and oval cells in adults exhibit similar characteristics (Shiojiri et al. 1991, Tian et al. 1997, Tanaka et al. 2009), suggesting common origin of these cells. In adulthood, oval cells develop in injured livers and form cholangiocytes that express CK19 (Grozdanov et al. 2006). Cells reacting faintly to CK19 were seen in fetuses and neonates on days 1 and 4; these cells might have properties of oval cells. Cholangiocytes forming bile ducts on neonate days 8-21 and at adult weeks have a strong reaction to CK19. In addition to the usefulness of AE1/AE3 antibody, CK19 antibody will detect not only oval cells but also bile duct epithelia.

In conclusion, this study showed basic data on the kinetic and distribution of macrophages, HSCs and cholangiocytes in the developing rat liver. Macrophages have heterogeneous immunophenotypes and different distribution. HSCs show various cytoskeletal proteins, and primitive HSCs were found to express desmin and GFAP. CK19-expressing cells seen in early hepatogenesis may be oval cells capable of organizing into bile ducts. Rats are widely used in toxicity studies as a laboratory animal (Laskin and Pilaro 1986, Warheit 2007). There are many hepatotoxicants, and chemically-induced hepatic lesions develop by complicated mechanisms involving interaction between parenchymal hepatocytes and non-parenchymal cells or between live-constituting cells and inflammatory cells. The information of this study would be useful for investigations of experimentally-induced rat liver lesions.

Summary

Non-parenchymal cells in the liver consist mainly of Kupffer cells, hepatic stellate (HS) cells and cholangiocytes. To establish base-line data and clarify the nature, this study investigated immunohistochemically the kinetics of these cell populations in developing liver of F344 rats. Samples were collected from fetuses on days 18 and 20, neonates on days 1, 4, 8, 15, and 21, and adults at weeks 5-35. ED1 (CD68)-positive macrophages showed highest number as early as fetal day 18, and then decreased gradually until adulthood. The numbers of macrophages reacting to ED2 (CD163), SRA-E5 (scavenger receptor A, CD204) and OX6 (MHC class II), increased after birth (early neonates), and ED2- and SRA-E5-positive cell numbers were maintained until adulthood, but OX6-positive cell number decreased at late stages of neonates and adulthood. ED2- and SRA-E5-positive cells appeared along the sinusoids, indicating Kupffer cells, whereas OX6-positive cells were limited in the Glisson's sheath. Vimentin-positive hepatic stellate cells (HSCs) were seen consistently from fetuses to adulthood. Desmin- and glial fibrillary acidic protein (GFAP)-positive HSCs tended to be seen in fetuses and early stages of neonates. HSCs reacting to α-smooth muscle actin (α-SMA) were not detectable. Cholangiocytes, reacting to cytokeratin 19 and AE1/AE3, began to be seen on fetus day 18 with faint reaction, and interlobular bile ducts were completed in the Glisson's sheath by neonatal day 8. This study shows that there are heterogeneous macrophage populations and that HSCs can show various cytoskeletal proteins in rat hepatogenesis.

Table 1. Primary antibodies used for immunohistochemistry

Antibody	Dilution	Source	Specificity
Anti-ED1	1:100	Chemicon International, Inc, Temecula, CA, USA	Exudate macrophages (monocytes)
Anti-ED2	1:100	Serotec, Oxford, UK	Resident macrophages (Kupffer cells)
Anti-OX6	1:100	Serotec	Dendritic cells, activated macrophages
Anti-SRA-E5	1:100	TransGenic Inc, Kumamoto, Japan	Macrophages, Kupffer cells
Anti-Vimentin	1:400	DakoCytomation, Glostrup, Denmark	Cells of mesenchymal origin
Anti-Desmin	1:200	Dako	Smooth muscle cells
Anti-α-SMA	1:100	Dako	Smooth muscle cells, myofibroblasts
Anti-GFAP*	1:500	Dako	Astroglial cells
Anti-CK19	1:100	Novocastra Laboratories Ltd, Newcastle, UK	Cholangiocytes
Anti-AE1/AE3	predilution	Dako	Cholangiocytes

*; Rabbit polyclonal antibody; the rest are mouse monoclonal antibodies. **α-SMA**: α-smooth muscle actin, **GFAP**: glial fibrillary acidic protein, **CK19**: cytokeratin 19. ED1 for CD68, ED2 for CD163, OX6 for MHC class II, SRA-E5 for CD204.

Table 2. Oligonucleotide sequences of primers used in the real-time PCR

Gene	Primers	Oligonucleotide sequences	Size of amplicon (bp)
CSF-1	Sense	5’-ACAGGTGGAACTGCCAGTGTAGAA-3’	89
	Anti-sense	5’-GGTGGACGTTGCCATAATGTCTC-3’	
Rps18	Sense	5’-AAGTTTCAGCACATCCTGCGAGTA-3’	140
	Anti-sense	5’-TTGGTGAGGTCAATGTCTGCTTTC-3’	

CSF-1: colony stimulating factor-1, **Rps18**: ribosomal protein s18 (an internal control gene).

Figure Legends

Fig. 1. Tissue sections of developing rat livers on fetus days 18 (A) and 20 (B), neonate days 1 (C) and 21 (D). Erythroblasts with a round nucleus are diffusely or sporadically distributed among hepatocytes; the erythroblasts gradually decrease with age (A-C). Distinct hepatic lobules including central veins (CV), interlobular vein (IV), interlobular arteriole (IA) and interlobular bile ducts (IBs) are shown on neonate day 21 (D). **V**: vein. HE.

Fig. 2. The kinetics of macrophages reacting to ED1 (A), ED2 (B), SRA-E5 (C) and OX6 (D) in rat hepatogenesis. ED1-reactive macrophages are greatest before birth and decreased in post-natal days (A), whereas ED2-, SRA-E5- and OX6-reactive macrophages begin to be increased after birth (B-D). **F**: fetus, **N**: neonate, **Adult**: adults at weeks 5-35, **Average**: mean macrophage count of periportal and perivenular areas on N4-21 and at adulthood (*; $P<0.05$ to F18).

Fig. 3. Tissue sections showing diffuse distribution of macrophages reacting to ED1 (A, B) and ED2 (C, D) in the hepatic parenchyma on neonate day 8. SRA-E5-positive macrophages are present along the sinusoids on neonate day 4 (E, F). OX6-positive macrophages are seen exclusively in the Glisson's sheath at adult week 10 (G, H). Immunohistochemistry, counterstained with hematoxylin.

Fig. 4. Expression of CSF-1 mRNA relative to that on fetus day 18 and normalized by Rps18 mRNA from fetus day 18 until adulthood. Data are expressed as mean ± SD. The expression level increases on neonate day 15 and shows tendency to increase on neonate day 21 and at adulthood (*; $P<0.05$ to F18).

Fig. 5. The kinetics of hepatic stellate cells (HSCs) reacting to vimentin (A), desmin (B) and glial fibrillary acidic protein (GFAP) (C) in developing rat liver from fetus day 18 until adulthood. The vimentin is expressed consistently from fetus day 18 until adulthood (A), whereas HSCs reacting to desmin (B) and GFAP (C) are decreased

in late stages of neonates and adulthood. Average is the mean number of cells in periportal and perivenular areas on neonate (N) days N4-21 and at adulthood (*; $P<0.05$ to F18).

Fig. 6. Tissue sections showing sporadically distributed HSCs reacting to vimentin (A), desmin (B) and GFAP in parenchyma on neonate days 4, 8 and 1, respectively. Immunohistochemistry, counterstained with hematoxylin.

Fig. 7. Tissue sections showing cholangiocytes on fetus day 18 (A, arrows) and bile duct formed by cholangiocytes on neonate day 8 (B, arrows) reactive to cytokeratin (CK) 19. Cholangiocytes react faintly (A) or strongly (B) to CK19. Immunohistochemistry, counterstained with hematoxylin.

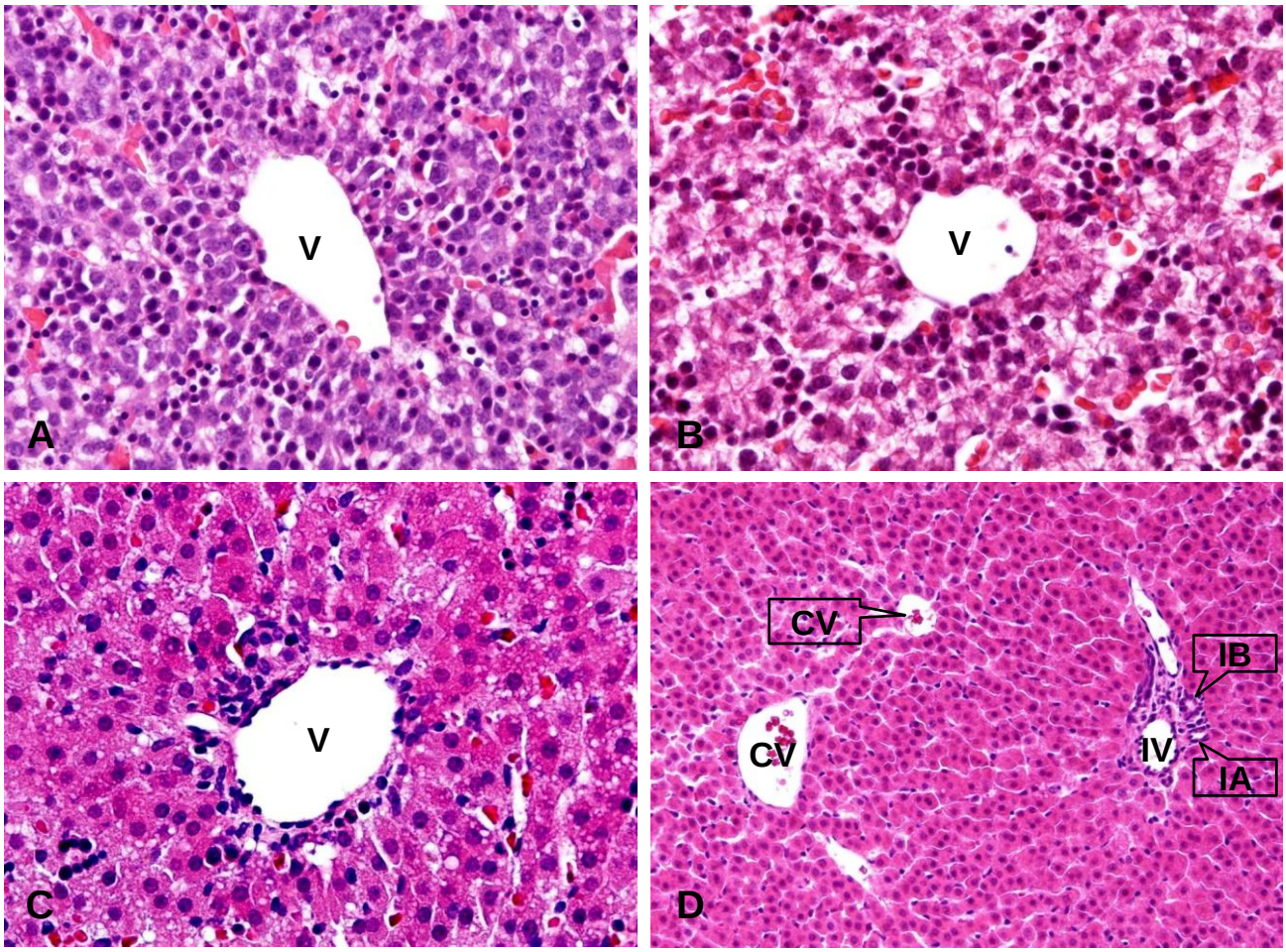

Fig. 1

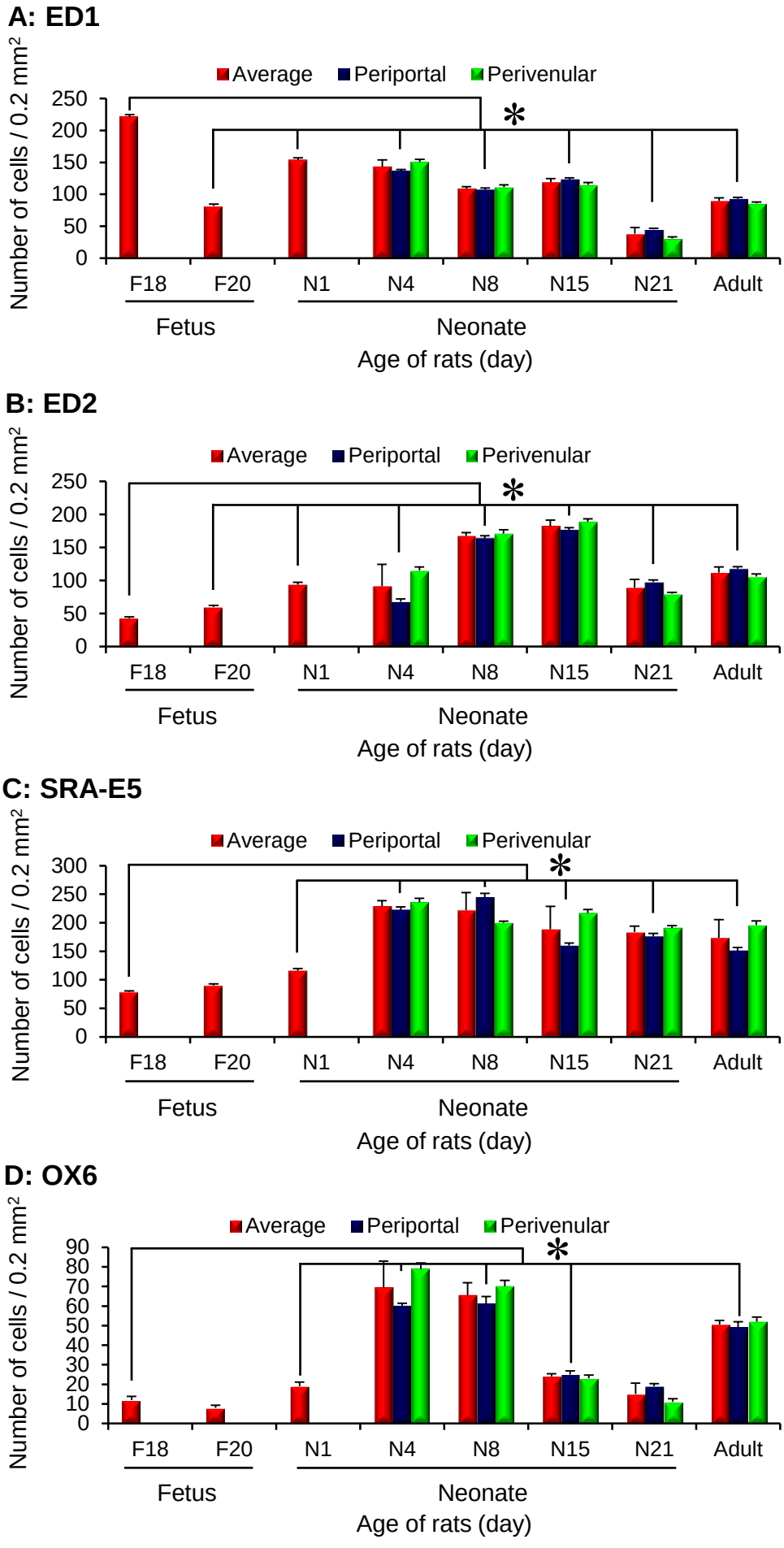
A: ED1
Number of cells / 0.2 mm²
Average
Periportal
Perivenular
250
200
150
100
50
0
*
F18
F20
N1
N4
N8
N15
N21
Adult
Fetus
Neonate
Age of rats (day)
B: ED2
Number of cells / 0.2 mm²
Average
Periportal
Perivenular
250
200
150
100
50
0
*
F18
F20
N1
N4
N8
N15
N21
Adult
Fetus
Neonate
Age of rats (day)
C: SRA-E5
Number of cells / 0.2 mm²
Average
Periportal
Perivenular
300
250
200
150
100
50
0
*
F18
F20
N1
N4
N8
N15
N21
Adult
Fetus
Neonate
Age of rats (day)
D: OX6
Number of cells / 0.2 mm²
Average
Periportal
Perivenular
90
80
70
60
50
40
30
20
10
0
*
F18
F20
N1
N4
N8
N15
N21
Adult
Fetus
Neonate
Age of rats (day)

Fig. 2

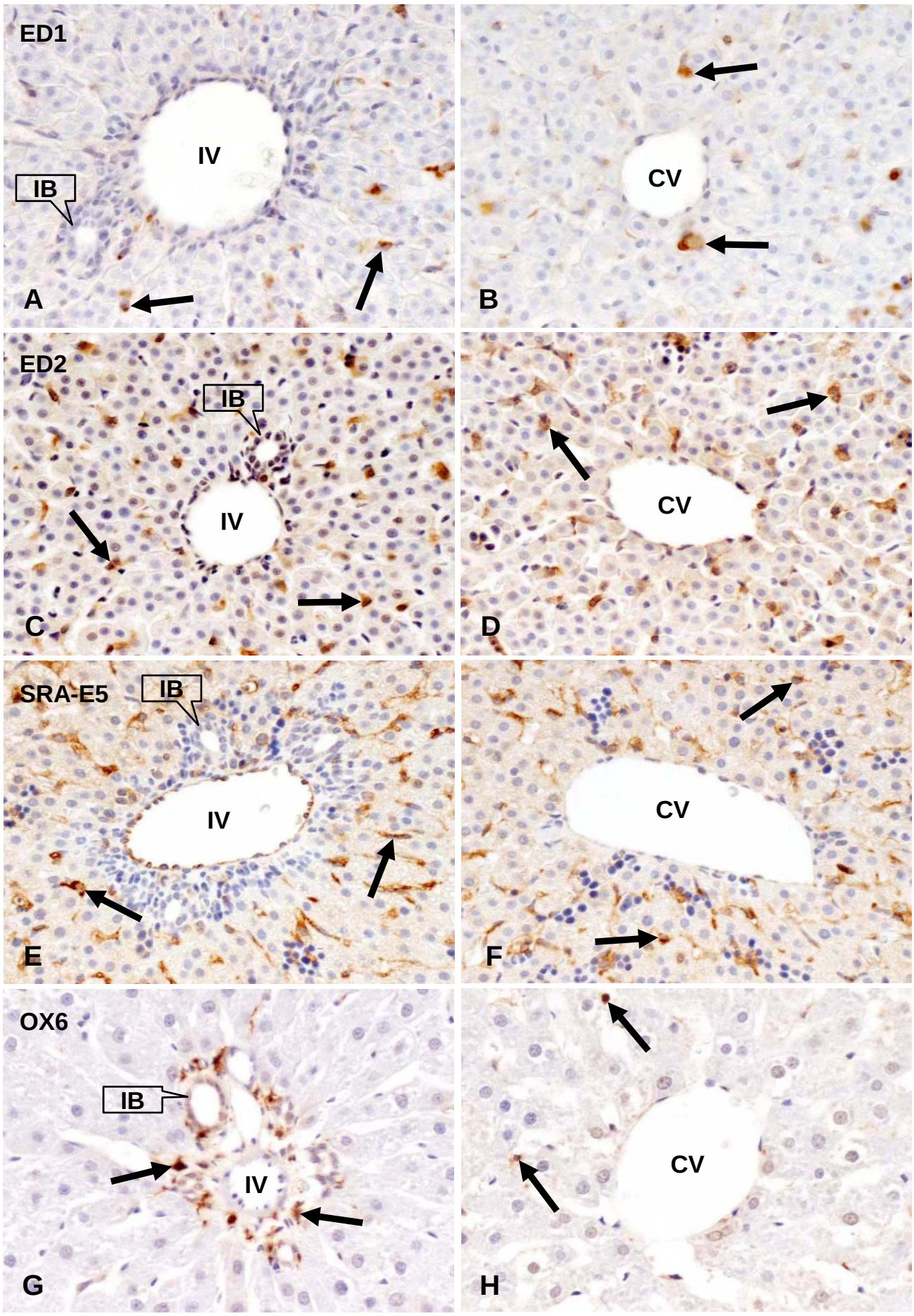

Fig. 3

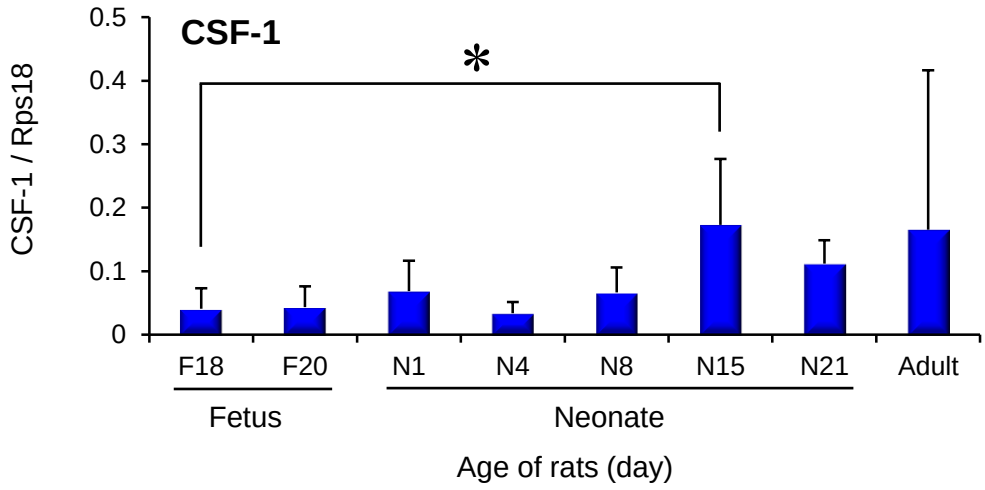
CSF-1
*
CSF-1 / Rps18
0.5
0.4
0.3
0.2
0.1
0
F18
F20
N1
N4
N8
N15
N21
Adult
Fetus
Neonate
Age of rats (day)

Fig. 4

A: Vimentin

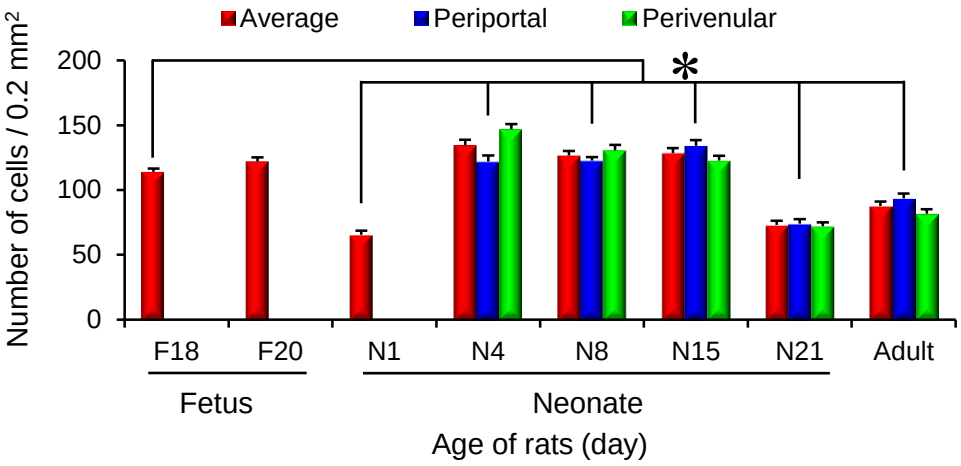

B: Desmin

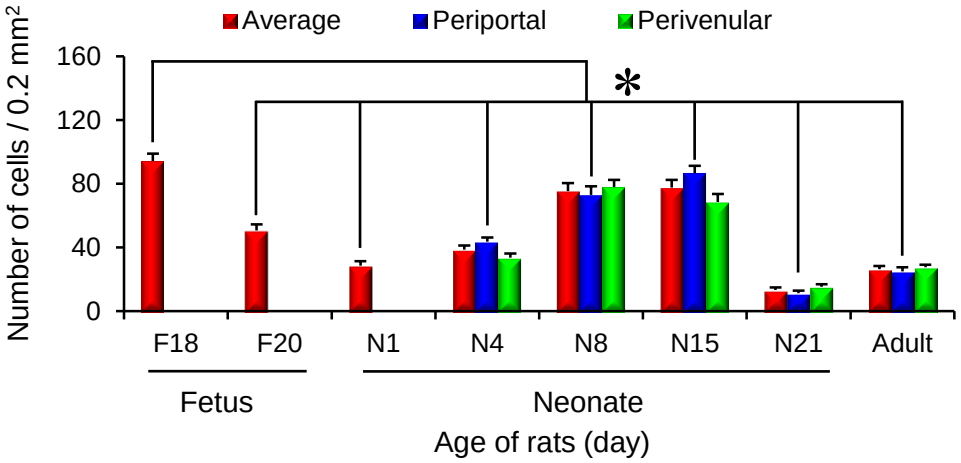

C: GFAP

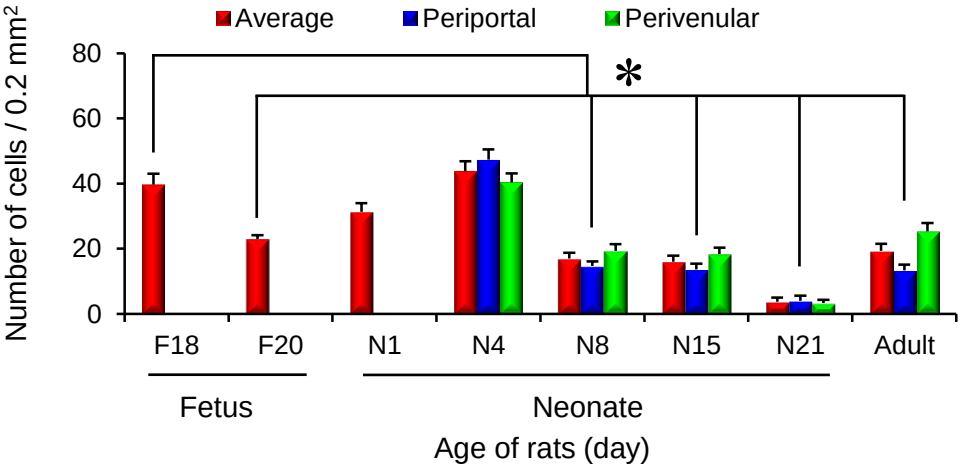

Fig. 5

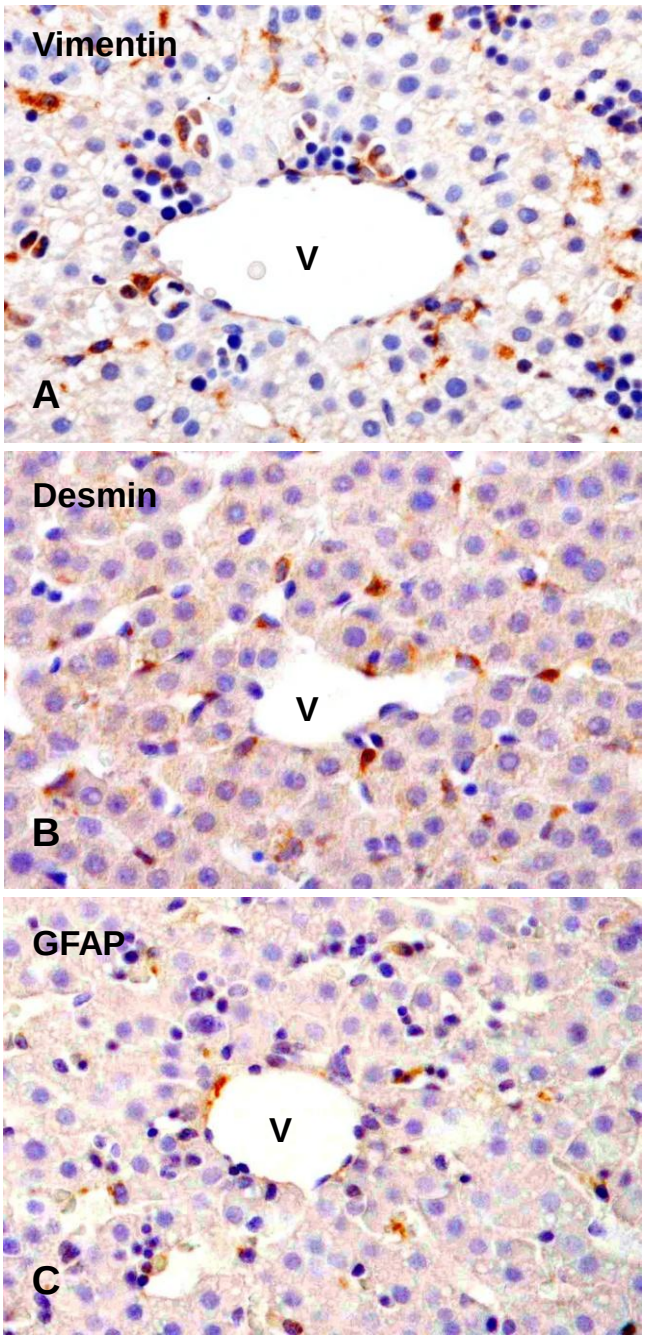

Fig. 6

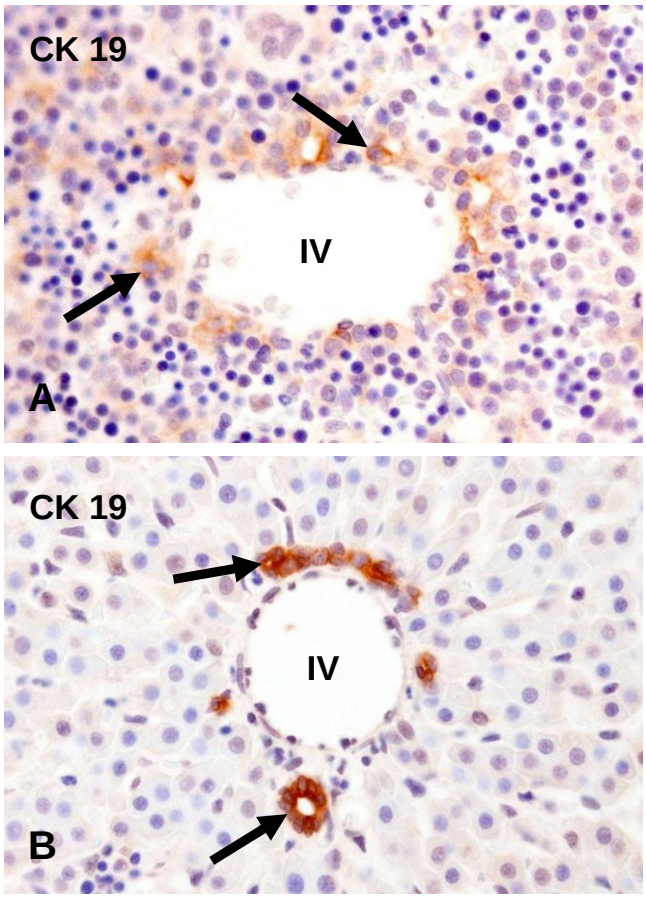

Fig. 7

Chapter 2

Immunohistochemical Characterization of Macrophages and Myofibroblasts in Cirrhotic Liver Lesions due to *Fasciola* Infection in Cattle

Introduction

Biliary fibrosis is the outcome of wound healing responses due to persistent or repeated injuries to cholangiocytes in cholangiopathies (Lazaridis et al. 2004, Penz-Österreicher et al. 2011). Uncontrolled biliary fibrosis progresses toward cirrhosis, culminating in hepatic insufficiency (Wynn and Barron 2010). Cholangiopathies in humans such as sclerosing cholangitis, drug-induced cholangiocyte damage, autoimmunity and obstruction of bile ducts due to cholelithiasis have been implicated in abnormal remodeling of bile ducts leading finally to biliary fibrosis in the Glisson's sheath. In veterinary medicine, along with aforementioned causes, liver fluke (*Fasciola* spp.) infections are important for hepatic failure in cattle. In the infection, hepatocyte damage is caused by migration of immature parasites at the acute stage; then, adult parasites invade into bile ducts in the Glisson's sheath and settle within the bile ducts (Andrews 1999) at the chronic stage. The infection causes cholangitis, cholangiocyte hyperplasia and biliary fibrosis, and cirrhosis may be developed in cattle in severe and consistent infection (Marcos et al. 2007); this condition may result in poor weight gain, reduced milk and meat yield, and infertility at the final stage (Ngategize et al. 1993, Kusiluka and Kambarage 1996). Such significant economic loss due to liver fluke infection is a major public health problem in some parts of the world, especially in East Asia, East Europe, Africa and Latin America (Marcos et al. 2008, Marcos et al. 2011, Young et al. 2011). However, the pathological events in liver fluke infection-associated biliary fibrosis have not been investigated in detail at cellular levels, although the appearance of eosinophils is well known (Marcos et al. 2007).

Fibrosis is a complex process characterized by inflammatory cell infiltrates and excessive deposition of extracellular matrices (ECMs). Out of the inflammatory cells, macrophages play a central role in fibrogenesis via production of fibrogenic factors (Bataller and Brenner 2005, Strieter et al. 2007); the most effective factor is transforming growth factor-β (TGF-β) (Inagaki and Okazaki 2007). The macrophages appearing in

fibrotic lesions induced in rats by hepatotoxicants have been demonstrated to be heterogeneous in immunophenotypes (Ide et al. 2002). Based on immunoexpressions with different antibodies for macrophages, macrophages in rat hepatic fibrosis have properties such as phagocytic activity, pro-inflammatory factor production, and MHC class II expression (Mori et al. 2009). These hepatic macrophages may be recruited from Kupffer cells, blood monocytes and interstitial dendritic cells present in the Glisson's sheath (Mori et al. 2009, Golbar et al. 2011). The ECMs are produced by myofibroblasts. In the hepatic fibrosis after parenchymal injury, myofibroblasts has been considered to be derived from hepatic stellate cells (HSCs) (Hautekeete and Geerts 1997, Friedman 2000). On the other hand, pre-existing fibroblasts may be the precursor of myofibroblasts in biliary fibrosis (Ramadori and Saile 2004, Beaussier et al. 2007, Golbar et al. 2011). The myofibroblasts can express variously cytoskeletons such as vimentin, desmin and α-smooth muscle actin (α-SMA). The cellular properties have not yet been characterized in liver fluke infection-induced biliary fibrosis in cattle.

In order to shed some light behind the pathogenesis of biliary fibrosis, in this study, the author investigated the properties of macrophages and myofibroblasts in liver fluke infection-induced cattle liver lesions by using the immunohistochemistry with a panel of antibodies for detection of macrophages and myofibroblasts. This study shows that macrophages with heterogenous phenotypes participate in the lesions, and myofibroblasts express various mesenchymal cytoskeletons, particularly vimentin and α-SMA.

Materials and Methods

Samples

Fasciola-infected cattle livers involving biliary cirrhosis (n=8) obtained at two abattoirs in Osaka, Japan were used in this study. Para-cirrhotic normal tissues of the same livers (n=4) served as controls. Macroscopic examination of the livers revealed whitish discoloration and *Fasciola* spp. in the bile ducts on the cut surface. The study protocol conformed to the institutional guidelines of Osaka Prefecture University for handling and use of biological specimens for experimental purposes.

Histopathology and immunohistochemistry

Cirrhotic and normal liver tissues were fixed in 10% neutral buffered formalin and Zamboni's fixative (0.21% picric acid and 2% paraformaldehyde in 130 mM phosphate buffer, pH 7.4) (Ide et al. 2005). These tissues were dehydrated and embedded in paraffin. Deparaffinized sections of 4 μm thick were stained with hematoxylin and eosin (HE) and azan-Mallory methods for histopathology. Deparaffinized sections were also used for immunohistochemical staining with monoclonal mouse anti-CD68, anti-AM-3K, and anti-SRA-E5 (a macrophage scavenger receptor, CD204) antibodies, as well as rabbit polyclonal anti-ionized calcium binding adaptor molecule-1 (Iba-1) antibody for macrophages; monoclonal mouse anti-vimentin, anti-desmin and anti-α-SMA antibodies for mesenchymal cells/myofibroblasts; monoclonal mouse anti-cytokeratin (CK) 19 antibody for bile duct epithelial cells. The detail information of these antibodies is given in Table 1. After pretreatment with heat (microwave in citrate buffer for 20 minutes), trypsin (0.1% trypsin in phosphate buffered saline (PBS) for 30 minutes at 37°C) or proteinase K (10 μg/ml proteinase K in PBS for 15 minutes) as shown in Table 1, tissue sections were treated with 3% H_2O_2 in PBS to quench endogenous peroxidase, and then with 5% skimmed milk in PBS to inhibit nonspecific reactions. The sections were incubated with

each primary antibody overnight (two overnight for anti-CD163 antibody) at 4ºC, followed by reaction with the secondary antibody (Histofine Simple Stain MAX-PO, Nichirei, Tokyo, Japan). Positive reactions were visualized with 3, 3'-diaminobenzidine (DAB Substrate Kit, Vector Laboratories, Inc., Burlingame, CA, USA). Sections stained with non-immunized mouse/rabbit sera instead of primary antibodies were all negative and served as control. Sections were counterstained lightly with hematoxylin.

Cell count and statistical analyses

Cells showing a distinct immunopositive reactions for CD68, AM-3K, SRA-E5 and Iba-1 were counted in five randomly selected areas (0.2 mm^2) of each sample at the periportal (including the Glisson's sheath) and perivenular areas of the normal livers, as well as portal fibrotic tissues and pseudo-lobules of the cirrhotic livers at a magnification of ×400 using ImageJ software version 1.44 (NIH, Bethesda, MD, USA). Cells positive for vimentin, desmin and α-SMA were evaluated semi-quantitatively using grades as shown in Table 2. Obtained data represented mean ± standard deviation (SD), and statistical analysis was performed using Tukey's test. Significance was set at $P < 0.05$.

Results

Histopathology

As control livers, the author used livers without any lesions (Fig. 1A). Grossly, the liver fluke-infected livers had irregular surface, and there were liver flukes in some dilated bile ducts. Histopathologically, the affected livers consisted of pseudo-lobules and fibrotic areas. The fibrotic areas were composed of inflammatory cells, spindle-shaped cells, and proliferation of collagen fibers, forming bridges by which pseudo-lobules were separated (Fig. 1B). The greatest fibrotic areas were found to be developed exclusively in the Glisson's sheath, because there were interlobular veins, interlobular arteries, and interlobular bile ducts. Eosinophils were frequently seen in the fibrotic areas (Fig. 1C, inset), and mononuclear cells were also observed often. The proliferation of collagen fibers forming bridges was clearly demonstrated by azan-Mallory methods (Fig. 1D). In addition to the ductular reaction, called pseudo-bile ducts, in the affected Glisson's sheath, newly-formed blood vessels were frequently seen. Based on histopathological findings, the liver fluke-infected livers were regarded as cirrhotic lesions at the advanced stage.

Macrophage immunophenotypes

The numbers of macrophages positive for CD68, AM-3K, SRA-E5, and Iba-1 were counted in control and cirrhotic livers, the statistical evaluation data are presented in Fig. 2. In control livers, the numbers of macrophages reacting to CD68 (Fig. 2A), AM-3K (Fig. 2B), SRA-E5 (Fig. 2C) and Iba-1 (Fig. 2D) were all greater in the periportal (PP) areas (including the Glisson's sheath) than those of perivenular (PV) areas. On the other hand, in cirrhotic livers (CL), the numbers of macrophages reactive for CD68 (Fig. 2A) and AM-3K (Fig. 2B) were higher in the portal connective tissues (PCT) compared to those in the parenchyma in the pseudo-lobules (PSL). By contrast, the numbers of macrophages positive for SRA-E5 (Fig. 2C) and Iba-1 (Fig. 2D) were lower in the PCT compared to

those in the PSL. The author next compared the average number of macrophages between normal livers (NL) and cirrhotic livers (CL); overall, macrophages expressing CD68 and AM-3K in the CL were significantly increased in contrast to those in the NL (Fig. 2A, B); on the other hand, those positive for SRA-E5 and Iba-1 showed a significant decrease in CL than NL (Fig. 2C, D).

In the control livers, CD68-, AM-3K-, SRA-E5- and Iba-1-positive macrophages were sporadically distributed in the hepatic parenchyma and the periportal areas (including the Glisson's sheath) (Fig. 3A, C, E, G, respectively). The cytoplasm of the SRA-E5-positive macrophages appeared to be slightly enlarged (Fig. 3E) in contrast to macrophages reacting to CD68, AM-3K and Iba-1. Based on the distribution of these macrophages, it was considered that Kupffer cells located along the sinusoids of the liver lobules and tissue macrophages in the Glisson's sheath reacted to these antibodies in varying degrees. In cirrhotic livers including the Glisson's sheath, macrophages reacting to CD68 (Fig. 3B), AM-3K (Fig. 3D), SRA-E5 (Fig. 3F) and Iba-1 (Fig. 3H) were often seen; particularly, the numbers of cells reacting to CD68 and AM-3K were greater in CL as mentioned in the statistical evaluation (Fig. 2A-D).

Immunophenotypes of mesenchymal cells and myofibroblasts in the Glisson's sheath

Semi-quantitative analysis on the expressions of vimentin, desmin and α-SMA in control and cirrhotic livers is presented in Table 2. Pre-existing and newly-formed vascular smooth muscles were reactive for desmin and α-SMA, which then were excluded from the evaluation. In control cattle livers, spindloid cells reacting to vimentin (Fig. 4A), desmin (Fig. 4C) and α-SMA (Fig. 4E) were present along the sinusoid, indicating that HSCs may react to these antibodies for mesenchymal markers. Additionally, vimentin-positive cells seen in the Glisson's sheath are considered to be pre-existing mesenchymal cells/portal

fibroblasts; on the contrary, desmin and α-SMA-positive cells were rarely seen in the Glisson's sheath.

In the cirrhotic livers including the Glisson's sheath, mesenchymal cells reacting to vimentin (Fig. 4B), desmin (Fig. D) and α-SMA (Fig. F) were seen more frequently. Particularly, vimentin and α-SMA-positive cells (Fig. 4B, F, respectively) were greater than that of desmin-positive cells (Fig. 4D) in the fibrotic areas. Interestingly, α-SMA-positive cells appeared surrounding the hyperplastic interlobular bile ducts (Fig. 4F, arrows). As mentioned above, smooth muscle cells in newly formed blood vessels reacted strongly to α-SMA (Fig. 4F, arrowheads).

Immunohistochemistry for cholangiocytes

Immunoreactivity for CK19, a marker of cholangiocyte, was limited to the epithelial cells of interlobular bile ducts in the Glisson's sheath in the control livers (Fig. 5A). By contrast, CK19-immunopositive cholangiocytes in the interlobular bile ducts involved in the fibrotic lesions were clearly seen (Fig. 5B). Additionally, CK19-positive cells were observed in the fibrotic lesions; some of them were sporadically present as a single cell or clusters consisting of a few cells, and the others formed ducts without clear lumen (Fig. 5C). Therefore, the frequency of CK19-positive cholangiocytes was increased in the cirrhotic livers.

Discussion

Histopathology

Biliary cirrhosis is the advanced stage of hepatic fibrosis which is frequently associated with ductular reactions (hyperplasia/proliferation which form pseudo-bile ducts) and structural alteration (Schuppan and Afdhal 2008, Lin et al. 2010). The present cattle cirrhotic livers were characterized by pseudo-lobule formation, proliferation/hyperplasia of bile ducts and fibrotic bridges. The fibrotic bridges were formed between portal and portal areas, between portal and central vein areas, or central vein and central vein areas (Rockey and Chung 1998). Ductular reaction is regarded as "pacemaker of portal fibrosis" and used as an indicator for assessment of degrees of hepatic fibrosis (Clouston et al. 2005, Richardson et al. 2007, Penz-Österreicher et al. 2011). In the current study, significant ductular reaction was observed by the immunoreactivity with CK19 antibody, indicating the advanced stage of hepatic fibrosis for the present cases examined. The ductular reaction may be derived from metaplasia of hepatocytes without function (Yoshioka et al. 2004). A single epithelial cell and cellular clusters consisting of a few epithelial cells, which were reactive for CK19, may be metaplastic cells of hepatocytes, because cholangiocytes and hepatocytes have been considered to be generated from the common progenitors, termed as oval cells (Yoshioka et al. 2004, Tanaka et al. 2011). Periportal region with advancing fibrosis might serve as a niche for the metaplasia of progenitor cells (Gleiberman et al. 2005).

Macrophages

Eosinophil infiltration was clearly observed as the major inflammatory cell type in the present case as reported previously in cattle livers infected with *Fasciola* spp. (Tanimoto et al. 1998). In addition to eosinophils, mononuclear cells were observed in the

fibrotic lesions. The mononuclear cells were regarded as macrophages by the immunohistochemistry. Macrophages have been demonstrated to have crucial roles in fibrogenesis. TGF-β1, a potent fibrogenic factor, produced by macrophages can incite myofibroblast development (Bataller and Brenner 2005, Inagaki and Okazaki 2007, Strieter et al. 2007). Previously, the appearance of macrophages has been demonstrated to play roles in *Schistosoma*-infected livers in mice (Wynn et al. 2004). The current study showed that macrophages appeared in close proximity with collagen-producing myofibroblasts in the portal connective tissues in *Fasciola*-induced biliary cirrhosis, indicating involvement of macrophages in fibrogenesis due to liver fluke infection (Fascioliasis). Factors produced by cholangiocytes in ductular reaction, which is commonly observed in *Fasciola*-infection, might recruit macrophages in the Glisson's sheath favoring fibrogenesis (Jafri et al. 2009, Brancato and Albina 2011). However, the factors remain to be investigated in future studies. In the present study, the author attempted to investigate the immunophenotypes of macrophages. In the control cattle livers, macrophages reacting to CD68, AM-3K, SRA-E5, and Iba-1 were detected along the sinusoids; these findings for the first time showed that these antibodies would be useful for the detection for hepatic macrophages in cattle. Furthermore, the present study demonstrated that macrophages reacting to the four antibodies were greater in the number in the periportal areas than in the perivenular areas, indicating that Kupffer cells are more predominant in the periportal areas (Parker and Picut 2005). CD68 up-expression may imply the activated phagocytosis, because CD68 is located on the lysosomal membrane, especially phagolysosome of blood monocyte-derived exudate and resident macrophages (Damoiseaux et al. 1994, Song et al. 2011). CD163 is a cell-surface glycoprotein receptor, which is highly expressed in resident macrophages (Fabriek et al. 2005), and triggers the production of proinflammatory mediators such as tumor necrosis factor (TNF)-α, interleukin (IL)-1β and IL-6 (Polfliet et al. 2006), and it may also acts as endocytic scavenger receptor for hemoglobin-haptoglobin complex which can mediate clearance of free hemoglobin from the circulation (Graversen et al. 2002); therefore, the AM-3K, a

clone of CD163, expressing macrophages may be related to the proinflammatory cytokine production, and phagocytosis. SRA-E5s are principal receptors of macrophages whose major function is to eliminate target ligands such as modified low density lipoprotein (Haworth et al. 1997, Suzuki et al. 1997, Platt et al. 2002). Iba-1, also known as allograft inflammatory factor-1 (AIF1), is critically involved in motility-associated rearrangement of the actin cytoskeleton (Ohsawa et al. 2000, Kohler 2007).

Interestingly, in the fibrotic areas of cattle cirrhosis, the numbers of macrophages positive for CD68 and AM-3K were more increased than in controls, whereas macrophages reacting to SRA-E5 and Iba-1 were decreased. Although the reason should be investigated further, macrophages in the fibrotic lesions might have been considered to show increased phagocytosis and inflammatory factor production rather than lipid metabolism and mobility. At least, it was considered that macrophages with different functions might participate in the cattle liver fibrosis infected with liver fluke. To the best of the author's knowledge, such investigations on macrophages are the first trial for the liver fluke-infected cattle cirrhosis.

Myofibroblasts in the Glisson's sheath with fibrosis

Myofibroblasts are identified by immunoexpressions of cytoskeletons such as α-SMA, vimentin and desmin, and the myofibroblasts play important roles in hepatic fibrosis by producing extracellular matrices (Magness et al. 2004, Hinz et al. 2007). HSCs along the sinusoids and pre-existing fibroblasts in the Glisson's sheath may be the precursors of myofibroblasts (Beaussier et al. 2007). The portal fibroblasts are characterized by vimentin positivity but do not react to desmin, and HSCs in normal rat livers are identified by both vimentin and desmin reactions (Penz-Österreicher et al. 2011). α-SMA expression is seen in well-differentiated myofibroblasts in advanced fibrosis (Novo et al. 2009, Wynn and Barron 2010). In the present cattle cirrhotic livers, desmin-positive cells were infrequently

seen, and vimentin-positive cells were moderately or frequently present. Interestingly, α-SMA-positive cells were markedly increased in the fibrotic areas. These findings indicated that myofibroblasts expressing α-SMA might be derived from the pre-existing portal fibroblasts rather than HSCs, as have been mentioned in rat biliary cirrhosis (Beaussier et al. 2007, Dranoff and Wells 2010).

In summary, in addition to the availability of different antibodies (against CD68, AM-3K, SRA-E5 and Iba-1) for macrophage detection in cattle tissues, this study demonstrates that macrophage immunopositive to these antibodies are present more predominantly in the periportal areas than in the perivenular areas. Furthermore, it was found that CD68- and AM-3K-positive macrophages participated in the fibrotic lesions of cattle; on the other hand, SRA-E5- and Iba-1-positive macrophages were less in the number. On the basis of possible functions demonstrable with the immunohistochemistry with these antibodies, macrophages appearing in the fibrotic areas might have functions such as phagocytosis and proinflammatory factor productions. It was found that myofibroblasts, which are considered to contribute to fibrogenesis, reacted moderately or strongly to vimentin and α-SMA; however, desmin-positive cells were rarely seen. It has been considered that eosinophils might be responsible for the development of hepatic fibrosis by producing TGF-β1 (Shen et al. 2008). Along with eosinophils, this study showed that macrophages also participated in the liver *Fasciola*-infected cattle cirrhosis, in relation to development of myofibroblasts expressing vimentin and α-SMA. These data would be useful to analyze the billiary fibrosis as spontaneous lesions.

Summary

Histopathologically, cirrhosis in *Fasciola*-infected cattle livers were characterized by inflammatory cell infiltration such as eosinophils and macrophages, pseudo-lobule, pseudo-bile ducts and fibrotic bridges separating pseudo-lobules; the fibrotic lesions were developed in the Glisson's sheath. Pseudo-bile ducts consisting of epithelial cells reacted clearly to cytokeratin (CK) 19, a phenotype indicative of cholangiocyte. Immunophenotypes of macrophages and myofibroblasts were investigated in the fibrotic livers. Macrophages positive for CD68 (reflecting phagocytosis) and AM-3K (CD163, representing proinflammatory cytokine production) were increased and those for SRA-E5 (CD204, implying lipid metabolism) and Iba-1 (a calcium binding protein playing role in chemotaxis) decreased in cirrhotic liver tissues, compared to para-cirrhotic normal livers. Spindle-shaped myofibroblasts positive for vimentin, desmin and α-smooth muscle actin (α-SMA) increased in the peribiliary connective tissues, although the desmin positive cells were fewer. In addition to the usefulness of these antibodies for macrophage detection in cattle livers, this study shows that macrophages with different immunophenotypes participate in *Fasciola*-infected cattle livers, in relation to development of myofibroblasts expressing mainly vimentin and α-SMA.

Table 1. Primary antibodies used for immunohistochemistry

Antibody	Dilution	Pretreatment	Source of antibody	Specificity
Anti-CD68	1:50	Proteinase K	DakoCytomation, Glostrup, Denmark	Exudate macrophages (monocytes)
Anti-AM-3K	1:50	Proteinase K	TransGenic Inc, Kumamoto, Japan	Resident macrophages (Kupffer cells)
Anti-SRA-E5	1:100	Heat	TransGenic Inc.	Macrophages, Kupffer cells
Anti-Iba-1*	1:100	Heat	Wako Pure Chemical Industries Ltd, VA, USA	Macrophages
Anti-Vimentin	1:400	Heat	Dako	Cells of mesenchymal origin
Anti-Desmin	1:200	Heat	Dako	Smooth muscle cells
Anti-α-SMA	1:100	Proteinase K	Dako	Smooth muscle cells, myofibroblasts
Anti-CK19	1:100	Trypsin	Novocastra Laboratories Ltd, Newcastle, UK	Cholangiocytes

*; Rabbit polyclonal antibody; the rest are mouse monoclonal antibodies. **α-SMA**: α-smooth muscle actin, **CK19**: cytokeratin 19. AM-3K for CD163, SRA-E5 for CD204.

Table 2. Semi-quantitative analyses of HS cells/myofibroblasts

Antibody \ Sample	PP NL	PV NL	PCT CL	PSL CL
Anti-α-SMA	±	+	++ ~ +++	+
Anti- Vimentin	± ~ +	± ~ +	++ ~ +++	±
Anti- Desmin	±	±	+	−

PP: periportal (including Glisson's sheath), **NL**: normal liver, **PV**: perivenular, **PCT**: portal connective tissue, **CL**: cirrhotic liver, **PSL**: pseudolobule, **α-SMA**: α-smooth muscle actin.

Semi-quantitative grades: –; no positive cells, ±; occasional positive cells, +; few positive cells, ++; moderate number positive cells, +++; many positive cells.

Figure Legends

Fig. 1. Histopathology of *Fasciola*-induced biliary cirrhosis in cattle. Representative section of a para-cirrhotic normal liver showing no apparent changes (A). Cirrhotic liver section shows prominent fibrosis in the Glisson's sheath, fibrotic bridges between adjacent portal areas (arrows), formation of pseudo-lobules (asterisks) and infiltration of inflammatory cells (B). The affected Glisson's sheath (C, higher magnification of outlined area in B) consists of bile duct hyperplasia (arrows) and the inflammatory cells involve mainly eosinophils (inset, arrow). Fibrotic tissues, demonstrable with collagen staining (blue), around a pseudo-lobule (asterisk) and in the portal to portal connection is seen (D). **IA**: interlobular arteriole, **IB**: interlobular bile duct, **IV**: interlobular vein. HE (A-C) and azan-Mallory method (D).

Fig. 2. The kinetics of macrophages reacting to CD68 (A), AM-3K (B), SRA-E5 (C) and Iba-1 (D) in the biliary cirrhosis. In normal liver, macrophage populations are greater in periportal (PP) areas than those in perivenular (PV) areas (A-D). In cirrhotic liver, macrophages positive for CD68 and AM-3K are greater in portal connective tissues (PCT) than those in the parenchyma of pseudo-lobule (PSL) (A, B). By contrast, macrophages reactive for SRA-E5 and Iba-1 are smaller in PCT than in the parenchyma of PSL (C, D). Compared to normal livers, the number of macrophages positive for CD68 and AM-3K are increased and those for SRA-E5 and Iba-1 are decreased in cirrhotic livers. Student's *t*-test. *; $P<0.05$.

Fig. 3. The distributions of macrophages positive for CD68 (A, B), AM-3K (C, D), SRA-E5 (E, F) and Iba-1 (G, H) in the biliary cirrhosis. Immunopositive macrophages are sporadically distributed in the periportal areas including the Glisson's sheath in normal livers (A, C, E, G). A significant number of macrophages positive for CD68 (B) and AM-3K (D) are detectable in the portal connective tissues (PCT) in cirrhotic livers. In contrast, macrophages reactive for SRA-E5 (F) and Iba-1 (H) are

a few in the PCT in CL. **IA**: interlobular arteriole, **IB**: interlobular bile duct, **IV**: interlobular vein. Arrows indicate representative cells in each staining. Immunohistochemistry, counterstained with hematoxylin.

Fig. 4. The distributions of mesenchymal cells/myofibroblasts positive for vimentin, desmin and α-SMA in the biliary cirrhosis. A few cells expressing vimentin (A), desmin (C) and α-SMA (E) are seen in the periportal areas (including the Glisson's sheath) in the normal livers. In contrast to normal livers, the number of cells expressing vimentin (B), desmin (D) and α-SMA (F) are increased in the Glisson's sheath in cirrhotic livers. Note that desmin expressing cells are relatively fewer (D), and the number of blood vessels in the Glisson's sheath, reactive for α-SMA (F, arrowheads), are increased. **IA**: interlobular arteriole, **IB**: interlobular bile duct, **IV**: interlobular vein. Arrows indicate representative cells in each staining. Immunohistochemistry, counterstained with hematoxylin.

Fig. 5. The distribution of cholangiocytes in the biliary cirrhosis. Cytokeratin (CK) 19-positive cholangiocytes are detectable only in the bile ducts (arrows) in the Glisson's sheath in normal liver (A). Hyperplasia of bile ducts is seen in biliary cirrhosis (B, arrows). The hyperplastic bile ducts are irregular in shape and often devoid of lumen (C, outlined area in B; arrows). Individual cholangiocyte or clusters of cholangiocytes, reacting to CK19, are seen in the periportal parenchyma (C, arrowheads). Immunohistochemistry, counterstained with hematoxylin.

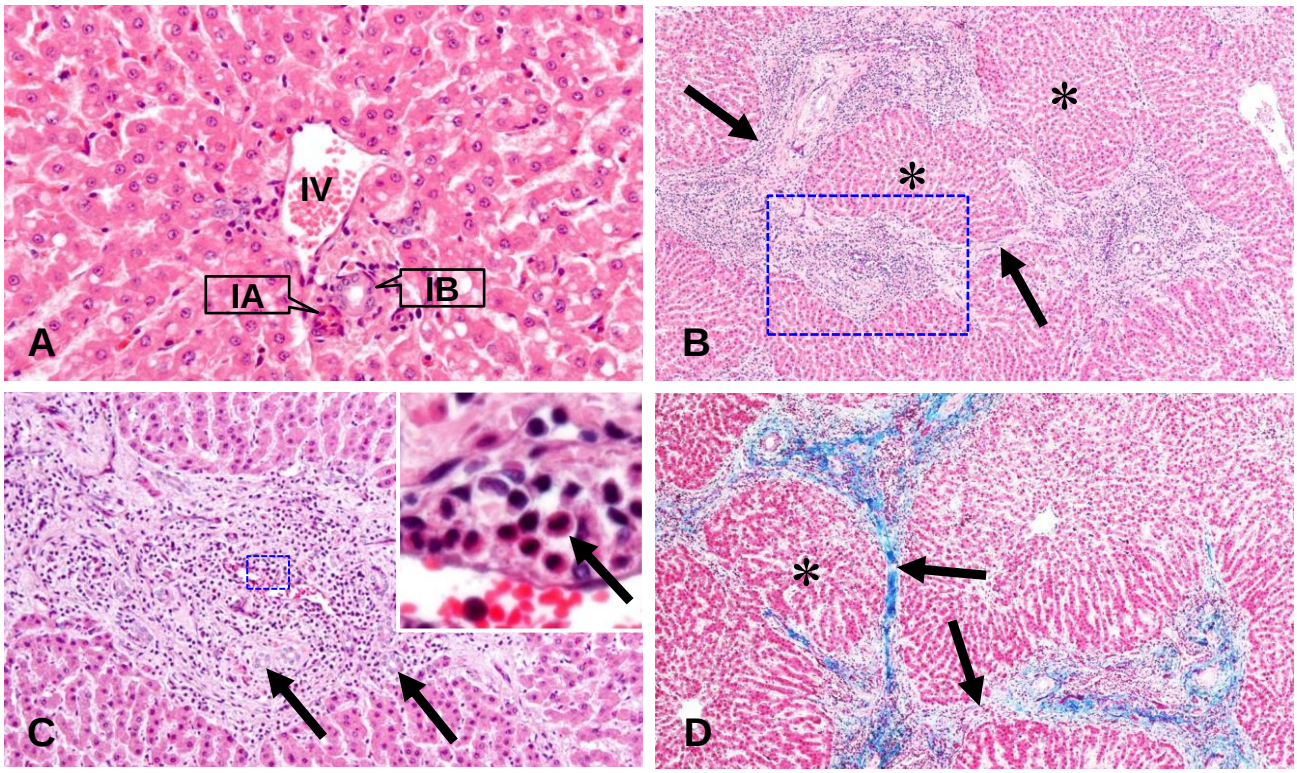

Fig. 1

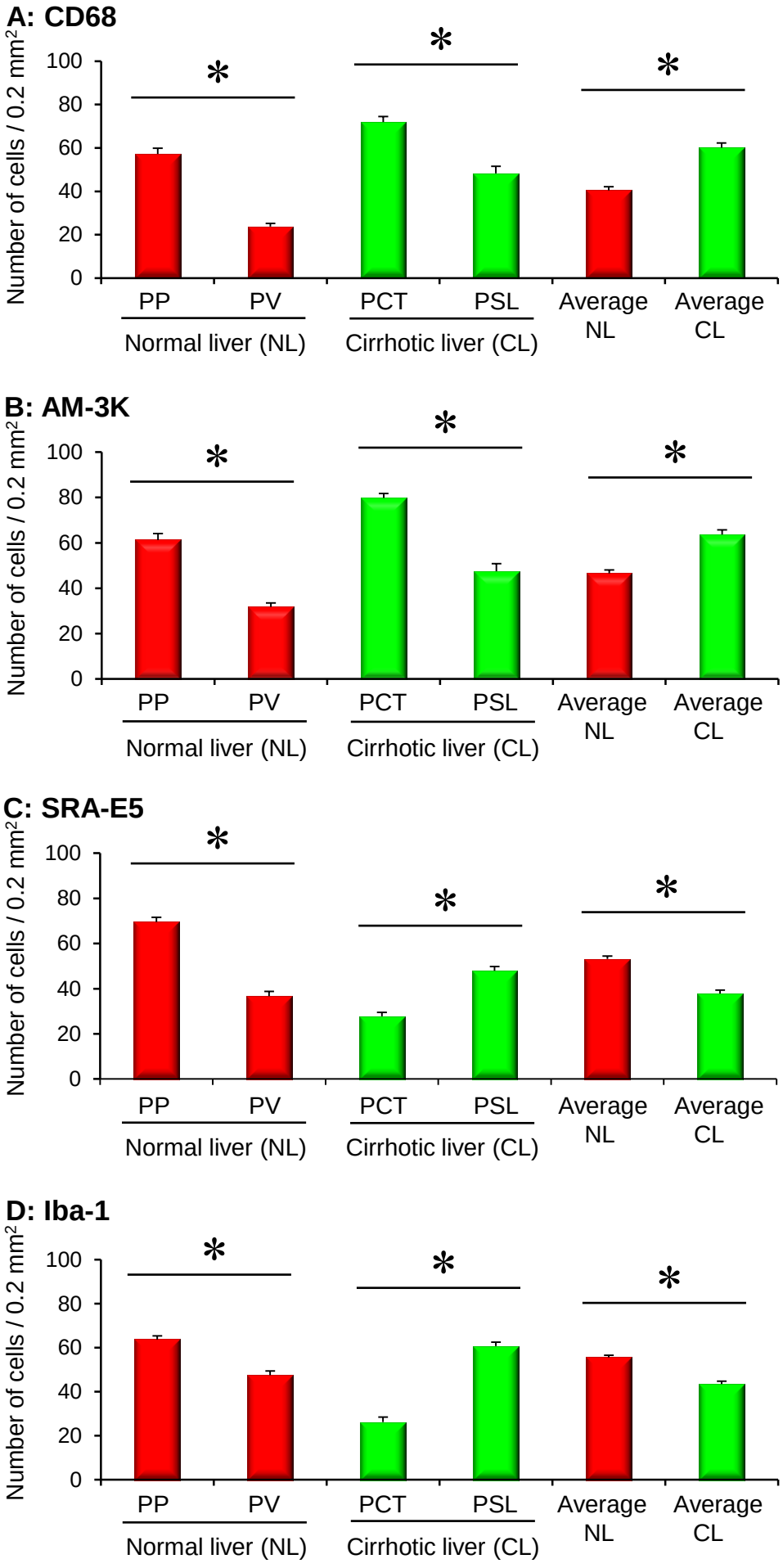
A: CD68
B: AM-3K
C: SRA-E5
D: Iba-1
Number of cells / 0.2 mm²
100
80
60
40
20
0
*
PP
PV
PCT
PSL
Average NL
Average CL
Normal liver (NL)
Cirrhotic liver (CL)

Fig. 2

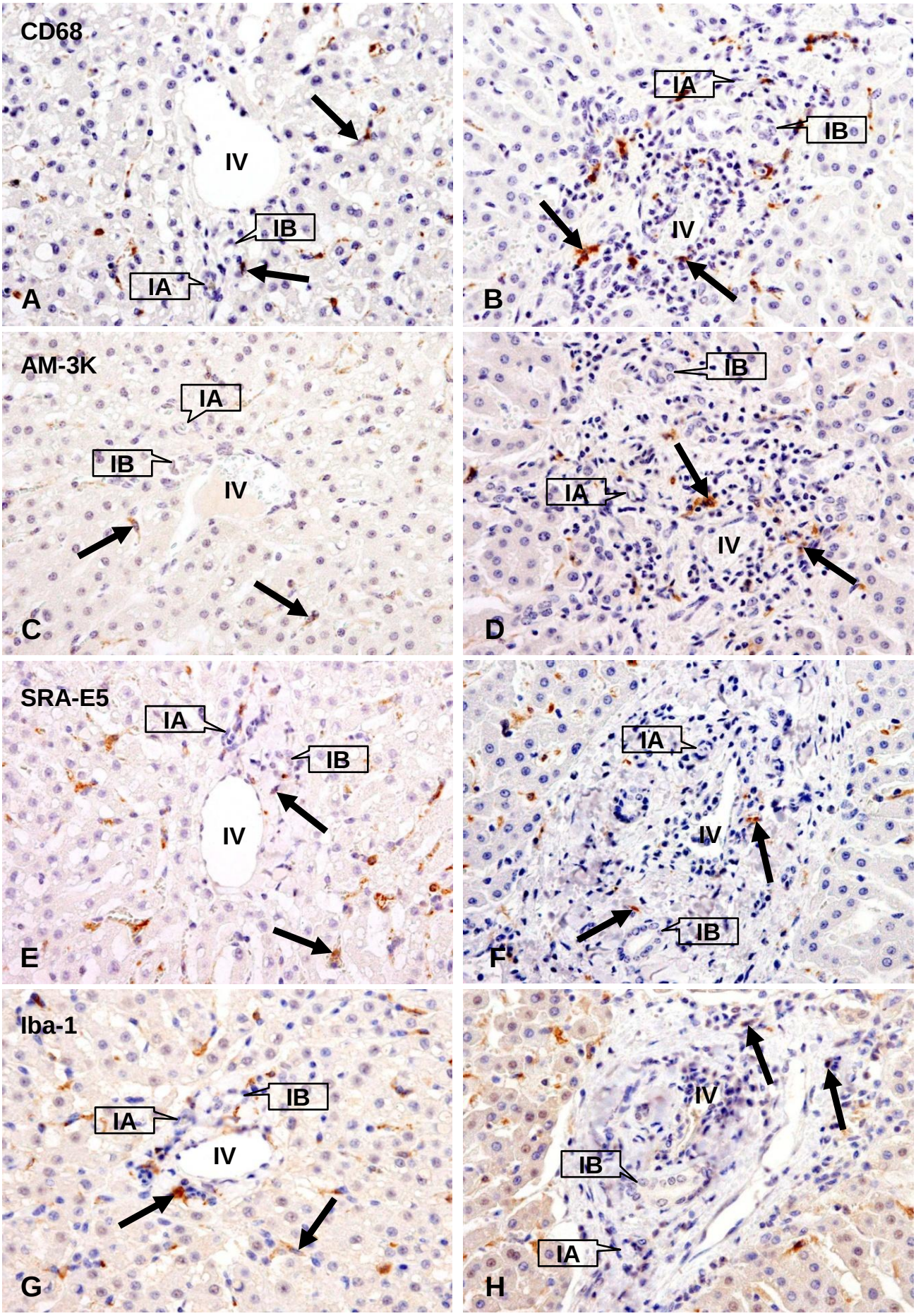
CD68
IV
IB
IA
A
IA
IB
IV
B
AM-3K
IA
IB
IV
C
IB
IA
IV
D
SRA-E5
IA
IB
IV
E
IA
IV
IB
F
Iba-1
IB
IA
IV
G
IV
IB
IA
H

Fig. 3

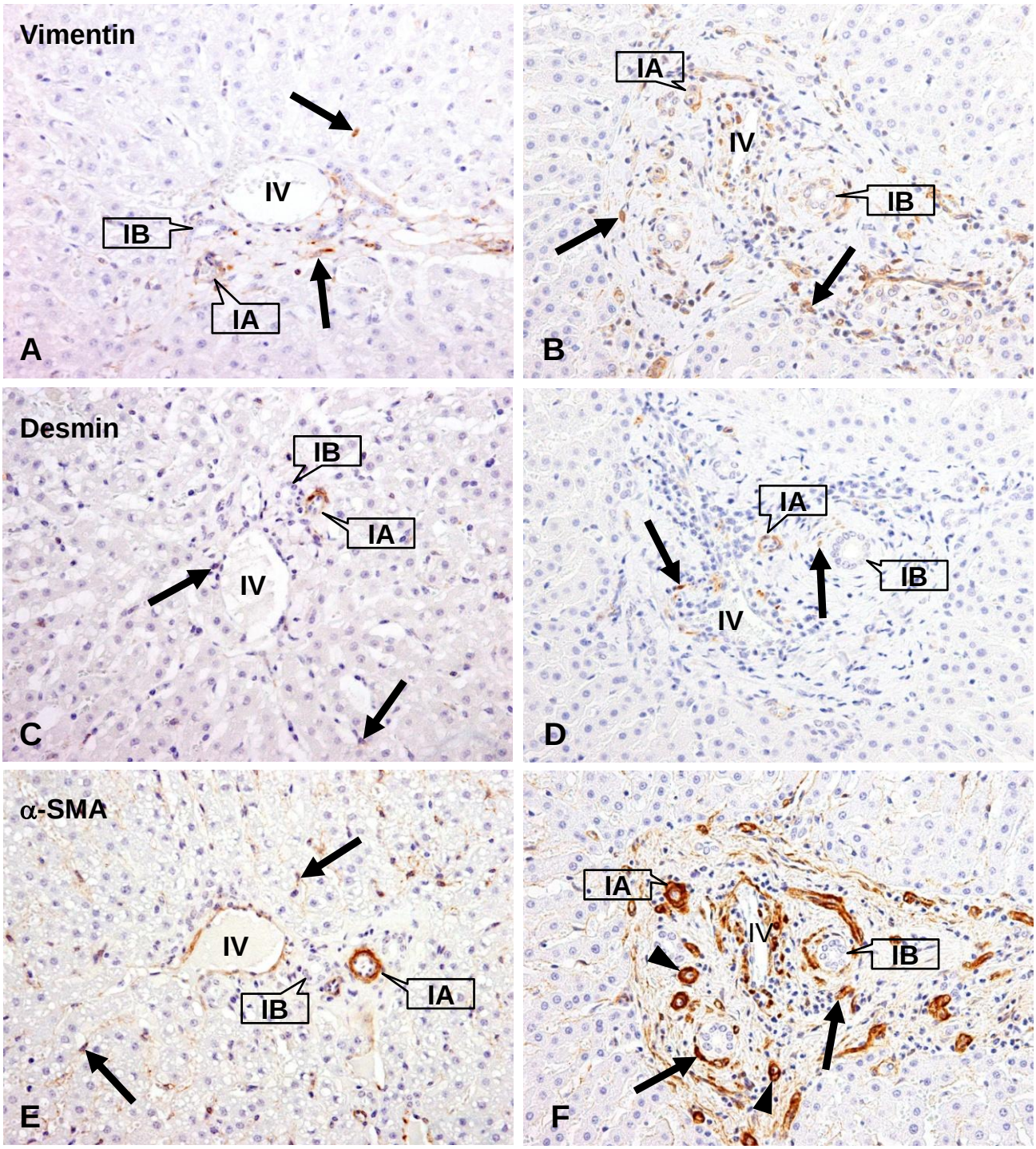
Vimentin
IV
IB
IA
A
IA
IV
IB
B
Desmin
IB
IA
IV
C
IA
IB
IV
D
α-SMA
IV
IB
IA
E
IA
IV
IB
F

Fig. 4

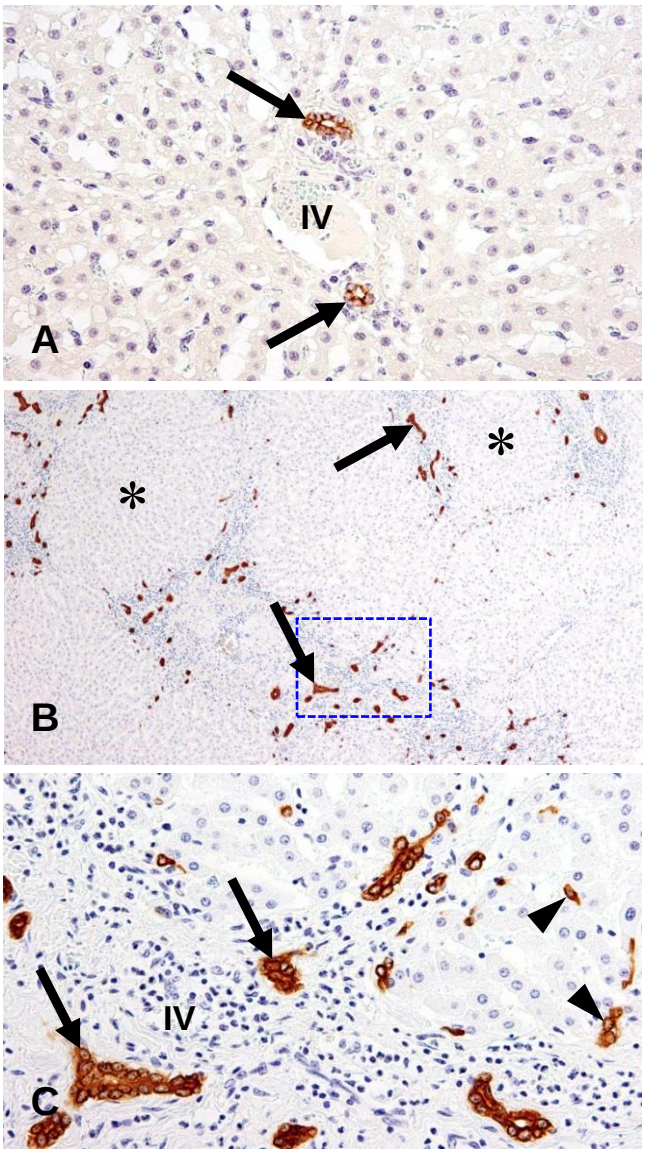

Fig. 5

Chapter 3

Immunohistochemical Characterization of Macrophages and Myofibroblasts in α-Naphthylisothiocyanate (ANIT)-induced Bile Duct Injury and Subsequent Fibrogenesis in Rats

Section I

Immunophenotypes of Macrophages and Myofibroblasts in ANIT-induced Biliary Fibrosis in Rats

Introduction

Biliary fibrosis is a pathological process observed in cholangiopathies such as primary sclerosing cholangitis, bile duct stenosis/obstruction and drug-induced bile duct damage, resulting in hepatic insufficiency and cirrhosis (Lazaridis et al. 2004). The abnormal interplay between injured cholangiocytes, mesenchymal cells (hepatic stellate cells (HSCs), portal fibroblasts, and vascular smooth muscle cells), and inflammatory cells (neutrophils, macrophages, and lymphocytes) has been implicated in cholangiopathy-related biliary fibrosis (Lazaridis et al. 2004, Strazzabosco et al. 2005). Perhaps because of these complicated interactions, the pathogenesis of biliary fibrosis remains poorly understood.

It has been recently reported that macrophages and myofibroblasts are two major cell components with crucial roles in hepatic and renal fibrogenesis (Mo et al. 1999, Schuppan et al. 1999, Ide et al. 2001). Macrophages secrete soluble factors responsible for the induction of myofibroblasts capable of producing extracellular matrices (Wynn 2008). Therefore, fibrotic lesions may be abrogated by modulation of macrophage functions. Macrophages appearing in hepatic lesions show heterogeneous functions, demonstrable with immunohistochemical methods (Ide et al. 2005, Mori et al. 2009). Myofibroblasts have been regarded as contractile mesenchymal cells expressing various cytoskeletons such as vimentin, desmin and α-smooth muscle actin (α-SMA) (Yamate et al. 2005, Hinz et al. 2007); the origin and properties have not yet been clarified in biliary fibrosis. In the

present study, the author investigated the immunophenotypes of macrophages and myofibroblasts in relation to biliary fibrosis in alpha-naphthylisothiocyanate (ANIT)-induced cholestatic rat liver lesions. ANIT is a well-characterized hepatotoxicant known to cause cholestatic liver injury (Kossor et al. 1993). Because the expression of colony stimulating factor-1 (CSF-1), monocyte chemoattractant protein-1 (MCP-1) and transforming growth factor-β1 (TGF-β1) are correlated with the extent of hepatic injury (Kim et al. 1998, Qi et al. 1999, Zhang et al. 2004, Bataller and Brenner 2005, Guo et al. 2006, Pinzani et al. 2008), the author examined the expression patterns of these factors. The present study demonstrates that macrophages and myofibroblasts, each showing heterogeneous immunophenotypes, participate in post-bile duct injury fibrosis, and that their appearance correlates with the cytokines examined, in particular MCP-1.

Materials and Methods

Animals and ANIT-induced hepatic lesions

Five-week-old, male F344 rats (100 to 120 g body weight) were purchased from Charles River Japan (CRJ, Hino, Shiga, Japan). These animals were housed in an animal room at a controlled temperature of 21 ± 3˚C and with a 12-hour light-dark cycle; they were provided a standard diet for rats (MF, Oriental Yeast Co. Ltd., Tokyo, Japan) and tap water *ad libitum*. After a one week acclimatization period, they were divided into control (three rats) and ANIT injection groups (twenty-one rats). The animals in the ANIT group were given a single intraperitoneal (IP) injection of ANIT at a dose of 75 mg/kg body weight dissolved in olive oil (Calvo et al. 2001). Three rats were euthanized by exsanguination under ether anesthesia on each of post-injection (PI) days 1, 2, 3, 5, 7, 9 and 12. Control rats received an equal volume of olive oil and were euthanized immediately after the injection (PI day 0). One hour before euthanasia, all the rats received IP injection of 5-bromo-2′-deoxyuridine (BrdU: Sigma-Aldrich Co., St. Louis, MO, USA) at the dose of 50 mg/kg body weight.

At necropsy, blood was collected from the abdominal artery and serum samples were tested for aspartate transaminase (AST), alanine transaminase (ALT), alkaline phosphatase (ALP) and total bilirubin (T. Bil) with a Clinical Analyzer 7170 (Hitachi, Tokyo, Japan).

The animal experiments were conducted under the institutional guidelines approved by the ethical committee of Osaka Prefecture University for animal care.

Histopathology and immunohistochemistry

Tissues from the left external lobe of the livers were fixed in 10% neutral buffered formalin, Zamboni’s fixative (0.21% picric acid and 2% paraformaldehyde in 130 mM

phosphate buffer, pH 7.4) and periodate-lysine-paraformaldehyde (PLP) solutions (Ide et al. 2003). These tissues were dehydrated and embedded in paraffin. Deparaffinized sections, cut at 4 μm in thickness, were stained with hematoxylin and eosin (HE) for histopathology. Zamboni's solution- or PLP-fixed tissue sections were used for the immunohistochemistry with mouse monoclonal antibodies against macrophages (ED1 (for CD68), ED2 (for CD163), OX6 (for major histocompatibility complex (MHC) class II), SRA-E5 (for CD204)), mesenchymal cytoskeletal proteins (vimentin, desmin, and α-SMA), bile duct epithelia (CK19) and incorporated BrdU for proliferating cholangiocytes (Table 1). After pretreatments with heat (microwave in citrate buffer for 20 minutes), trypsin (0.1% trypsin in phosphate buffered saline (PBS) for 30 minutes at 37°C) or proteinase K (10 μg/ml proteinase K in PBS for 15 minutes) as shown in Table 1, tissue sections were treated with 3% H_2O_2 in PBS to quench endogenous peroxidase, and then with 5% skimmed milk in PBS to inhibit nonspecific reactions. The sections were incubated with each primary antibody overnight at 4ºC, followed by reaction with the secondary antibody (Histofine Simple Stain MAX-PO, Nichirei, Tokyo, Japan). Positive reactions were visualized with 3, 3'-diaminobenzidine (DAB Substrate Kit, Vector Laboratories, Inc., Burlingame Inc., CA, USA). Non-immunized mouse IgG served as a negative control. Sections were counterstained lightly with hematoxylin.

Cells showing a distinct immunopositive reaction for ED1, ED2, OX6 or SRA-E5 were counted in five randomly selected areas (0.2 mm^2) of each rat at the periportal area (including the Glisson's sheath) of the hepatic lobule at a magnification of ×400 using ImageJ software version 1.44 (NIH, Bethesda, MD, USA). Cells positive for vimentin, desmin and α-SMA in the periportal area including the Glisson's sheath was evaluated semi-quantitatively using grades as shown in Table 2.

Immunofluorescence stainings

Double immunofluorescence labeling was carried out using ANIT-induced fresh frozen liver sections obtained on PI day 3. The combinations in the dual immunofluorescence labeling were ED1/OX6, ED2/OX6, desmin/vimentin, α-SMA/vimentin, desmin/α-SMA, CK19/vimentin or CK19/α-SMA. Briefly, after fixation in cold acetone/methanol (1:1) for 10 minutes, the sections were incubated with 10% normal goat serum for 30 minutes. The sections were reacted with the primary antibody overnight at 4ºC, and then with the secondary antibody conjugated with Alexa 488 (Invitrogen, Carlsbad, CA, USA) for 1 hour at room temperature. The sections were incubated with the second primary antibody followed by Cy3 conjugated secondary antibody (Jackson Immunoresearch Laboratories Inc., Baltimore, PA, USA). Alexa fluor™ 488 labeled OX6 (AbD Serotec, Oxford, UK) and Hilyte fluor™ 555 (Dojindo Molecular Technologies, Inc., Tokyo, Japan) labeled anti-vimentin antibodies were used for ED1/OX6 and ED2/OX6, as well as CK19/vimentin combinations, respectively. The sections were covered with Vectashield® mounting medium containing 4' 6 diamidino-2-phenylindole (DAPI) (Vector Laboratories, Inc., Burlingame, CA, USA) for nuclear staining and analyzed by a laser scanning confocal microscope system (C1si, Nikon, Tokyo, Japan). Non-immunized mouse IgG was used as a negative control, and PBS was used as washing solution between steps.

Reverse transcriptase polymerase chain reaction (RT-PCR)

Liver samples were immersed in RNAlater™ (Qiagen GmbH, Hilden, Germany) and stored at −80˚C. The extraction of RNA was carried out by using an SV total RNA isolation system kit® (Promega Corporation, Madison, WI, USA). After the isolation, concentration of RNA was measured on a nanodrop1000™ spectrophotometer (Thermo Scientific, Wilmington, DE, USA) and then reverse transcribed to cDNA with the

superscript II transcriptase system® (Invitrogen, Carlsbad, CA, USA) (Ide et al. 2003) and amplified, in duplicate, with the SYBR® Green Real-time PCR Master Mix (Toyobo Co. Ltd, Osaka, Japan) using the LineGene system (Bioflux, Tokyo, Japan) for each of the specific primers of rat MCP-1, TGF-β1, CSF-1 and ribosomal protein S18 (Rps18; an internal control gene). The PCR conditions for MCP-1 used were initial denaturation at 95ºC for 1 minute followed by 40 cycles of 15 seconds of denaturation at 95ºC, 15 seconds of annealing at 62ºC, and 20 seconds of extension at 72ºC. The same PCR conditions were used for TGF-β1 and CSF-1 except annealing temperatures of 64ºC and 60ºC, respectively. The oligonucleotide sequences used for PCR are shown in Table 3. The PCR products were electrophoresed in 2% agarose gel, and DNA was stained with ethidium bromide on the gel.

Statistical analyses

Obtained data represented mean ± standard deviation (SD), and statistical analysis was performed using the Tukey's test or Student's *t*-test. Significance was accepted at $P < 0.05$.

Results

ANIT-induced hepatic lesions

The body weight was decreased slightly on PI days 1 and 2, in contrast to that on day 0, indicating possible influence of the ANIT injection (Fig. 1). Histopathologically, no significant changes were seen in the livers of control rats (Fig. 2A). In ANIT-injected rats, lesions were seen mainly in the Glisson's sheath and in the adjacent areas. On PI day 1, desquamation of necrotic cholangiocytes of the interlobular bile ducts in the Glisson's sheath was seen, accompanied by edema and infiltration of a small number of neutrophils; sinusoidal dilation containing a few inflammatory cells and degenerating hepatocytes with eosinophilic cytoplasm were observed in the vicinity of the Glisson's sheath (Fig. 2B). On PI day 2, in addition to a few neutrophils, mononuclear cells and spindle-shaped cells began to be seen in the affected Glisson's sheath, having more increased edematous change (Fig. 2C); these mononuclear cells and spindle-shaped cells were regarded as macrophages and myofibroblasts, respectively, as mentioned below. On PI day 3, epithelial cells with hyperchromatic nuclei began to surround the damaged interlobular bile ducts, indicating regeneration of the ducts; neutrophils almost disappeared, although mononuclear cells were still detectable (Fig. 2D). On PI days 5, 7 and 9, the severity of lesions compared to those seen on PI days 1-3 decreased gradually, along with decreased numbers of mononuclear cells, but the spindle-shaped cells became more prominent in the affected lesions, particularly on PI days 5 (Fig. 2E) and 7 (Fig. 2F). By PI day 12 the interlobular ducts were relatively normal and inflammatory changes, including cellular infiltrates and edema, had disappeared, although the fibrotic lesion was still present.

The values of AST on PI days 1 and 2, ALT on PI days 1-3 and ALP on PI days 2 and 3 showed a significant increase (Fig. 3A-C), indicating transient hepatic damage due to the action of ANIT. The T. Bil levels were significantly increased on PI day 1, peaked on PI day 2, and then gradually decreased on PI days 3 to 12; however, values did not return

to control levels until day 12 (Fig. 3D), indicative of persistent cholestasis in ANIT-induced hepatic lesions.

Immunohistochemistry for macrophages

The kinetics of macrophages reacting to ED1, ED2, SRA-E5, and OX6 is shown in Fig. 4. In the liver of controls, some ED1-positive cells were seen in the hepatic lobules and Glisson's sheath (Fig. 5A). Although a small number of ED2-positive cells were also observed in the Glisson's sheath, the positive cells were present mainly along the sinusoids of the hepatic lobule, indicative of Kupffer cells (Fig. 5C). SRA-E5-positive cells were present exclusively along the sinusoids, like ED2-positive Kupffer cells, but no SRA-E5-reacting cells were seen in the Glisson's sheath (Fig. 5E). On the other hand, OX6-positive cells were rarely seen in the hepatic lobules of the controls; the positive cells with spindle-like or dendritic appearances were present only in the Glisson's sheath (Fig. 5G).

The number of ED1-positive cells began to increase significantly as early as PI day 2, reaching a maximum on PI day 3, and thereafter maintained significantly increased numbers up to PI day 9 (Fig. 4A); these ED1-positive cells were round or spindle-shaped in appearance (Fig. 5B). Increased numbers of ED2-positive cells were present only on PI day 3, and the positive cells were round to oval in shape, having abundant cytoplasm (Fig. 5D). The number of SRA-E5-positive cells was significantly increased on PI days 2 to 12, except day on day 3, suggesting a consistent increment in cell numbers (Fig. 4C); the positive cells were more prominent in the sinusoids in the vicinity of the Glisson's sheath, and they exhibited round to fusiform shapes (Fig. 5F). The OX6-positive cell number showed a consistent, significant increase on PI days 2 to 12 (Fig. 4D); the positive cells were large round or stellate in shape, and distributed mainly in the Glisson's sheath (Fig. 5H).

The double immunofluorescence labeling on PI day 3 for OX6 and ED1 (Fig. 6A-C) or ED2 (Fig. 6D-F) revealed that 56 % and 26 % of the OX6-positive macrophages in the Glisson's sheath were reactive for ED1 and ED2, respectively.

Immunohistochemistry for myofibroblasts using cytoskeletal markers such as vimentin, desmin and α-SMA

In the Glisson's sheath of control livers (Fig. 7A, C, E), vascular smooth muscle cells reacted weakly for desmin (Fig. 7C) and strongly for α-SMA (Fig. 7E). However, no mesenchymal cells positive for desmin or α-SMA were apparent. Vimentin-positive cells were sporadically seen in the Glisson's sheath and along the sinusoids (Fig. 7A) in the vicinity of Glisson's sheath; the latter were regarded as HSCs.

In ANIT-injected rats, vimentin-positive cells (Fig. 7B) began to increase on PI day 1 and peaked on PI days 2 and 3 (Table 2). Desmin-positive cells showed the highest number as early as PI day 1 and the increased number persisted until PI day 3 (Table 2). In contrast, α-SMA-positive cells gradually increased from PI days 1 to 9, and slightly decreased onwards (Table 2). Desmin- and α-SMA-positive cells were located around the interlobular bile ducts (Fig. 7D, F), whereas vimentin reactivity was seen not only in spindle cells in the Glisson's sheath but also a few HSCs present along the sinusoids (Fig. 7B). These spindle cells in the Glisson's sheath showed co-expression of vimentin, desmin and α-SMA in the double immunofluorescence labeling on PI day 3 (Fig. 8A-I). Interestingly, regenerating cholangiocytes were also reactive for vimentin (Fig. 7B).

Immunohistochemistry for cholangiocytes

Anti-CK19 antibody is useful for the detection of cholangiocytes (Chapter 1). The CK19 reactivity of injured cholangiocytes on PI days 1 to 3 was decreased or lost (Fig. 9A-

C), and on PI days 5 to 12, it gradually increased with reconstitution of bile ducts (Fig. 9D). In addition, vimentin immunoreactivity was seen in regenerating cholangiocytes (Fig. 7B), as mentioned above. To confirm the findings, double immunofluorescence staining for CK19 and vimentin was conducted using liver samples on PI days 2 and 3, and co-expression of these markers was confirmed in regenerating cholangiocytes (Fig. 10A-C). Vimentin expression was seen at the basal surface of the cholangiocytes. Double immunofluorescence staining for CK19 and α-SMA revealed no co-localization (Fig. 10D-F).

The BrdU-immunohistochemistry demonstrated that injured cholangiocytes started to proliferate on PI day 2 and continued until PI day 7 (Fig. 11) with a peak on PI day 3 (Table 2).

Expression of mRNAs

Consistent with the increased number of macrophages, MCP-1 mRNA was increased significantly on PI days 1 and 2; on subsequent days (PI days 3 to 12), MCP-1 expression returned to control levels (Fig. 12A). The expression of TGF-β1 mRNA was significantly increased only on PI day 9 (Fig. 12B). CSF-1 mRNA did not show any significant change (Fig. 12C).

Discussion

ANIT-induced hepatic lesions

ANIT-induced hepatic lesions were characterized by bile duct epithelial cell necrosis/desquamation and infiltration of inflammatory cells in the Glisson's sheath, as well as degeneration of hepatocytes in the vicinity of the Glisson's sheath. These histopathological changes are consistent with those reported previously (Kossor et al. 1993). Additionally, hepatic injury due to ANIT injection was indicated by markedly increased levels of AST, ALT, ALP and T. Bil at early stage. The mechanism behind ANIT-induced liver injury has not yet been fully characterized. However, it has been suggested by others that, after direct injury of cholangiocytes by ANIT excreted in bile, inflammatory cells in the Glisson's sheath produce oxidative factors (oxidants), resulting in hepatocyte injury (Dietrich et al. 2001, Kodali et al. 2006).

In the present study, cholangiocytes began to regenerate on PI days 2 and 3, demonstrable by the BrdU immunohistochemistry. Following regeneration, CK19-positive cholangiocytes were noted around the injured bile ducts, indicating remodeling of the bile duct. Although vimentin is generally specific for mesenchymal cells (Azumi and Battifora 1987, Sappino et al. 1990), the double immunofluorescence staining showed that CK19-positive regenerating cholangiocytes also reacted to vimentin. Interestingly, vimentin expression was characteristically seen at the basal cytoplasm adjacent to the basement membrane. Vimentin expression in regenerating cholangiocytes indicated reconstitution of cholangiocytes in the bile duct system (Milani et al. 1989). In the present ANIT-induced lesions, it is interesting to note that biliary fibrosis began to develop on PI day 2 and, on subsequent days, the fibrosis advanced gradually with increased numbers of myofibroblasts. The finding that T. Bil level did not return to control levels until PI day 12 is consistent with cholestasis due to the biliary fibrosis observed.

Macrophages

Some investigators have suggested that neutrophils play important roles in the pathogenesis of ANIT-induced hepatic lesions (Dietrich et al. 2001). In the present study, neutrophils were temporarily seen only on day 1. In contrast, macrophages appeared as the major cell component from day 2 onwards. To the author's knowledge, this is the first report of macrophage appearance using different macrophage-specific antibodies in ANIT-induced hepatic lesions.

Macrophages can be divided into three categories: blood monocyte-derived exudative macrophages, resident macrophages (Kupffer cells) and antigen-presenting dendritic cells. They differ in ontogeny, morphology, immunophenotype, tissue distribution and function; the immunophenotypes and functions may be changed depending on microenvironmental conditions (Takahashi et al. 1996, Yamate et al. 2000). In this study, the author used four different antibodies (ED1, ED2, OX6, and SRA-E5) to detect the appearance and distribution of macrophages.

ED1 antibody recognizes CD68, which is located on lysosomes, especially phagosomes of blood monocyte-derived infiltrating macrophages and resident macrophages. Expression implies enhanced phagocytosis (Damoiseaux et al. 1994, Suda et al. 1998). In the present study, the number of ED1-positive cells increased as early as PI day 2 and the level was maintained until PI day 9. ED1-positive cells are likely to have phagocytic activity for cell debris after ANIT-induced tissue injury. ED2 labels resident macrophages (Kupffer cells) in normal livers (Golbar et al. 2012). Recently, it has been reported that CD163, the antigen recognized by ED2, functions as a scavenger receptor for hemoglobin-haptoglobin complexes, that the presence of CD163 in lesions reflects the production of inflammatory mediators such as IL-6 and TNF-α (Polfliet et al. 2006). The ED2-positive cell number was transiently increased on PI day 3, which could be attributable to the production of such inflammatory factors during ANIT-induced lesion development.

The SRA-E5 antibody was generated by immunizing scavenger receptor knockout mice with recombinant human type I scavenger receptor protein (CD204) (Tomokiyo et al. 2002). CD204 expression is related to lipid metabolism in macrophages via the scavenger receptor (Greaves et al. 1998). The SRA-E5-positive cell number showed a consistent increase on PI days 2 to 12. The consistent increase in numbers of SRA-E5-positive cells suggests that abnormal metabolism of lipid may be occurring in the affected liver due to ANIT injection.

Interestingly, compared with SRA-E5-positive cells, which were observed exclusively along the sinusoids, the distribution of OX6-positive macrophages was limited to the affected Glisson's sheath, suggesting differences in the properties of SRA-E5- and OX6-positive cells. The increased number of OX6-positive cells was consistently seen on PI days 2 to 12, in general agreement with the kinetics of SRA-E5- and ED1-positive cells (Fig. 4A, C, D). The MHC class II molecule recognized by OX6 is expressed in activated macrophages and dendritic cells (Zhang et al. 1993, Yamashiro et al. 1994, Ide et al. 2005, Zhao et al. 2006). Dendritic cells are major antigen-presenting cells, consisting of the interstitial dendritic cells, interdigitating follicular cells of the spleen and lymph nodes, and Langerhans cells of the epidermis (Gao et al. 2007, Zimmerli and Hauser 2007). Interstitial dendritic cells are widely distributed in connective tissues, including the Glisson's sheath (Takahashi et al. 1996). Intriguingly, the present double immunofluorescence labeling demonstrated that 56% of the OX6-positive cells also reacted to ED1, suggesting that macrophages, which phagocytose cell debris, might also express MHC class II in ANIT-induced lesions. MHC class II expression is related to subsequent induction of CD4+ T cells (Perrigoue et al. 2009). Although the reason why the OX6-positive cells showed a consistent increase remains to be investigated, the positive cells could potentially play vital roles in regeneration of injured cholangiocytes or development of biliary fibrosis in ANIT-induced rat liver lesions.

MCP-1 is a member of the C-C chemokine family and acts as a monocyte/macrophage chemotactic agent in injured tissues (Schecter et al. 1997, Marra et

al. 1998, Sakai et al. 2006). In the present study, MCP-1 mRNA was increased significantly on PI days 1 and 2 in ANIT-injected rat livers, suggesting that a transient increase of MCP-1 at early stage might mediate macrophage infiltration into injured areas. Besides chemotaxis, MCP-1 has important roles in fibrogenesis (Gharaee-Kermani et al. 1996, Tsuruta et al. 2004, Sakai et al. 2006). The role of MCP-1 in fibrogenesis is evident by the *in vitro* finding that human peripheral CD14-positive monocytes showed enhanced TGF-β1 mRNA expression when MCP-1 was added (Sakai et al. 2006). TGF-β1 is a well-known fibrogenic factor produced mainly by macrophages in injured livers (Zhang et al. 2004, Guo et al. 2006). It has also been reported that MCP-1-added to a rat macrophage cell line *in vitro* enhanced expression of CD68 (ED1) and CD163 (ED2) molecules (Mori et al. 2009). Therefore, the increased mRNA level of MCP-1 at the early stage could have enhanced macrophage immunophenotypes and mediated subsequent biliary fibrosis, although increased TGF-β1 mRNA was seen only on PI day 9 which might be related to the late stage of biliary fibrosis.

Mesenchymal cells in Glisson's sheath

Fibrogenesis is evoked by the development of myofibroblasts capable of producing collagens (Abdel-Aziz et al. 1991). The myofibroblasts are mesenchymal cells expressing vimentin; in addition to vimentin, they can express various cytoskeletal proteins (desmin and α-SMA) under fibrogenic factor stimuli (Yamate et al. 2005). After injury of cholangiocytes, vimentin- and desmin-positive cells were increased on days 1 to 3 in the Glisson's sheath; thereafter, expression was gradually decreased, whereas α-SMA-positive cells appeared instead, showing the greatest expression on days 5 to 9. Although the double immunofluorescence labeling revealed that there were myofibroblasts co-expressing vimentin/desmin, desmin/α-SMA or vimentin/α-SMA, it was shown that immunophenotypes of myofibroblasts were changed depending on stages of the lesions in the Glisson's sheath; vimentin and desmin expression were enhanced at the early stage,

whereas α-SMA expression was seen at the mid and late stages. Particularly, the appearance of α-SMA-expressing cells appeared to be related to the development of progressing biliary fibrosis. Myofibroblasts expressing α-SMA have been considered to be most active for collagen production (Wynn 2008). The derivation of myofibroblasts in biliary fibrosis has not been clarified. The vimentin-positive cells co-expressing desmin or α-SMA were located around the regenerating bile ducts at the early stage and, subsequently, α-SMA-positive cells expanded throughout the Glisson's sheath at the late stage. The pre-existing mesenchymal cells around the bile ducts might differentiate into myofibroblasts leading to the biliary fibrosis. After hepatocyte injury, HSCs can differentiate into myofibroblasts (Li and Friedman 1999, Friedman 2003). HSCs present in the vicinity of the Glisson's sheath might represent another possible precursor of the myofibroblasts in biliary fibrosis, because HSCs can express desmin (Asahina et al. 2009).

In conclusion, the present study demonstrates, for the first time, that macrophages positive for ED1, ED2, SRA-E5, and OX6 appear in ANIT-induced hepatic lesions, showing different distribution and kinetics. Based on the immunophenotypes, these macrophages might have functions such as phagocytic activity, inflammatory factor production, lipid metabolism, and antigen-presentation. In addition, the participation of myofibroblasts variously expressing mesenchymal cytoskeletal markers was confirmed in the injured Glisson's sheath; the cells expressed vimentin and desmin at the early stages, and α-SMA at the mid and late stages. Collectively, it is likely that interaction between macrophages and myofibroblasts is important in the progressive biliary fibrosis after cholangiocyte injury due to ANIT injection. The mechanisms of cholangiopathies are very complicated. ANIT-induced hepatic lesions and subsequent biliary fibrosis would be beneficial to investigate the molecular mechanisms. Additionally, the immunohistochemical analyses used in the present study might be useful when hepatotoxicant-induced hepatic lesions are evaluated pathologically.

Summary

To investigate pathogenesis of post-bile duct injury fibrosis, interlobular bile duct epithelial cell injury was induced in male F344 rats by a single IP injection of α-naphthylisothiocyanate (75 mg/kg body weight) and rats were observed for 12 days. On days 1-2, cholangiocytes were injured and desquamated. On days 3-5, the affected bile ducts began to regenerate, showing positive staining for CK19 and vimentin. On days 5-9, fibrotic areas gradually developed around regenerating bile ducts in the Glisson's sheath. These consisted of cells positive for vimentin, desmin and α-SMA; vimentin- and desmin-positive cells were increased in the early stage (days 1-3), whereas α-SMA-positive cells appeared in the mid (days 4-7) and late stages (days 8-12), although there were cells co-expressing these cytoskeletons. On day 12, bile duct regeneration almost completed, with reduced fibrosis. Macrophages positive for ED2 (CD163) increased transiently in the early stage, whereas those reacting to ED1 (CD68), OX6 (MHC class II) and SRA-E5 (CD204) showed a consistent increase throughout experiment. Interestingly, OX6-positive cells were limited to the Glisson's sheath, whereas SRA-E5-positive cells were seen exclusively along the sinusoids of hepatic lobules. MCP-1 mRNA increased significantly in the early stage. This study shows that macrophages exhibiting different immunophenotypes and distributions participate in post-bile duct injury fibrosis associated with myofibroblasts expressing various mesenchymal cytoskeletons.

Table 1. Primary antibodies used for the immunohistochemistry and immunofluorescence staining

Antibody	Dilution	Pretreatment	Source
Anti-ED1	1:100	Proteinase K	Millipore, Billerica, MA, USA
Anti-ED2	1:100	Proteinase K	Serotec, Oxford, UK
Anti-OX6	1:100	Proteinase K	Serotec
Anti-SRA-E5	1:100	Microwave	TransGenic Inc, Kumamoto, Japan
Anti-Vimentin	1:400	Microwave	DakoCytomation, Glostrup, Denmark
Anti-Desmin	1:200	Microwave	Dako
Anti-α-SMA	1:100	Proteinase K	Dako
Anti-CK19	1:100	Trypsin	Novocastra Laboratories Ltd, Newcastle, UK
Anti-BrdU	1: 100	4N HCl and 0.1% Trypsin	Dako

ED1 for CD68, ED2 for CD163, OX6 for MHC class II, SRA-E5 for CD204.

α-SMA: α-smooth muscle actin, **CK 19**: cytokeratin19, **BrdU**: 5-bromo-2′-deoxyuridine.

Table 2. Semi-quantitative analyses of mesenchymal cells and cholangiocytes in the Glisson's sheath

Post injection		Mesenchymal cells			Cholangiocytes		
	(PI) day	Vimentin	Desmin	α-SMA	CK19	Vimentin	BrdU
Control (0)		+	−	−	++	−	−
Early stage	1	++	+ ++	+	+ ~ ++	+	−
	2	+++	+++	++	+	+++	++
	3	+++	+++	++	± ~ +	+++	+++
Mid stage	5	++	++	+++	+ ~ ++	++ ~ +++	+
	7	++	+	+++	++ ~ +++	++	+
Late stage	9	+	±	++ ~ +++	+++	+	−
	12	+	−	+	+++	± ~ +	−

α-SMA: α-smooth muscle actin, **CK19**: cytokeratin19, **BrdU**: 5-bromo-2′-deoxyuridine. Desmin and α-SMA-positive vascular smooth muscle cells were excluded for the evaluation.

Semi-quantitative grades: For vimentin, desmin, α-SMA and BrdU : –; no positive cells, ±; occasional positive cells, +; a few positive cells, ++; moderate number of positive cells, +++; many positive cells. For CK19 : ±; faintly stained, +; lightly stained, ++; moderately stained, +++; intensely stained.

Table 3. Oligonucleotide sequences of primers used in the real-time PCR

Gene	Primers	Oligonucleotide sequences	Size of amplicon (bp)
MCP-1	Sense	5’-GCTTCTGGGCCTGTTGTTC-3’	156
	Anti-sense	5’-CTGCTGCTGGTGATTCTCTTGT-3’	
TGF-β1	Sense	5’-CTTCAGCTCCACAGAGAAGAACTGC- 3’	298
	Anti-sense	5’-CACGATCATGTTGGACAACTGCTCC- 3’	
CSF-1	Sense	5’-ACAGGTGGAACTGCCAGTGTAGAA-3’	89
	Anti-sense	5’-GGTGGACGTTGCCATAATGTCTC-3’	
Rps18	Sense	5’-AAGTTTCAGCACATCCTGCGAGTA-3’	140
	Anti-sense	5’-TTGGTGAGGTCAATGTCTGCTTTC-3’	

MCP-1: monocyte chemoattractant protein-1, **TGF-β1**: transforming growthfactor-β1, **CSF-1**: colony stimulating factor-1, **Rps18**: ribosomal protein s18.

Figure Legends

Fig. 1. Body weight changes in rats on days 0 (control), 1, 2, 3, 5, 7, 9, and 12 following a single injection of α-naphthylisothiocyanate (ANIT). **Cont**: control.

Fig. 2. Histopathology in control (A) and ANIT-injected (B-F) rats. The Glisson's sheath in control consists of interlobular arteriole (IA), interlobular vein (IV) and interlobular bile ducts (IBs), as well as fibroblastic cells (A). In ANIT-injected rats, desquamation of IB epithelial cells, edema, and infiltration of a small number of neutrophils (arrows) are seen in the affected Glisson's sheath on post-injection (PI) day 1 (B); on PI day 2, regenerating cholangiocytes in IBs, edema and infiltration of mononuclear cells are observed (arrows) (C); almost regenerated IBs, less edema and infiltrating mononuclear cells (arrows) are seen on PI day 3 (D). In the affected Glisson's sheath, on PI day 5 a greater number of mononuclear cells are present (E), and on PI day 7 (F), spindle-shaped fibroblastic cells (arrows) are developed around the IB, indicating biliary fibrosis. HE.

Fig. 3. Blood biochemical analyses in control and in ANIT-injected rats (PI days 1-12). Aspartate transaminase (AST) (A), alanine transaminase (ALT) (B), alkaline phosphatase (ALP) (C) and total bilirubin (T. Bil) (D). **Cont**: control. Student's *t*-test. *; $P< 0.05$, significantly different from controls.

Fig. 4. The kinetics of macrophages in the Glisson's sheath and hepatic lobule around the Glisson's sheath in livers of control and ANIT-injected (PI days 1-12) rats. The number of macrophages positive for ED1 (for CD68) significantly increases on PI days 2-9 (A), and that for ED2 (for CD163) increases transiently on PI day 3 (B). The macrophage number for SRA-E5 (for CD204) (C) and OX6 (for MHC class II) (D) shows a consistent increase on PI days 2-12 (except on PI day 3 for SRA-E5). Tukey's test. *; $P<0.05$, significantly different from controls.

Fig. 5. Distribution of macrophages in the Glisson's sheath and the surrounding hepatic lobule of control (A, C, E, G) and ANIT-induced liver lesions on PI day 3 (B, D, F, H). As compared with controls (A, C, E, G), ED1(B)-, ED2(D)-, SRA-E5(F)-, and OX6(H)-positive macrophages show increased numbers in the affected areas. Interestingly, ED2-positive cells in control are along the sinusoids (C), indicating Kupffer cells; increased numbers of ED1(B)- and ED2(D)-positive cells are seen in the affected Glisson's sheath; SRA-E5-positive cells are seen mainly along the sinusoids (F) of hepatic lobule around the Glisson's sheath, whereas the appearance of OX6-positive cells are limited to the Glisson's sheath (H). Arrows indicate positive cells. No signal was observed in negative control sections. **IA**: interlobular arteriole, **IB**: interlobular bile duct, **IV**: interlobular vein. Immunohistochemistry, counterstained with hematoxylin.

Fig. 6. Immunofluorescence staining for OX6 and ED1 or OX6 and ED2 in the Glisson's sheath of ANIT-treated livers on PI day 3. Photomicrographs show macrophages positive for OX6 (green, A and D; arrows) and ED1 (red, B; arrows) or ED2 (red, E; arrows) and the digital merges (yellow, C for OX6 and ED1 or F for OX6 and ED2; arrows). The number of macrophages co-expressing OX6/ED1 (C) is greater than those of OX6/ED2 (F). No signal was observed in negative control sections. **IV**: interlobular vein. Immunofluorescence, DAPI for nuclear staining.

Fig. 7. Mesenchymal cells reacting to vimentin (A, B), desmin (C, D) and α-smooth muscle actin (α-SMA) (E, F) in the Glisson's sheath in control (A, C, E) and in ANIT-induced liver lesions on PI day 3 (B, D, F). In control livers, a few vimentin positive cells are distributed in the hepatic parenchyma (A, arrows). In ANIT-induced livers, vimentin-positive mesenchymal cells in the hepatic lobule and affected Glisson's sheath are seen (B, arrows); desmin (D, arrows)- and α-SMA (F, arrows)-positive mesenchymal cells are present mainly around regenerating bile ducts in the affected Glisson's sheath. Note that regenerating cholangiocytes

rimming the interlobular bile ducts react to vimentin (B, arrowheads). No signal was observed in negative control sections. **IA**: interlobular arteriole, **IB**: interlobular bile duct, **IV**: interlobular vein. Immunohistochemistry, counterstained with hematoxylin.

Fig. 8. Immunofluorescence staining for vimentin-, desmin-, and α-SMA-positive myofibroblasts in the Glisson's sheath of ANIT-treated livers on PI day 3. There are myofibroblasts showing immunofluorescence labeling for desmin (A, green; arrows) and vimentin (B, red; arrows), and co-expressing desmin and vimentin (C, digital merge, yellow; arrows); those for α-SMA (D, green; arrows) and vimentin (E, red; arrows), and co-expressing α-SMA and vimentin (F, digital merge, yellow; arrows); those for α-SMA (G, green; arrows) and desmin (H, red; arrows), and co-expressing α-SMA and desmin (I, digital merge, yellow; arrows). No signal was observed in negative control sections. **IV**: interlobular vein. Immunofluorescence, DAPI for nuclear staining.

Fig. 9. Immunohistochemistry for cholangiocytes in the Glisson's sheath in control (A) and in ANIT-induced livers (B-D). Cholangiocytes in the interlobular bile ducts (IBs) are strongly reactive for cytokeratin (CK) 19 in control liver (A). Loss of IB epithelial cells (arrows) with edematous change is shown on PI day 1, although cholangiocytes (arrowhead) in some IBs are still reactive for CK19 (B). On the other hand, weak immunoreactivity for CK19 in regenerating cholangiocytes on PI day 3 (C, arrow) and intense immunoreactivity for CK19 in completely regenerated cholangiocytes in IBs on PI day 12 (D, arrow) are seen. No signal was observed in negative control sections. **IV**: interlobular vein. Immunohistochemistry, counterstained with hematoxylin.

Fig. 10. Immunofluorescence staining for CK19, vimentin, and α-SMA in the Glisson's sheath of ANIT-treated livers on PI day 3. There are regenerating cholangiocytes positive for CK19 (A, green; arrow) and vimentin (B, red; arrow), and co-

expressing CK19 and vimentin (C, digital merge, yellow; arrow); insets in B for vimentin and C for co-expression indicate a dotted rectangle (inset) in A for CK19. Although the regenerating cholangiocytes give a positive reaction to CK19 (E, red; arrows), the cells do not react to α-SMA (D, green for α-SMA; F, digital merge for CK19 and α-SMA). No signal was observed in negative control sections. **IV**: interlobular vein. Immunofluorescence, DAPI for nuclear staining.

Fig. 11. Proliferating cells in the affected Glisson's sheath on PI day 2 using the BrdU immunostaining**.** Regenerating cholangiocytes show a positive reaction for BrdU (S-phase in cell cycle) (arrows). Some mesenchymal cells also react to BrdU (arrowheads), indicating proliferating myofibroblasts. No signal was observed in negative control sections. **IV**: interlobular vein. Immunohistochemistry, counterstained with hematoxylin.

Fig. 12. mRNA expressions of monocyte chemoattractant protein-1 (MCP-1) (A), transforming growth factor-β1 (TGF-β1) (B), and colony stimulating factor-1 (CSF-1) in control and ANIT-injected rats on PI days 1-12 by the RT-PCR methods. **Cont**: control. Student's *t*-test. *; $P<0.05$, significantly different from controls.

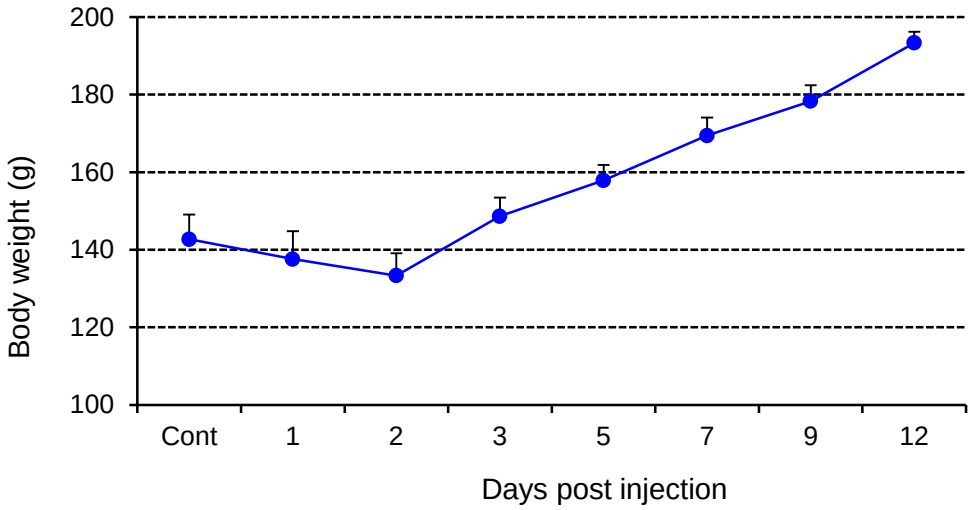
200
180
160
140
120
100
Body weight (g)
Cont
1
2
3
5
7
9
12
Days post injection

Fig. 1

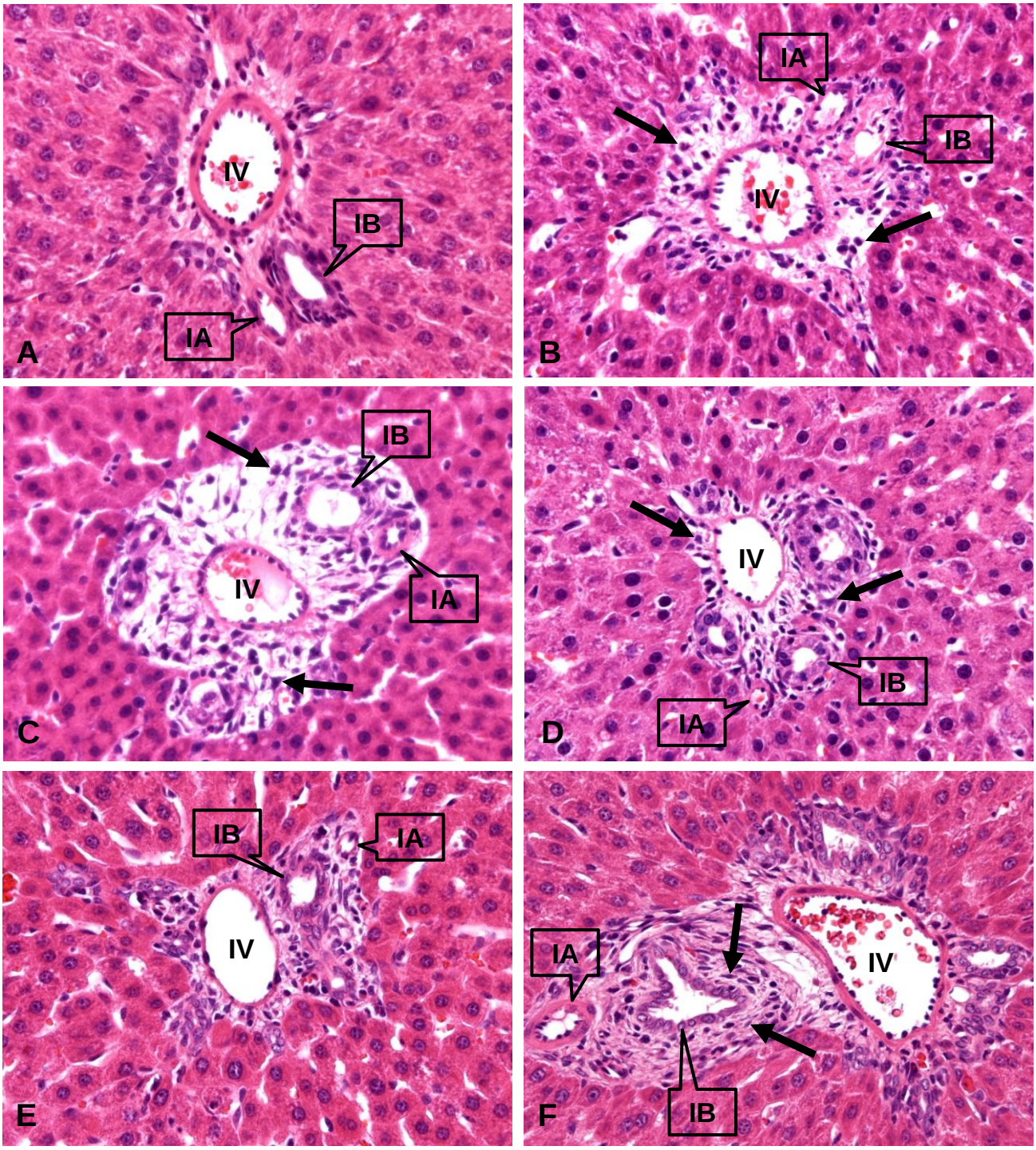

Fig. 2

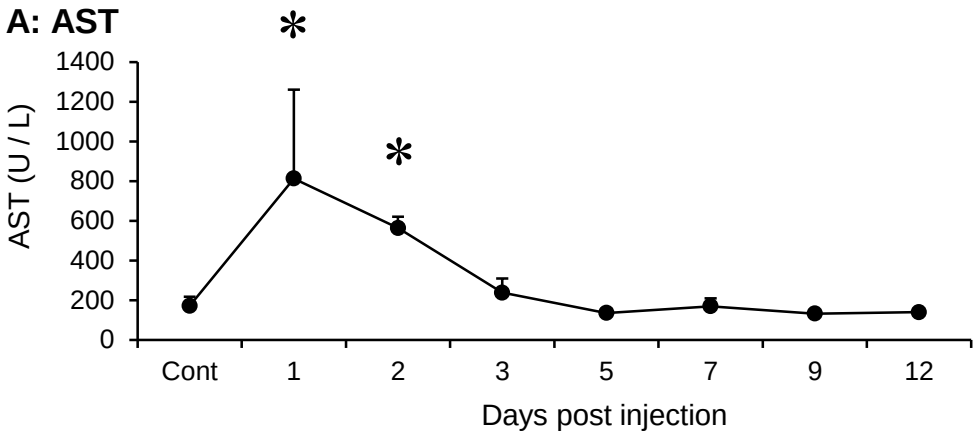
A: AST
AST (U / L)
1400
1200
1000
800
600
400
200
0
Cont
1
2
3
5
7
9
12
Days post injection

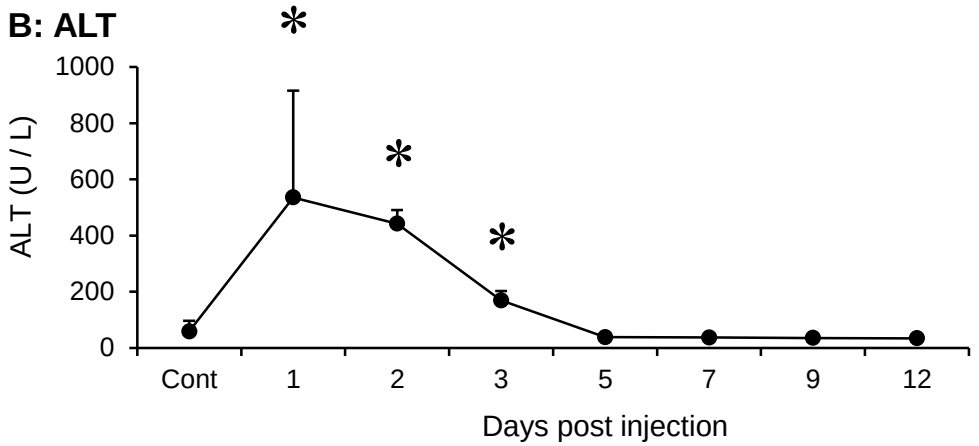
B: ALT
ALT (U / L)
1000
800
600
400
200
0
Cont
1
2
3
5
7
9
12
Days post injection

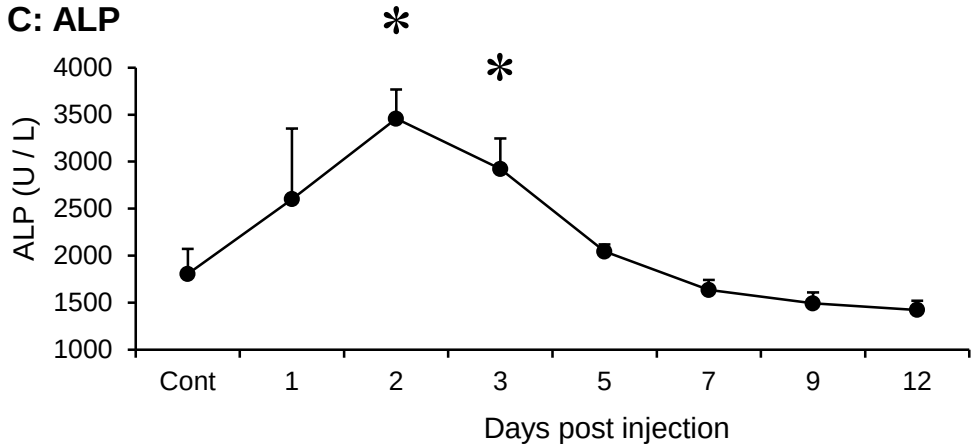
C: ALP
ALP (U / L)
4000
3500
3000
2500
2000
1500
1000
Cont
1
2
3
5
7
9
12
Days post injection

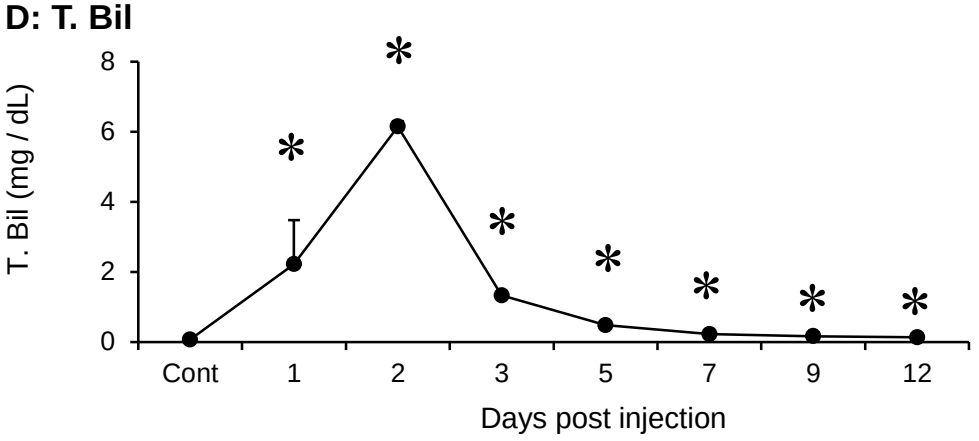
D: T. Bil
T. Bil (mg / dL)
8
6
4
2
0
Cont
1
2
3
5
7
9
12
Days post injection

Fig. 3

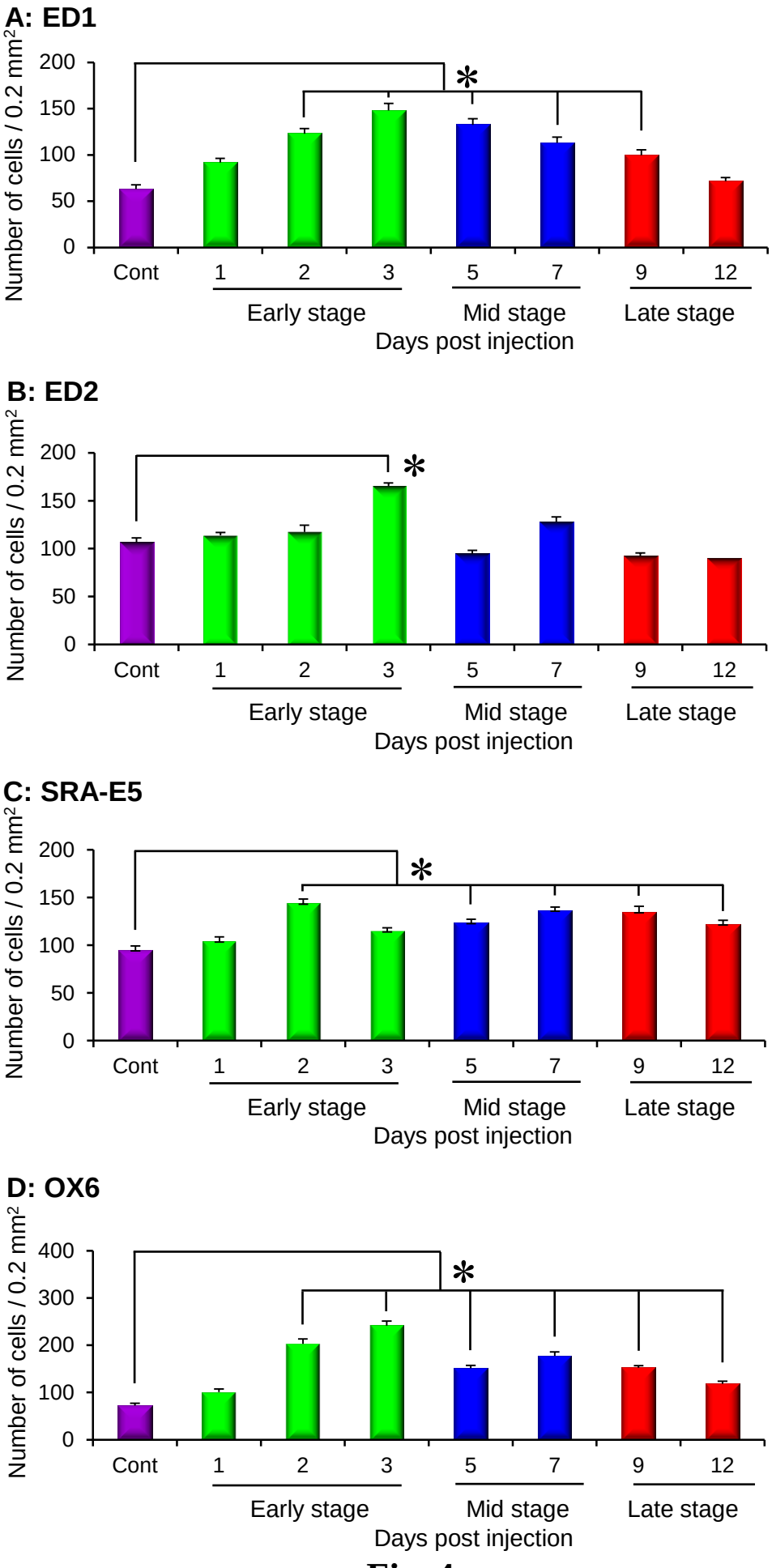
A: ED1
Number of cells / 0.2 mm²
200
150
100
50
0
*
Cont
1
2
3
5
7
9
12
Early stage
Mid stage
Late stage
Days post injection
B: ED2
Number of cells / 0.2 mm²
200
150
100
50
0
*
Cont
1
2
3
5
7
9
12
Early stage
Mid stage
Late stage
Days post injection
C: SRA-E5
Number of cells / 0.2 mm²
200
150
100
50
0
*
Cont
1
2
3
5
7
9
12
Early stage
Mid stage
Late stage
Days post injection
D: OX6
Number of cells / 0.2 mm²
400
300
200
100
0
*
Cont
1
2
3
5
7
9
12
Early stage
Mid stage
Late stage
Days post injection

Fig. 4

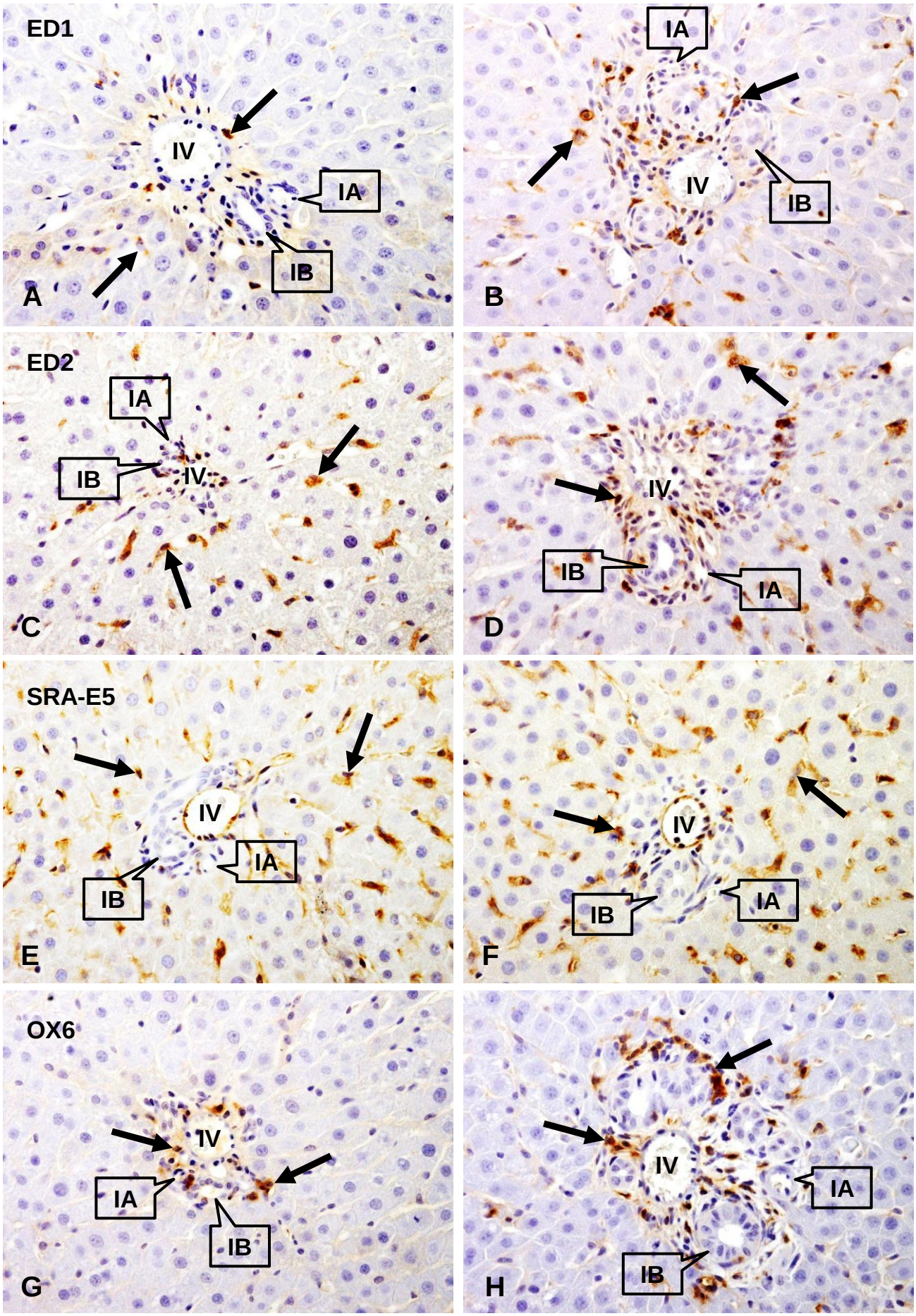
ED1
IV
IA
IB
A
IA
IV
IB
B
ED2
IA
IB
IV
C
IV
IB
IA
D
SRA-E5
IV
IA
IB
E
IV
IB
IA
F
OX6
IV
IA
IB
G
IV
IA
IB
H

Fig. 5

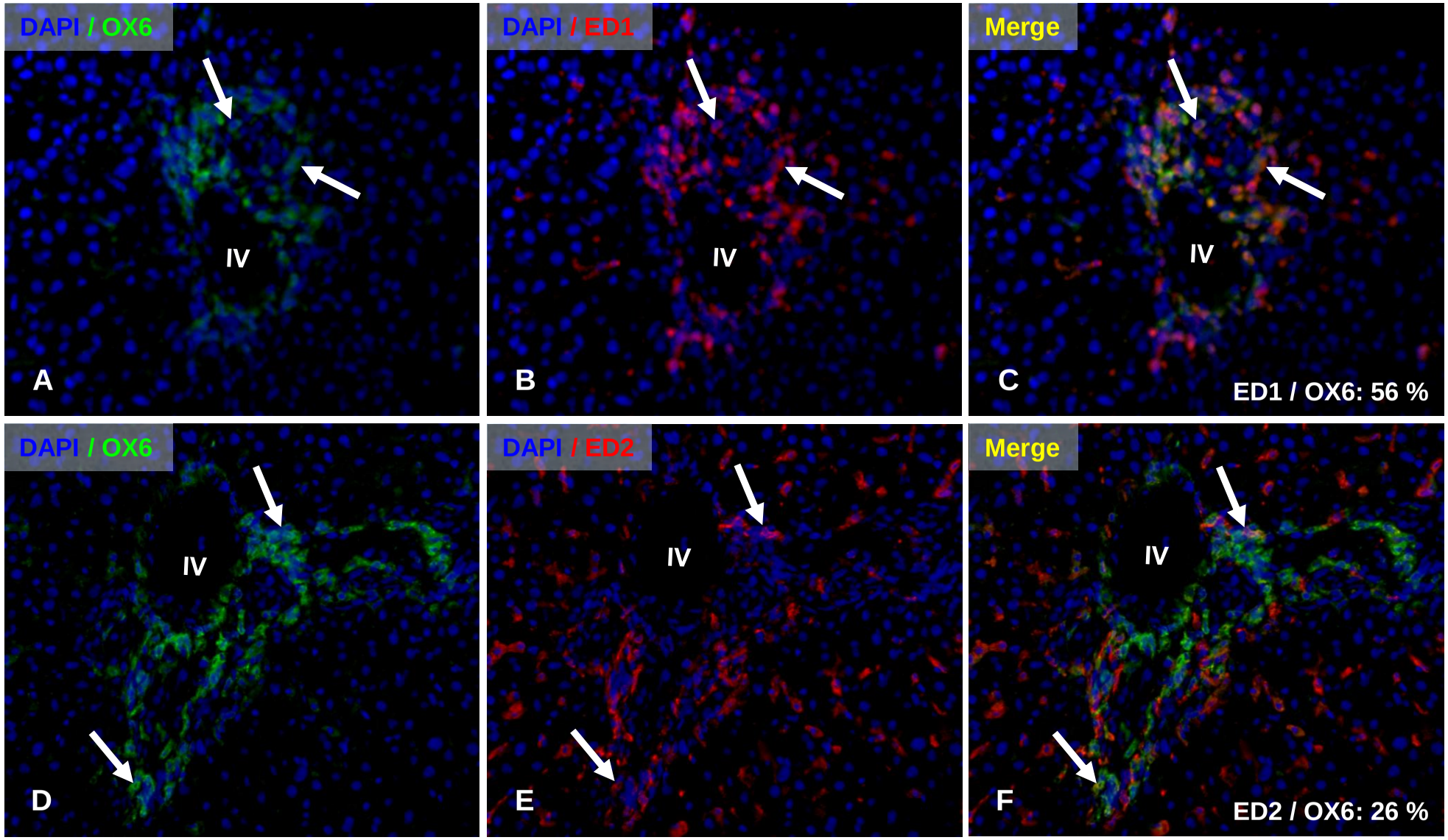
DAPI / OX6
IV
A
DAPI / ED1
IV
B
Merge
IV
C
ED1 / OX6: 56 %
DAPI / OX6
IV
D
DAPI / ED2
IV
E
Merge
IV
F
ED2 / OX6: 26 %

Fig. 6

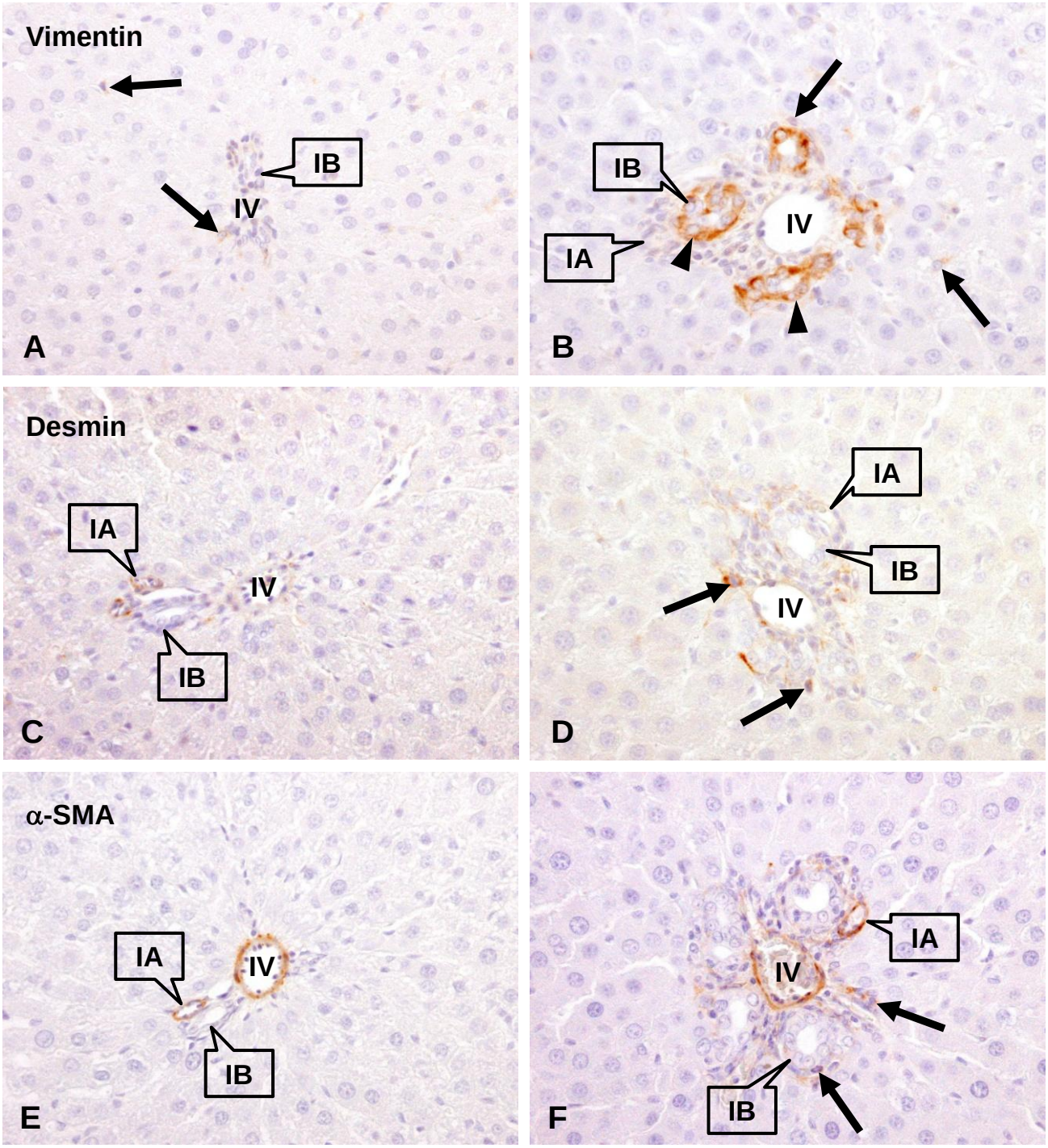
Vimentin
IB
IV
A
IB
IV
IA
B
Desmin
IA
IV
IB
C
IA
IB
IV
D
α-SMA
IA
IV
IB
E
IA
IV
IB
F

Fig. 7

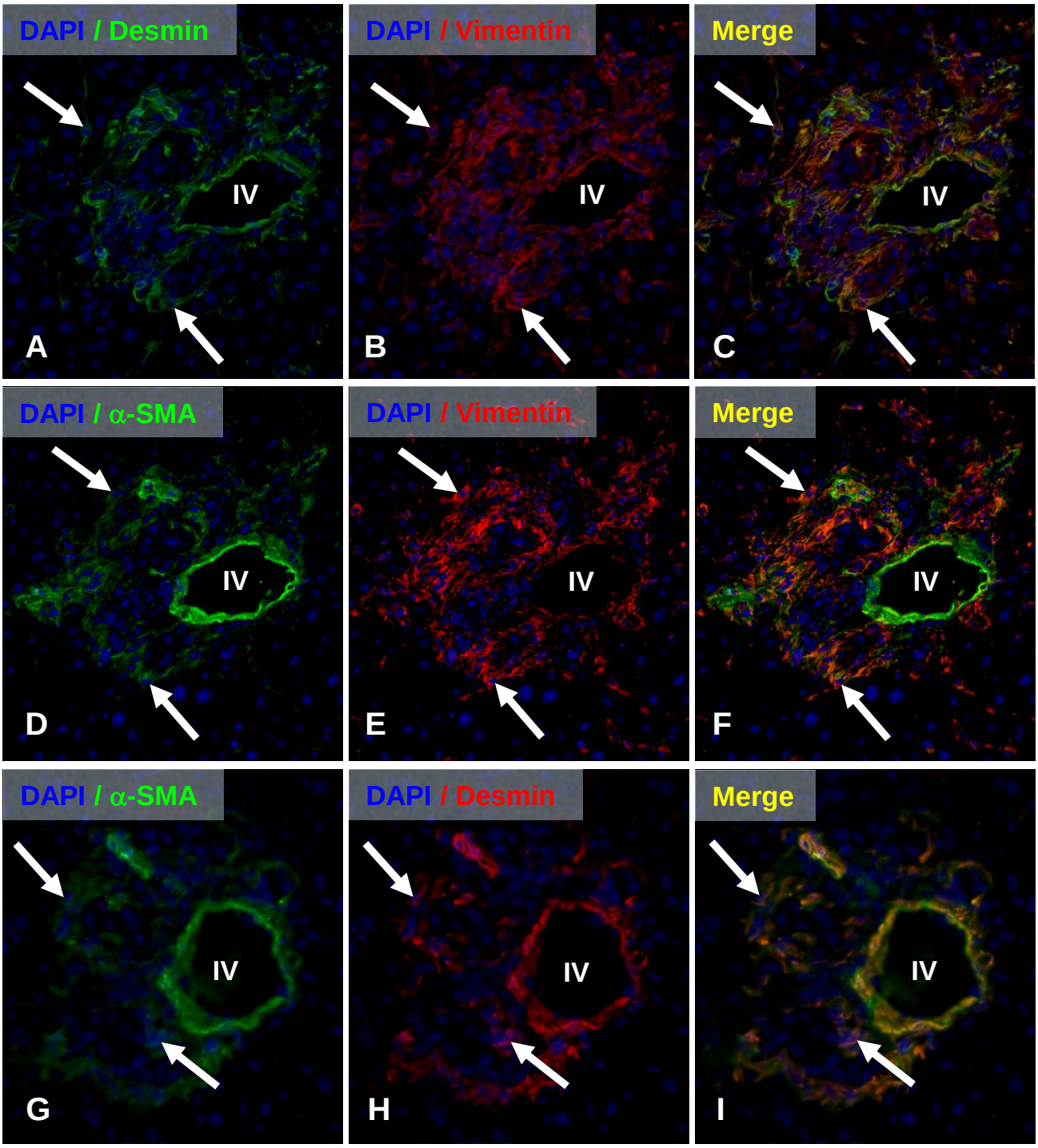
DAPI / Desmin
IV
A
DAPI / Vimentin
IV
B
Merge
IV
C
DAPI / α-SMA
IV
D
DAPI / Vimentin
IV
E
Merge
IV
F
DAPI / α-SMA
IV
G
DAPI / Desmin
IV
H
Merge
IV
I

Fig. 8

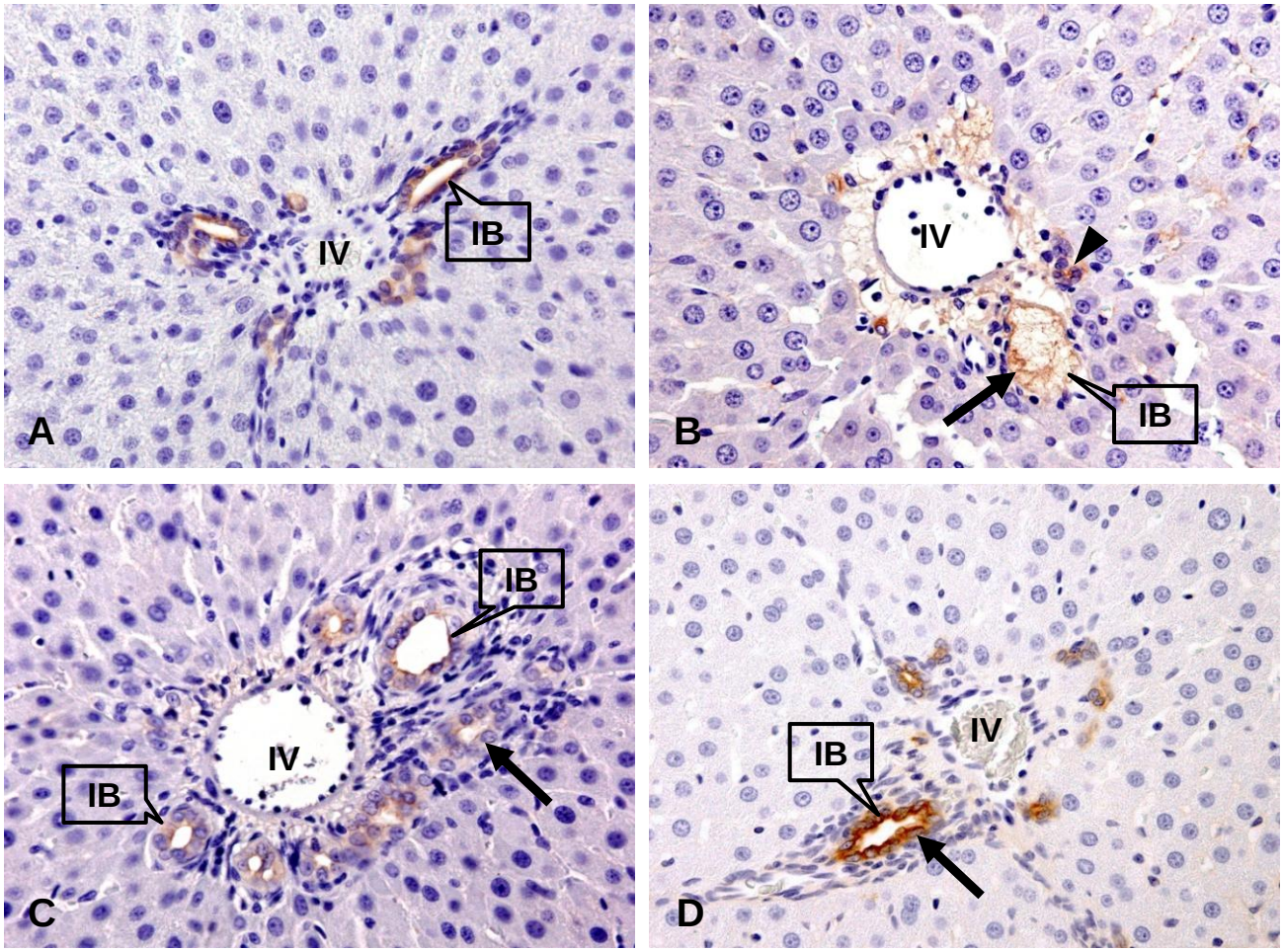

Fig. 9

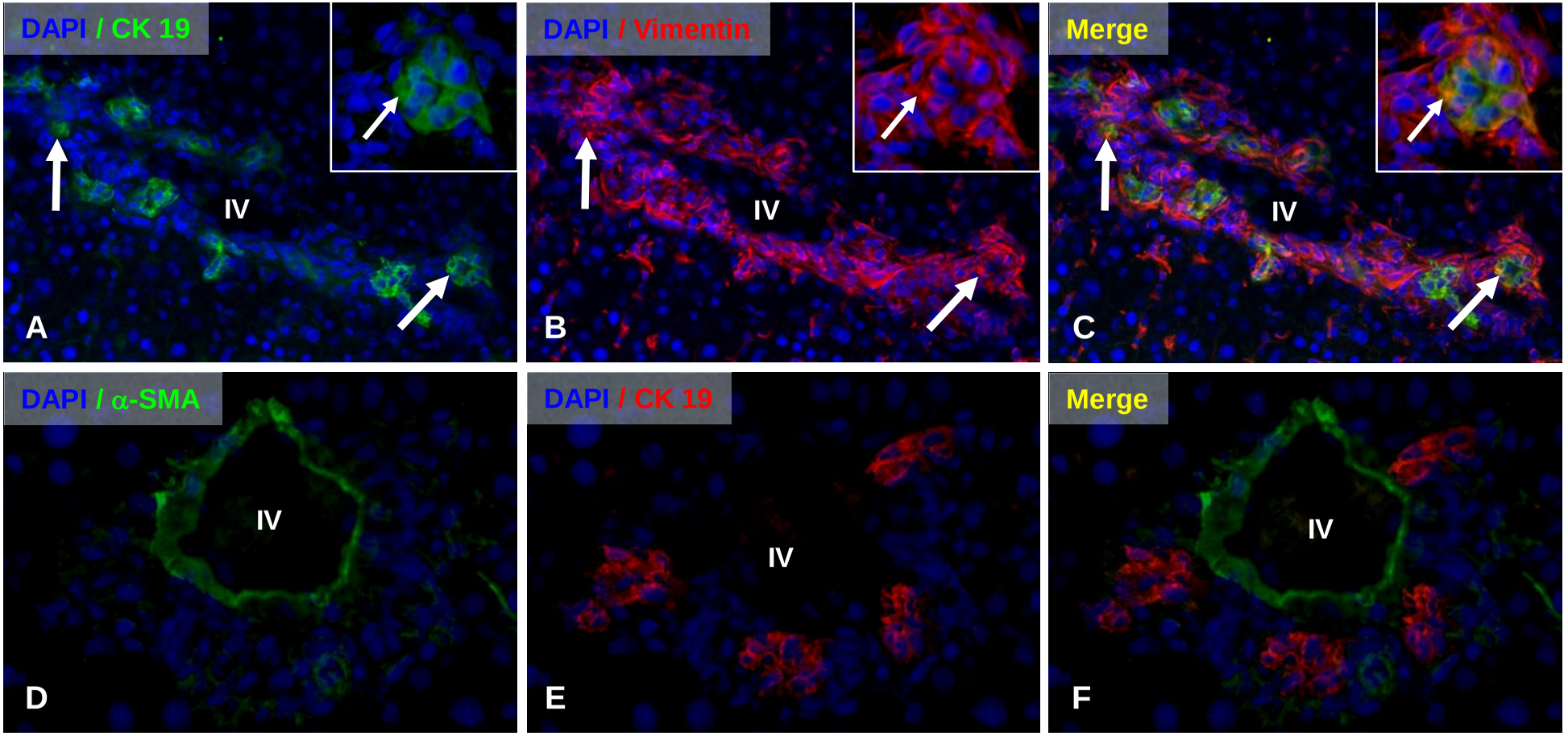
DAPI / CK 19
IV
A
DAPI / Vimentin
IV
B
Merge
IV
C
DAPI / α-SMA
IV
D
DAPI / CK 19
IV
E
Merge
IV
F

Fig. 10

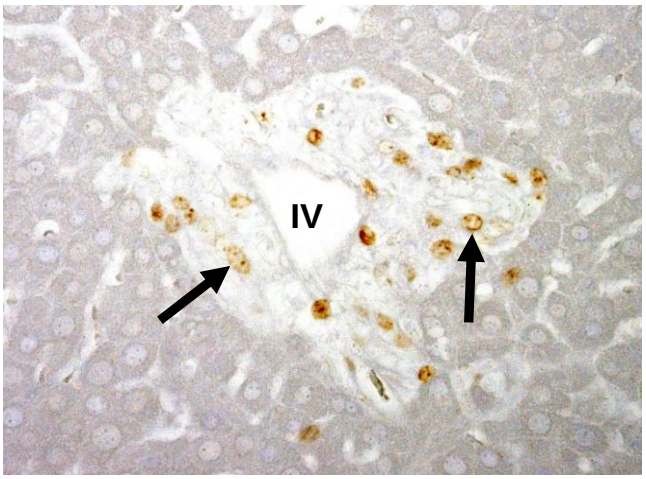

Fig. 11

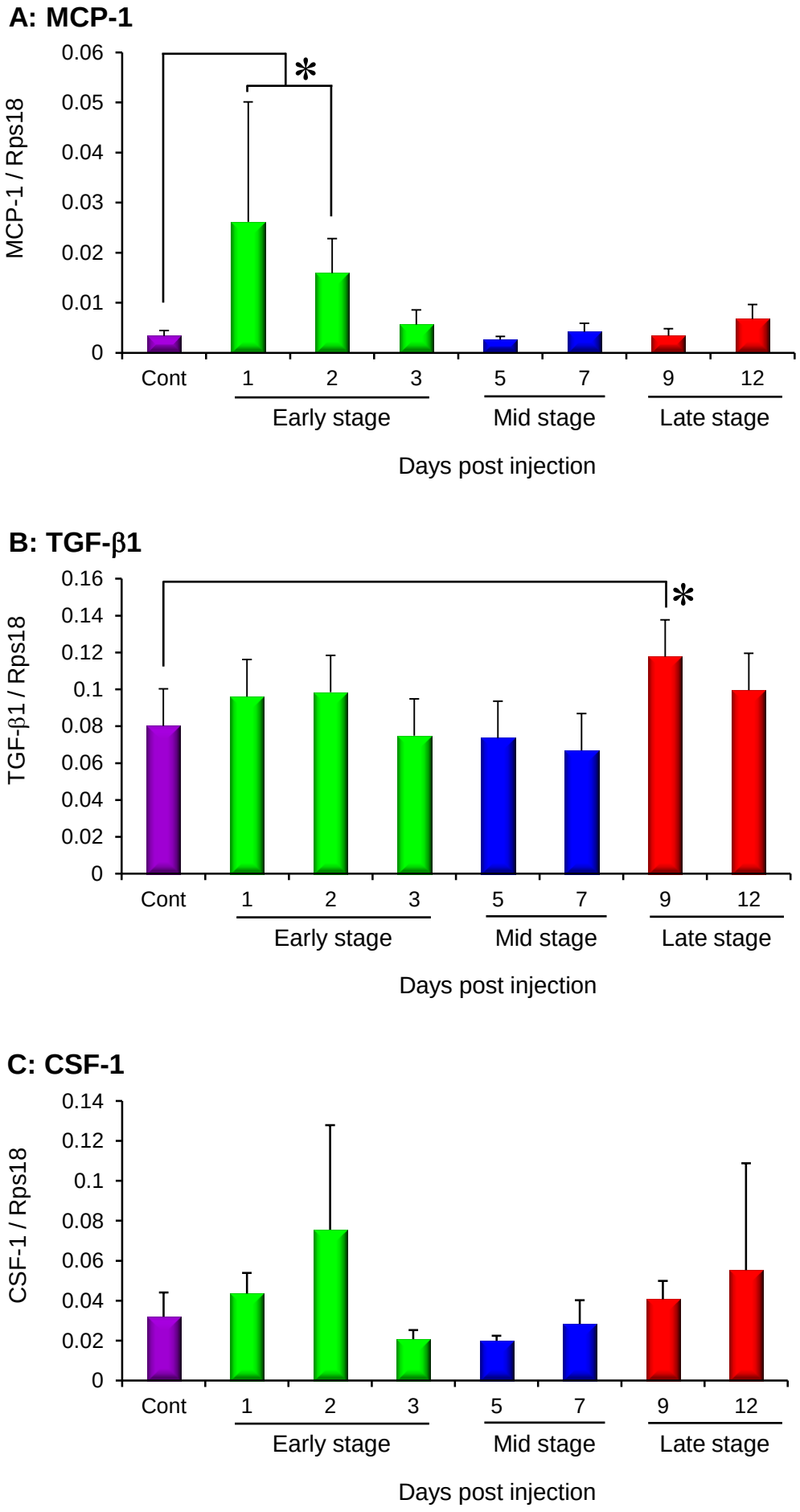
A: MCP-1
MCP-1 / Rps18
0.06
0.05
0.04
0.03
0.02
0.01
0
*
Cont
1
2
3
5
7
9
12
Early stage
Mid stage
Late stage
Days post injection
B: TGF-β1
TGF-β1 / Rps18
0.16
0.14
0.12
0.1
0.08
0.06
0.04
0.02
0
*
Cont
1
2
3
5
7
9
12
Early stage
Mid stage
Late stage
Days post injection
C: CSF-1
CSF-1 / Rps18
0.14
0.12
0.1
0.08
0.06
0.04
0.02
0
Cont
1
2
3
5
7
9
12
Early stage
Mid stage
Late stage
Days post injection

Fig. 12

Section II

Nestin Expression in ANIT-induced Acute Bile Duct Injury Lesions in Rats

Introduction

The enhanced capacity of stem/progenitor cells for proliferation, survival, and motility contributes to tissue homeostasis and injury repair (remodeling) (Kleeberger et al. 2007). Cholangiocytes are lining epithelial cells of interlobular bile ducts in the Glisson's sheath of liver with low replicative ability (LeSage et al. 1996). Minor injury to cholangiocytes is followed by successful regeneration, while repeated and severe injury results in permanent damage leading to ductopenia and peribiliary fibrosis (Omenetti et al. 2009, Golbar et al. 2011). Little is known about reasons why regeneration of cholangiocytes fails to keep pace with injury. Cytoskeletal intermediate filaments are critical and dynamic structural elements that control a variety of cell processes including proliferation, migration, survival and regeneration in patho-biological conditions (Coulombe and Wong 2004). Characterization on the expression dynamics of intermediate filaments may help improve understanding on the underlying mechanisms of cholangiocyte injury pathology, and may provide information on new therapeutic interventions.

Nestin is a class VI intermediate filament protein with a molecular weight 240-kDa. Initially, nestin expression was identified as a marker of neuroepithelial stem cells and progenitor cells in nervous system (Lendahl et al. 1990). Since then, nestin has been demonstrated to be expressed in non-neural progenitors and stem cells of pancreatic islets (Hunziker and Stein 2000, Zulewski et al. 2001, Lechner et al. 2002, Abraham et al. 2004), hematopoietic tissues (Walczak et al. 2004) and hair follicle sheath (Li et al. 2003,

Hoffman 2006). However, the function of nestin and the factors that may regulate its expression are currently unclear (Wiese et al. 2004). Additionally, nestin expression has not yet been investigated in the Glisson's sheath-constituting cells after damage.

This study investigated nestin expressions in α-naphthylisothiocyanate (ANIT)-induced acute cholangiocyte injury lesions in rat livers. This study demonstrates that nestin expression is up-regulated in regenerating cells of the Glisson's sheath-constituting cells such as cholangiocytes, mesenchymal cells, hepatic stellate cells (HSCs) and endothelial cells. Nestin expression may be used as an indicator for regeneration status in hepatotoxicity analyses.

Materials and Methods

Animals and ANIT-induced hepatic lesions

Five-week-old, male F344 rats (100 to 120 g body weight) purchased from Charles River Japan (CRJ, Hino, Shiga, Japan) were used. These animals were housed in an animal room at a controlled temperature of 21 ± 3˚C and with a 12-hour light-dark cycle; they were provided a standard diet for rats (MF, Oriental Yeast Co. Ltd., Tokyo, Japan) and tap water *ad libitum*. After a one week acclimatization period, they were divided into control (three rats) and ANIT injection groups (twenty-one rats). The animals in the ANIT group were given a single intraperitoneal (IP) injection of ANIT at a dose of 75 mg/kg body weight dissolved in olive oil (Calvo et al. 2001). Three rats were euthanized by exsanguination under isoflurane on each of post-injection (PI) days 1, 2, 3, 5, 7, 9 and 12. Control rats received an equal volume of olive oil and were euthanized immediately after the injection (PI day 0).

The animal experiments were conducted in compliance with the institutional guidelines and protocol approved by the ethical committee of Osaka Prefecture University for animal care.

Histopathology and immunohistochemistry

Tissues from the left external lobe of the livers were fixed in 10% neutral buffered formalin and Zamboni's fixative (0.21% picric acid and 2% paraformaldehyde in 130 mM phosphate buffer, pH 7.4). These tissues were dehydrated and embedded in paraffin. Deparaffinized sections, cut at 4 μm in thickness, were stained with hematoxylin and eosin (HE) for histopathology. Sections were also stained immunohistochemically with mouse monoclonal antibodies for cytokeratin (CK) 19 and nestin. The antibody information is presented in Table 1 and the detail staining protocol has been described elsewhere (Golbar

et al. 2011). Briefly, after pretreatment with trypsin (0.1% trypsin in phosphate-buffered saline (PBS), 20 minutes at 37ºC, for CK19) or heat (microwave in citrate buffer, 20 minutes, for nestin), tissue sections were treated with 3% H_2O_2 in PBS to quench endogenous peroxidase, and then with 5% skimmed milk in PBS to inhibit nonspecific reactions. The sections were incubated with the primary antibody overnight at 4ºC, followed by reaction with the secondary antibody (Histofine Simple Stain MAX-PO (M), Nichirei, Tokyo, Japan). Positive reactions were visualized with 3, 3'-diaminobenzidine (DAB Substrate Kit, Vector Laboratories, Inc., Burlingame, CA, USA). Sections stained with mouse N-universal negative control (Dako, Carpinteria, CA, USA) instead of the primary antibody produced no signal and served as control. Sections were counterstained lightly with hematoxylin. Cells showing distinct immunopositive reaction for nestin in the Glisson's sheath and in the vicinity were evaluated semi-quantitatively using grades as shown in Table 2.

Immunofluorescence staining

Double immunofluorescence labeling was carried out using ANIT-induced fresh frozen liver sections obtained on PI day 3. The combinations in the dual immunofluorescence labeling were nestin and CK19, vimentin, desmin, RECA-1, GFAP or α-SMA; vimentin and GFAP; Ki-67 and nestin, CK19, vimentin or desmin. The detail antibody information is given in Table 1. Briefly, after fixation in Zamboni's solution at 4ºC for 10 minutes, the sections were incubated with 10% normal goat serum for 30 minutes. The sections were allowed to react with the primary antibodies overnight at 4ºC and then with Alexa 488 conjugated secondary antibody (Invitrogen, Carlsbad, CA, USA) for 1 hour. The sections were incubated overnight with second primary antibody labeled with Hilyte Flour™ 555 (Dojindo Molecular Technologies, Inc., Tokyo, Japan) or second primary antibody followed by fluoresce conjugated secondary antibody. The sections were covered with SlowFade® Gold mounting medium containing 4' 6 diamidino-2-

phenylindole (DAPI) (Invitrogen, Eugene, OR, USA) for nuclear staining and were analyzed by a laser scanning confocal microscope system (C1si, Nikon, Japan). For control sections, primary antibodies were replaced with mouse/rabbit N-universal negative control (Dako, Carpinteria, CA, USA) and were all negative.

Results

ANIT-induced hepatic lesions

No significant changes were seen in control livers (Fig. 1A). In the ANIT-injected rats, on day 1, cholangiocyte desquamation in the interlobular bile ducts, infiltration of a few inflammatory cells (involving neutrophils) and edema in the Glisson's sheath as well as dilatation of the sinusoids and hepatocyte degeneration in the periportal parenchyma were observed (Fig. 1B). On PI day 2, cholangiocytes started to reappear in the Glisson's sheath to form bile ducts (Fig. 1C), which were almost completed by PI day 3 (Fig. 1D). Replacement of neutrophils by mononuclear cells and appearance of spindloid mesenchymal cells were seen on PI day 2 onwards: these cells were demonstrated as macrophages and myofibroblasts, respectively, by the immunohistochemical staining (section I). On PI day 5 onwards, the interlobular bile ducts were completely recovered and inflammatory changes such as cellular infiltrates and edema gradually disappeared.

Immunohistochemistry for cholangiocytes

In liver, CK19 is selectively expressed in bile duct epithelial cells and serves as a marker for cholangiocytes (Chapter 1). Cholangiocytes in the interlobular bile ducts of control livers were strongly reactive for CK19 (Fig. 2A). On PI day 1 after ANIT injection, CK19-positive cholangiocytes were almost undetectable, indicating complete desquamation by damage of ANIT, although there were some cholangiocytes reacting faintly to CK19 that escaped the necrotizing process (Fig. 2B). Regenerating cholangiocytes, which reappeared to form bile ducts on PI day 2, reacted faintly to CK19 (Fig. 2C). On PI day 3 (Fig. 2D) and subsequent days, the reactivity of cholangiocytes for CK19 gradually increased and recovered to level of controls.

Nestin expressing cells

In control liver sections, a small number of mesenchymal cells (+) and endothelial cells (+) in the Glisson's sheath expressed nestin, but cholangiocytes (-) did not (Table 2, Fig. 3A). A few HSCs in the hepatic parenchyma were reactive for nestin (Fig. 3A). As shown in Table 2, after the ANIT administration, nestin expression was seen in regenerating cholangiocytes, in spindle-shaped mesenchymal cells and endothelial cells mainly in the Glisson's sheath (Fig. 3B-D). The semi-quantitative analyses showed that nestin expression in mesenchymal cells and endothelial cells was seen on PI days 1-7 with a peak (+++) on PI days 3-5 and PI day 3, respectively. HSCs showed increased expression of nestin, the expression pattern being similar to mesenchymal cells in the Glisson's sheath reacting to nestin (Table 2, Fig. 3). Nestin in cholangiocytes began to be seen on PI day 2 and peaked on PI day 3 (+++); thereafter, the reactivity was decreased until PI day 5; on PI day 7 onwards, nestin expression was not seen.

Double immunofluorescence staining for nestin-positive cells

To further confirm the nestin expression in cholangiocytes, mesenchymal cells, endothelial cells and HSCs, the double immunofluorescence staining was performed. The double labeling showed that nestin was co-expressed in CK19-positive cholangiocytes (Fig. 4A-C), vimentin-positive mesenchymal cells (Fig. 4D-F), desmin-positive HSCs (mesenchymal cells) (Fig. 4G-I) and RECA-1-positive endothelial cells (Fig. 4J-L) in the Glisson's sheath and in the nearby hepatic lobules. GFAP-positive HSCs (Fig. 4M-O) and α-SMA-positive myofibroblasts did not express nestin. To confirm the absence of co-expression between nestin and GFAP, the double immunofluorescence staining for vimentin with GFAP was conducted. No co-expression for vimentin and GFAP was found.

Double immunofluorescence staining for Ki-67-positive cells

Ki-67-positive reaction was seen in nestin-positive mesenchymal cells (Fig. 5A-C). Furthermore, some Ki-67-positive cells were observed in CK19-positive cholangiocytes (Fig. 5D-F), vimentin-positive mesenchymal cells (Fig. 5G-I) and desmin-positive HSCs (Fig. 5J-L).

Discussion

ANIT-induced hepatic lesions

In this study, ANIT-induced damage was characterized by cholangiocyte desquamation, inflammatory cell reaction (neutrophils and macrophages) and edema in the Glisson's sheath; after the damage, biliary fibrosis developed moderately, consisting spindle-shaped mesenchymal cells (myofibroblasts). The remodeling of the Glisson's sheath-constituting cells after injury was almost completed until PI day 5. Macrophages and myofibroblasts, which might be related to biliary fibrosis, were characterized by the immunohistochemical staining in section I of the chapter 3. The CK19 immunohistochemical analyses showed that damaged cholangiocytes by desquamation developed no reaction and regenerating cholangiocytes gradually recovered the reaction until levels of controls. Vimentin-positive cells in the Glisson's sheath and desmin-positive cells in the hepatic lobules were regarded as myofibroblasts and HSCs, respectively. In section I, vimentin-positive cells could participate in the biliary fibrosis, and express α-SMA and desmin. At early stages, vimentin- and desmin-positive mesenchymal cells were predominant than α-SMA-positive cells in the affected Glisson's sheath. Therefore, co-expressions for nestin in vimentin- and desmin-positive cells were analyzed in the section II. RECA-1 selectively labeled endothelial cells (Yamanaka et al. 2011).

Nestin expression in cholangiocytes, mesenchymal cells, HSCs and endothelial cells

Although the function of nestin has not been fully determined, intermediate filaments such as nestin are critical as dynamic structural elements whose assembly and disassembly play important roles in influencing and responding to intracellular signaling cascades involved in cell proliferation, migration and survival (Coulombe and Wong 2004). A small number of HSCs and mesenchymal cells in the Glisson's sheath of controls reacted very faintly to nestin, suggesting homeostasis under normal conditions through replication.

Repopulating cholangiocytes after desquamation in the Glisson's sheath formed new bile ducts, expressing nestin; when bile duct formation was almost completed, nestin expression in cholangiocytes disappeared. Because Ki-67-positive proliferating cells were seen in the regenerating cholangiocytes, nestin expression may be related to regeneration or migration of cholangiocytes to form bile ducts.

More interestingly, the present study demonstrated that vimentin- and desmin-positive cells expressed nestin, and some of them reacted to Ki-67. As mentioned above, vimentin- and desmin-positive cells were considered to be mesenchymal cells (myofibroblasts in section I) and HSCs, respectively. Therefore, after injury, mesenchymal cells and HSCs also had capacity to proliferate or migrate, expressing nestin. Nestin is unable to self-assemble, because of very short N-terminus, a domain known to be essential for filament protein assembly (Herrmann and Aebi 2000); hence, nestin forms heterodimer and mixed polymer with other intermediate filaments such as vimentin (Marvin et al. 1998) and desmin (Sjoberg et al. 1994). Co-expressions of nestin with vimentin and desmin might have implied the mutual relationship of these intermediate cytoskeletons. However, nestin-positive cells did not co-express with GFAP, another intermediate filament protein of the category type III including vimentin and desmin. It was reported that HSCs might express GFAP at the neonatal stages or after parenchymal injury (Carotti et al. 2008, Golbar et al. 2012). Although there was a report describing co-expression of nestin and GFAP (Wiese et al. 2004), such findings were not confirmed in the present study of Glisson's sheath damage. α-SMA is expressed in well-differentiated mesenchymal cells (Kim et al. 2009). No mesenchymal cells co-expressing nestin and α-SMA in the affected Glisson's sheath indicated that α-SMA-positive myofibroblasts appear to have already no capacity to regenerate.

Additionally, the present study showed that RECA-1-positive endothelial cells co-expressed nestin. After endothelial injury, endothelial cells can regenerate (Paranthan et al.

2011). Nestin-expressing endothelial cells in the affected Glisson's sheath might be under regeneration.

In summary, this study demonstrated that nestin expression was seen in vimentin-positive mesenchymal cells, desmin-positive HSCs, RECA-1-positive endothelial cells and CK19-positive cholangiocytes in the Glisson's sheath in ANIT-induced hepatotoxicity. Nestin may be related to cell proliferation and migration. Because some of these cells reacted to Ki-67 (a proliferating marker), nestin-expressing cells were considered to be regenerating cells after injury. Therefore, nestin expression would be useful to detect regenerating cells in the damaged Glisson's sheath in hepatotoxicity.

Summary

The functions of nestin, an intermediate filament protein, is poorly understood, but may be related to cellular regeneration. The author investigated nestin expressions in α-naphthylisothiocyanate (ANIT)-induced cholangiocyte injury lesions in the Glisson's sheath in male F344 rats. Liver samples obtained at post-injection (PI) (75 mg/kg, IP) days 0 (control) and 1-12 were immunohistochemically stained for nestin, and nestin double-immunofluorescence was conducted with antibodies for mesenchymal cells (vimentin), hepatic stellate cells (desmin), endothelial cells (rat endothelial cell antigen (RECA)-1), cholangiocytes (cytokeratin (CK) 19), and proliferating cells (Ki-67). Nestin expressions were seen in mesenchymal cells, HSCs, endothelial cells and cholangiocytes in the affected Glisson's sheath and in the vicinity. The increased nestin expression was seen in mesenchymal- and endothelial cells on PI days 1-7, with a peaked level on PI days 3-5 for mesenchymal cells and on PI day 3 for endothelial cells. Nestin was expressed in cholangiocytes on PI days 2-5 with a peaked level on PI day 3. During the nestin expression, Ki-67-positive proliferating cells were observed in these cell populations. Based on these findings, it was considered that nestin expression might be related to regeneration of the Glisson's sheath-consisting cells after damage. The nestin antibody would be useful to analyze regenerating cells in the affected Glisson's sheath in hepatotoxicity.

Table 1. Primary antibodies used for immunohistochemistry/immunofluorescence staining

Antibody	Clone, dilution	Antibody sources	Staining specificity
Anti-CK19	B170, ×500 (×100)*	Novocastra Laboratories Ltd, Newcastle, UK	Cholangiocytes
Anti-nestin	Rat-401, ×500 (×500)*	Millipore, Temecula, CA, USA	Neuroepithelial stem cells
Anti-Vimentin	V9, ×500	DakoCytomation, Glostrup, Denmark	Mesenchymal cells
Anti-Desmin	D33, ×500	Dako	Smooth muscle cells
Anti-α-SMA	1A4, ×500	Dako	Myofibroblasts
Anti-GFAP**	-----, ×300	Dako	Astrocytes
Anti-RECA-1	HIS52, ×100	AbD Serotec, Oxford, UK	Endothelial cells
Ki-67**	-----, ×500	Abcam Inc, Kendall Square, Cambridge, MA, USA	Proliferating cells

*; Dilutions indicated in the parentheses were used for immunohistochemistry and the others were for immunofluorescence. **; Rabbit polyclonal antibodies; the rest are mouse monoclonal antibodies. **CK19**: cytokeratin 19, **α-SMA**: α-smooth muscle actin, **GFAP**: glial fibrillary acidic protein, **RECA-1**: rat endothelial cell antigen-1.

Table 2. Semi-quantitative analyses of nestin-positive cells in the Glisson's sheath

Post injection (PI) days	Control (0)	1	2	3	5	7	9	12
Mesenchymal cells	+	+ ~ ++	++	+++	+++	++ ~ +	+	+
Cholangiocytes	–	–	+ ~ ++	+++	+	–	–	–
Endothelial cells	+	+ ~ ++	++	+++	++	++	+	+

Semi-quantitative grades: –; no positive cells, +; few positive cells, ++; moderately number of positive cells, +++; many positive cells.

Figure Legends

Fig. 1. Histopathology in control (A) and ANIT-injected (B-D) rats. The Glisson's sheath in control consists of interlobular arteriole (IA), interlobular vein (IV) and interlobular bile ducts (IBs), as well as fibroblastic cells (A). In ANIT-injected rats, desquamation of IB epithelial cells, edema, and infiltration of a small number of neutrophils (arrows) are seen in the affected Glisson's sheath on post-injection (PI) day 1 (B); on PI day 2, regenerating cholangiocytes in interlobular bile ducts, edema and infiltration of mononuclear cells (arrows) are observed (C); almost regenerated IBs, less edema, mononuclear cells and spindle-shaped mesenchymal cells (arrows) are seen on PI day 3 (D). HE.

Fig. 2. Immunoreactivity for cytokeratin (CK) 19. Cholangiocytes in the intact bile ducts in control liver are strongly reactive for CK19 (A). No reactivity for CK19 is seen in desquamated cholangiocytes on PI day 1 (B, arrow). However, cholangiocytes in the smaller bile duct, which escaped the necrotizing process due to ANIT toxicity, are reactive for CK19 (B, arrowhead). Regenerating cholangiocytes on PI day 2 show a weak reactivity for CK19 (C, arrows). Increasing reactivity for CK19 in regenerating cholangiocytes is seen on PI day 3. **IA**: interlobular arteriole, **IB**: interlobular bile duct, **IV**: interlobular vein. Immunohistochemistry, counterstained with hematoxylin.

Fig. 3. Expressions of nestin in control (A) and ANIT-injected livers (B-D). In control livers, nestin expression is seen in mesenchymal cells in the Glisson's sheath (black arrows), endothelial cells in blood vessels (yellow arrows) and hepatic stellate cells (HSCs) in parenchyma (arrowhead). Nestin expression is seen in mesenchymal cells (black arrows), endothelial cells (yellow arrows) and HSCs (arrowhead) on post-injection (PI) day 1 (B). Up-regulation in nestin expression is seen in mesenchymal cells (arrows) and endothelial cells on PI day 2 (C). On PI day 3, in addition to the up-regulation in mesenchymal cells (black arrows), endothelial cells

(yellow arrows) and HSCs (arrowhead), nestin expression is seen in regenerating cholangiocytes (red arrows) (D). **IA**: interlobular arteriole, **IB**: interlobular bile duct, **IV**: interlobular vein. Immunohistochemistry, counterstained with hematoxylin.

Fig. 4. Immunofluorescence staining for nestin with cholangiocyte marker (CK19), mesenchymal cell marker (vimentin), hepatic stellate cell (HSC) markers (desmin, GFAP) and endothelial cell marker (rat endothelial cell antigen (RECA)-1) on PI day 3. Photomicrographs show cholangiocytes expressing CK19 (green, A; arrows), nestin (red, B; arrows) and the digital merges (yellow, C; arrows); nestin expression in mesenchymal cells around bile ducts is indicated by arrowheads (B, C). Photomicrographs show mesenchymal cells expressing vimentin (green, D; arrows), nestin (red, E; arrows) and the digital merges (yellow, F; arrows); HSCs expressing desmin (green, G; arrows), nestin (red, H; arrows) and the digital merges (yellow, I; arrows); endothelial cells expressing RECA-1 (green, J; arrows), nestin (red, K; arrows) and the digital merges (yellow, L; arrows). Nestin is not co-expressed with GFAP in HSCs (M, green for GFAP; N, red for nestin; O, the digital merge). **IV**: interlobular vein. Immunofluorescence, DAPI for nuclear staining.

Fig. 5. Immunofluorescence staining for cell proliferation marker Ki-67 with nestin, CK19, vimentin and desmin in the Glisson's sheath on PI day 3. There are mesenchymal cells positive for nestin (A, green; arrow) and Ki-67 (B, red; arrow), and co-expressing nestin and Ki-67 (C, digital merge, yellow; arrow); regenerating cholangiocytes positive for CK19 (D, green; arrow) and Ki-67 (E, red; arrow), and co-expressing CK19 and Ki-67 (F, digital merge, yellow; arrow); mesenchymal cells positive for vimentin (G, green; arrow) and Ki-67 (H, red; arrow), and co-expressing vimentin and Ki-67 (I, digital merge, yellow; arrow); HSCs positive for desmin (J, green; arrow) and Ki-67 (K, red; arrow), and co-expressing nestin and

Ki-67 (L, digital merge, yellow; arrow). **IV**: interlobular vein. Immunofluorescence, DAPI for nuclear staining.

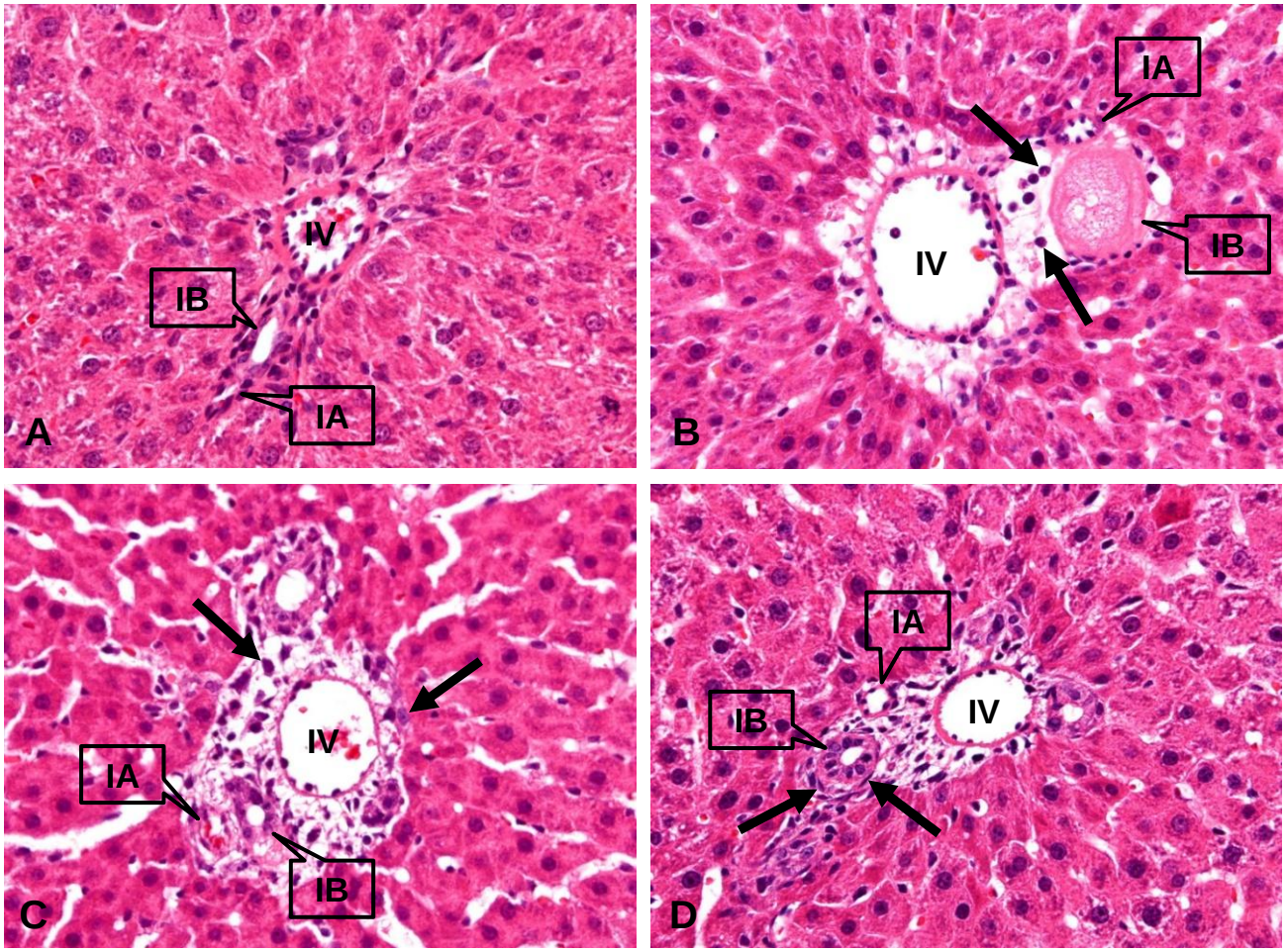

Fig. 1

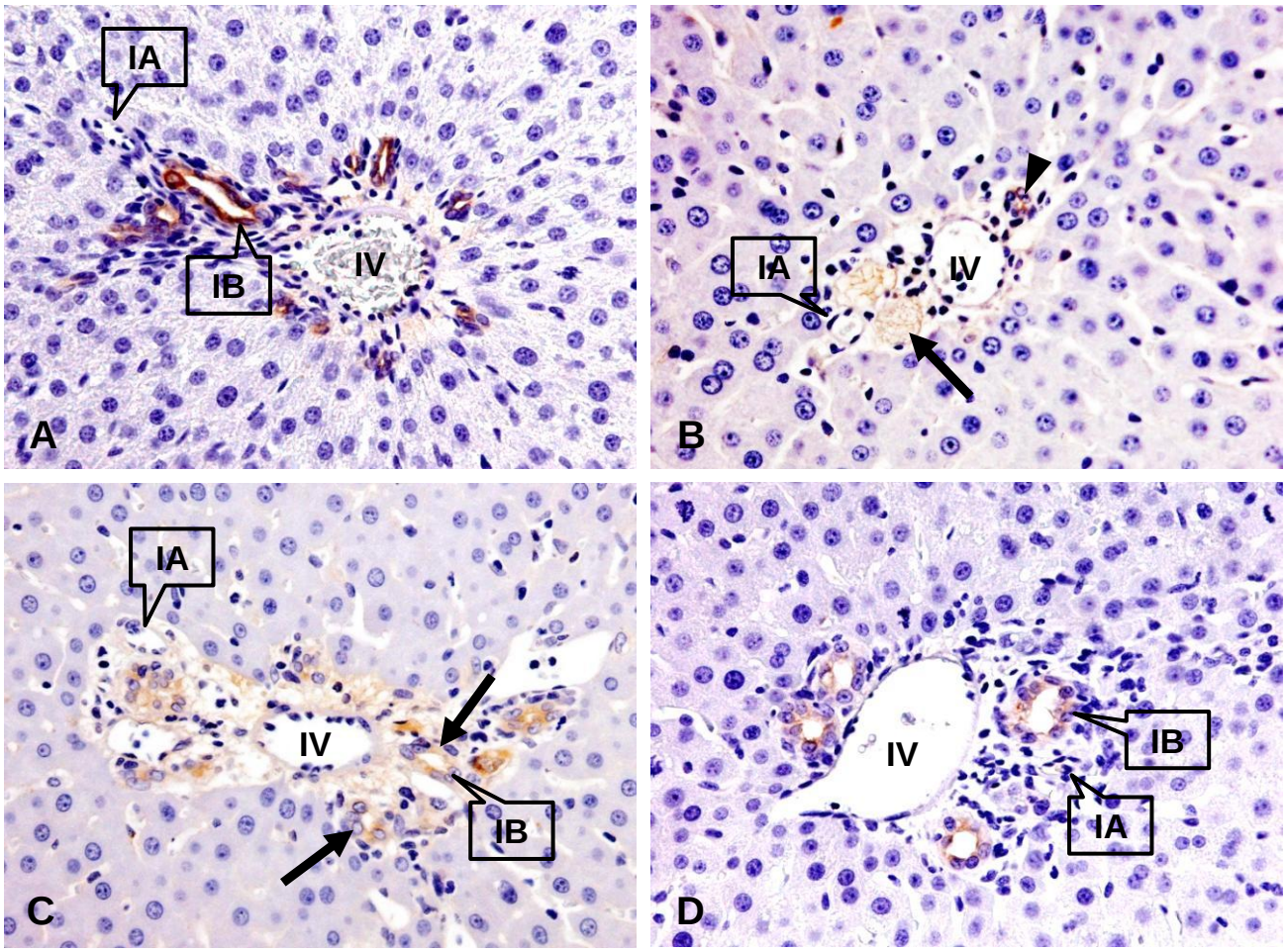

Fig. 2

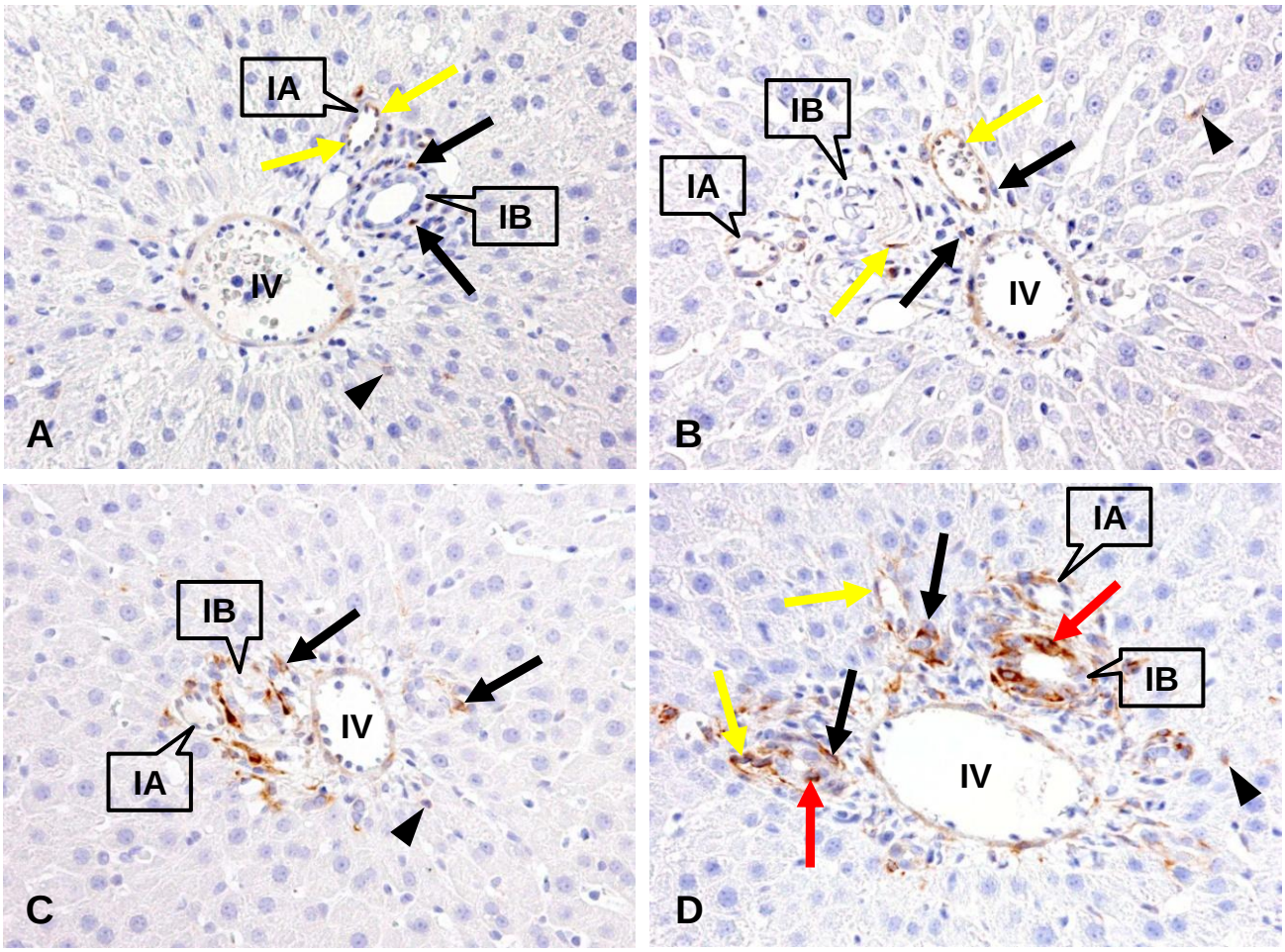

Fig. 3

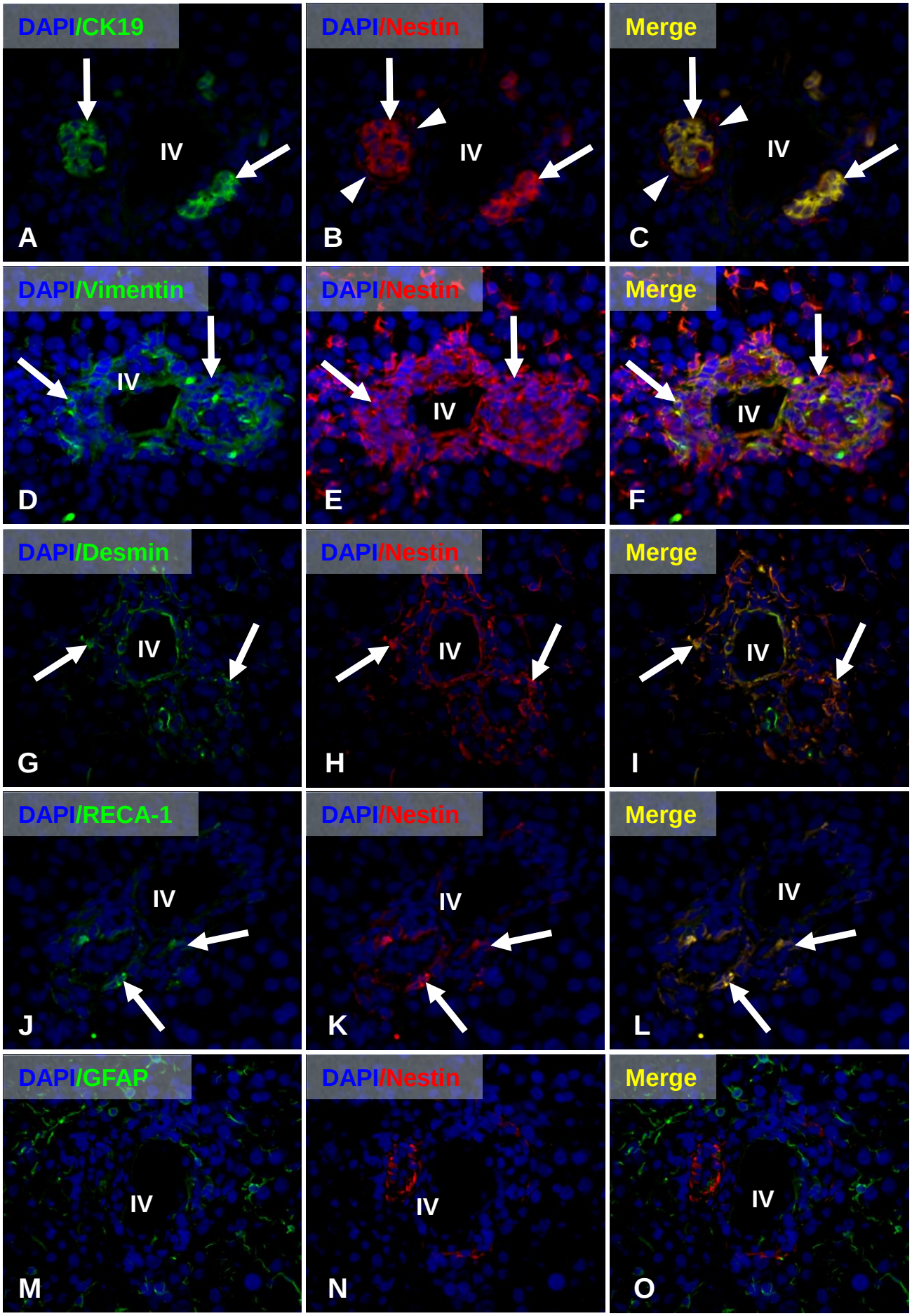
DAPI/CK19
IV
A
DAPI/Nestin
IV
B
Merge
IV
C
DAPI/Vimentin
IV
D
DAPI/Nestin
IV
E
Merge
IV
F
DAPI/Desmin
IV
G
DAPI/Nestin
IV
H
Merge
IV
I
DAPI/RECA-1
IV
J
DAPI/Nestin
IV
K
Merge
IV
L
DAPI/GFAP
IV
M
DAPI/Nestin
IV
N
Merge
IV
O

Fig. 4

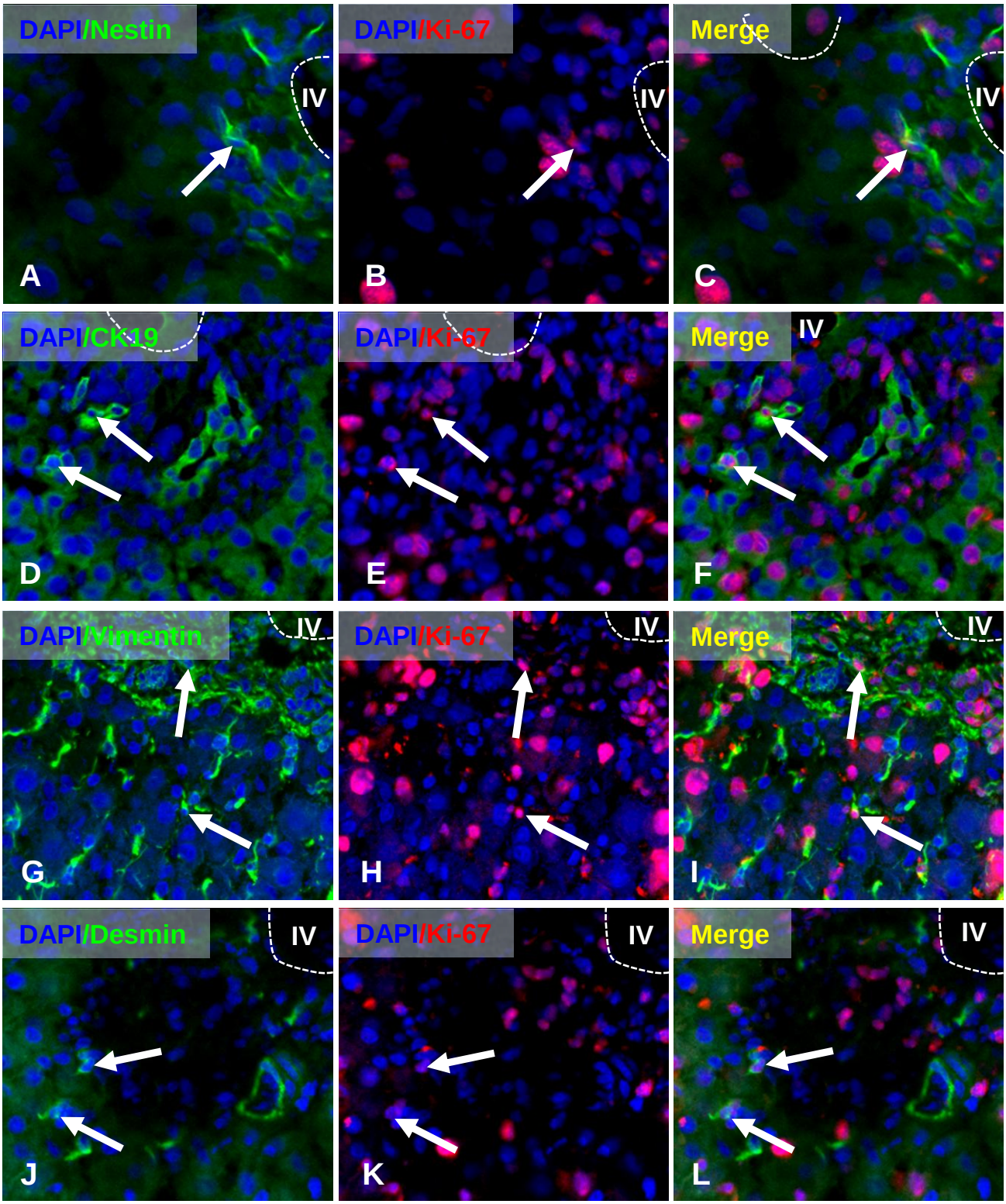
DAPI/Nestin
IV
A
DAPI/Ki-67
IV
B
Merge
IV
C
DAPI/CK19
D
DAPI/Ki-67
E
Merge
IV
F
DAPI/Vimentin
IV
G
DAPI/Ki-67
IV
H
Merge
IV
I
DAPI/Desmin
IV
J
DAPI/Ki-67
IV
K
Merge
IV
L

Fig. 5

Chapter 4

Slowly Progressive Cholangiofibrosis Induced in Rats by α-Naphthylisothiocyanate (ANIT), with Particular References to Characteristics of Macrophages and Myofibroblasts

Introduction

Cholangiofibrosis, also called cholangiohepatitis, is characterized by inflammation, bile duct proliferation/hyperplasia and abnormal accumulation of extracellular matrices (ECMs) in the Glisson's sheath, and develops in various pathological conditions such as sclerosing cholangitis, primary biliary sclerosis, obstructive cholestasis, and drug-associated cholangiocyte damage-related lesions; this condition finally leads to cirrhosis with hepatic insufficiency (Lazaridis et al. 2004), and may precede the development of cholangiocarcinoma (Hickling et al. 2010). Because of the complex etiology, comprehensive insights to the cholangiofibrosis are being pursuing. Experimental approaches to clarify the pathogenesis of cholangiofibrosis would be a pre-requisite for the exploitation of the effective and rational therapeutic strategies. To the author's knowledge, there have been few useful animal models of cholangiofibrosis. In this study, the author succeeded in establishment of cholangiofibrosis model in rats by repeated injections of α-naphthylisothiocyanate (ANIT) for a long time. ANIT is a well-known agrochemical having hepatotoxicity, particularly due to cholangiocyte damage, although the detailed mechanisms remain to be investigated (Ogawa et al. 2000, Dietrich et al. 2001).

Fibrosis is the process of healing response that engages a range of cell types and mediators (Friedman 2008). It has been reported that macrophages and myofibroblasts play important roles in the development of fibrotic lesions such as hepatic and renal fibrosis. In hepatic fibrosis, after parenchymal cell injury, hepatic stellate cells (HSCs) have been considered to be the origin that can differentiate into myofibroblasts capable of producing ECMs (Bataller and Brenner 2005); during the development, the myofibroblasts can express various intermediate cytoskeletons such as vimentin, desmin and α-smooth muscle action (α-SMA). For the differentiation into myofibroblasts and activation of HSCs, macrophages are getting attention on their unique roles; because, macrophages can secrete proinflammatory and fibrogenic mediators (Bataller and Brenner 2005, Karlmark et al. 2008, Wynn and Barron 2010). Transforming growth factor-β1 (TGF-β1) has been

considered the major factor capable of inducing the myofibroblasts. Additionally, macrophages have various functions such as phagocytosis and antigen presentation. Therefore, the relationship between macrophages and myofibroblasts should be crucial for the cholangiofibrosis. Functional roles of macrophages and characteristics of myofibroblasts in progressive cholangiofibrosis have not fully been determined yet.

In the present study, to shed light on the underlying pathogenesis, using ANIT-induced rat cholangiofibrosis model the author investigated characteristics of macrophages and myofibroblasts by the immunohistochemistry. Furthermore, the author examined expression patterns of fibrosis-related factors such as TGF-β1, monocyte chemoattractant protein-1 (MCP-1), and colony stimulating factor-1 (CSF-1). The present study shows that macrophages and myofibroblasts with divergent characteristics take part in ANIT-induced cholangiopathy in relation to fibrosis factors.

Materials and Methods

Animals and ANIT-induced hepatic lesions

Five-week-old, male F344 rats (100 to 120 g body weight) purchased from Charles River Japan (CRJ, Hino, Shiga, Japan) were used in this experiment. The rats were housed in an animal room at a controlled temperature of 21 ± 3˚C and with a 12-hour light-dark cycle; they were provided a standard diet for rats (MF, Oriental Yeast Co. Ltd., Tokyo, Japan) and tap water *ad libitum*. After a one week acclimatization, they were divided into control (eight rats) and ANIT-injection (twenty-four rats) groups. The rats in the ANIT group received weekly intraperitoneal (IP) injection of ANIT dissolved in olive oil at a dose of 30 mg/kg body weight (Calvo et al. 2001) for 5 weeks followed by 75 mg/kg body weight until 19 week. Four-rats were euthanized by exsanguinations under isoflurane anesthesia on each of post-first-injection (PFI) weeks 3, 7, 10, 13, 16, and 19. Control rats received an equal volume of vehicle only and were euthanized on PFI weeks 0 and 19; there were no differences in items examined between these control rats, and therefore, these rats were expressed as controls together.

At necropsy, blood was collected from the abdominal artery and separated serum samples were analyzed for aspartate transaminase (AST), alanine transaminase (ALT), alkaline phosphatase (ALP) and total bilirubin (T. Bil) with a Clinical Analyzer 7170 (Hitachi, Tokyo, Japan).

The animal experiments were performed in compliance with the institutional guidelines and protocol approved by the ethical committee of Osaka Prefecture University for animal care.

Histopathology and immunohistochemistry

Tissues from the left external lobe of the livers were fixed in 10% neutral buffered formalin, Zamboni's fixative (0.21% picric acid and 2% paraformaldehyde in 130 mM phosphate buffer, pH 7.4) and periodate-lysine-paraformaldehyde (PLP) solutions (Ide et al. 2005). These tissues were dehydrated and embedded in paraffin. Deparaffinized sections, cut at 4 μm in thickness, were stained with hematoxylin and eosin (HE) for histopathology. Tissue sections fixed in neutral buffered formalin or Zamboni's solution, or processed by PLP-AMeX (PLP-Acetone, methyl benzoate, and xylene) method were used for the immunohistochemistry with mouse monoclonal antibodies against macrophages of ED1 (for CD68), ED2 (for CD163), OX6 (for major histocompatibility complex (MHC) class II), and SRA-E5 (for CD204); additionally, antibodies against intermediate cytoskeletal proteins (vimentin, desmin, and α-SMA), bile duct epithelia (CK19) and cell proliferation (Ki-67) were used as primary antibody (Table 1). After pretreatment with heat (microwave in citrate buffer for 20 minutes), trypsin (0.1% trypsin in phosphate buffered saline (PBS) for 30 minutes at 37°C) or proteinase K (10 μg/ml proteinase K in Tris buffer, p^H 7.5 for 15 minutes) as shown in Table 1, tissue sections were treated with 3% H_2O_2 in PBS to quench endogenous peroxidase, and then with 5% skimmed milk in PBS to inhibit nonspecific reactions. The sections were incubated with each primary antibody overnight at 4ºC, followed by reaction with the secondary antibody (Histofine Simple Stain MAX PO, Nichirei, Tokyo, Japan). Positive reactions were visualized with 3, 3'-diaminobenzidine (DAB Substrate Kit, Vector Laboratories, Inc., Burlingame, CA, USA). Sections were counterstained lightly with hematoxylin. Controls obtained by replacing primary antibodies with non-immunized IgG were all negative.

Cells showing a distinct immunopositive reaction for ED1, ED2, OX6 or SRA-E5 were counted in five randomly selected areas (0.2 mm^2) including the Glisson's sheath and periportal area of the hepatic lobule at a magnification of ×400 using ImageJ software version 1.44 (NIH, Bethesda, MD, USA). Cells positive for vimentin, desmin and α-SMA

in the Glisson's sheath including the periportal area was evaluated semi-quantitatively using grades as shown in Table 2. Immunoreactivities for these cytoskeleton markers in blood vessels were excluded from these analyses.

Immunofluorescence staining

Double immunofluorescence labeling was carried out using ANIT-induced fresh frozen liver sections obtained on PFI weeks 10 and 19. The combinations in the dual immunofluorescence labeling were ED1/OX6, ED2/OX6, desmin/vimentin, α-SMA/vimentin, or desmin/α-SMA. Briefly, after fixation in Zamboni's solution for 15 minutes at 4°C, the sections were washed with 0.3% Triton X-100 and incubated with 10% normal goat serum for 30 minutes followed by reaction with the primary antibody overnight at 4ºC. Then the sections were allowed to react with the secondary antibody conjugated with Alexa 488 or Alexa 568 (Invitrogen, Carlsbad, CA, USA) for 1 hour at room temperature. The sections were incubated with the second primary antibody followed by fluorescent dye conjugated secondary antibody. Alexa fluor™ 488 labeled OX6 (AbD Serotec, Oxford, UK) was used for combinations of ED1/OX6 and ED2/OX6, and Hilyte fluor^{TM} 555 (Dojindo Molecular Technologies, Inc., Tokyo, Japan) labeled anti-vimentin antibodies were used for desmin/vimentin, and α-SMA/vimentin. The sections were covered with Vectashield® mounting medium containing 4' 6 diamidino-2-phenylindole (DAPI) (Vector Laboratories, Inc., Burlingame, CA, USA) for nuclear staining and analyzed by a laser scanning confocal microscope system (C1si, Nikon, Japan). No signal was observed in tissue sections stained by replacing primary antibodies with non-immunized mouse IgG and served as negative controls.

Reverse transcriptase polymerase chain reaction (RT-PCR)

Liver samples were immersed in RNAlater™ (Qiagen GmbH, Hilden, Germany) and stored at −80˚C. The extraction of RNA was carried out by using an SV total RNA isolation system kit® (Promega Corporation, Madison, WI, USA) according to manufacturer's instruction. After the isolation, concentration of RNA was measured on a nanodrop1000™ spectrophotometer (Thermo Scientific, Wilmington, DE, USA) and then reverse transcribed to cDNA with the superscript II transcriptase system® (Invitrogen, Carlsbad, CA, USA) and amplified, in duplicate, with the SYBR® Green Real-time PCR Master Mix (Toyobo Co. Ltd, Osaka, Japan) using the LineGene system (Bioflux, Tokyo, Japan) for each of the specific primers of rat MCP-1, TGF-β1, CSF-1 and ribosomal protein S18 (Rps18; an internal control gene). The PCR conditions for MCP-1 used were initial denaturation at 95ºC for 1 minute followed by 40 cycles of 15 seconds of denaturation at 95ºC, 15 seconds of annealing at 62ºC, and 20 seconds of extension at 72ºC. The same PCR conditions were used for TGF-β1 and CSF-1 except annealing temperatures of 64ºC and 60ºC, respectively. The oligonucleotide sequences used for PCR are shown in Table 2. The PCR products were electrophoresed in 2% agarose gel, and DNA was stained with ethidium bromide on the gel.

Statistical analyses

Quantitative data are presented as mean ± standard deviation (SD), and statistical analysis was performed using the Tukey's test or Student's *t*-test. Significance was set at $P < 0.05$.

Results

ANIT-induced hepatic lesions

The body weight gain in the ANIT group began to significantly decrease at PFI week 9 and at subsequent PFI weeks the decreased level was gradually marked with a significant change (Fig. 1). The level of T. Bil significantly increased from PFI weeks 7 to 19 (Fig. 2A). On the other hand, the levels of AST (Fig. 2B), ALT (Fig. 2C) and ALP (Fig. 2D) did not show any significant change.

No histopathological lesions were seen in controls at PFI weeks 0 and 19 (Fig. 3A). In the ANIT group, noticeable lesions were not found in rats at PFI week 3. At PFI week 7, a small number of inflammatory cells (mainly mononuclear cells) accompanied with slightly increased number of interlobular bile ducts started to be seen in the Glisson's sheath (Fig. 3B). At PFI weeks 10 onwards, the appearance of inflammatory cells and proliferating bile ducts became more prominent in the Glisson's sheath, and fibrosis consisting of spindle-shaped cells and collagen fibers was developed mainly around the proliferating bile ducts (Fig. 3C). Mononuclear cells and spindle-shaped cells were identified as macrophages and myofibroblasts, respectively, by the immunohistochemistry as stated below.

Cholangiocytes in interlobular bile ducts in the controls were clearly positive for CK19 (Fig. 4A). Although the intensity for CK19 immunohistochemistry was weaker, the proliferating bile ducts reacted to CK19 in the ANIT group at PFI weeks 7-19 (Fig. 4B). As compared with controls (Fig. 4C), the immunolabeling for Ki-67, a marker for cell proliferation, demonstrated a proliferating activity of cholangiocytes in the bile ducts of the affected Glisson's sheath (Fig. 4D). Interestingly, some spindle-shaped mesenchymal cells around the proliferating bile ducts reacted to Ki-67 (Fig. 4C, D).

Macrophage immunophenotypes

The author used four different antibodies (ED1, ED2, SRA-E5 and OX6) for detection of macrophages. The kinetics of macrophages reacting to these antibodies is shown in Fig. 5. Although the number at PFI week 10 did not show any significant change, the ED1-positive macrophage number significantly increased on PFI weeks 7, 13, 16, and 19. The ED2-positive macrophages showed a significantly increased number at PFI weeks 13-19. The numbers of macrophages reacting to SRA-E5 significantly increased at PFI week 7 and subsequent weeks until PFI week 19. The OX6-positive macrophages showed a significantly increased number from PFI week 3 to PFI week 19, indicating a consistent increase.

A few ED1-positive macrophages were seen in the Glisson's sheath of controls (Fig. 6A), whereas the positive cells were more frequently seen in the affected Glisson's sheath and in the periportal areas of the hepatic lobules of the ANIT group, showing round or spindle configuration (Fig. 6B). ED2-positive macrophages with round to oval in shape and having relatively abundant cytoplasm were distributed mainly along the sinusoids of the hepatic lobules of controls, indicative of Kupffer cells (Fig. 6C), and the positive cells were frequently seen in the affected Glisson's sheath (Fig. 6D). The SRA-E5-positive cells exhibited round to oval morphology, and a small number of the positive cells were located along the sinusoids in the hepatic lobules of the controls (Fig. 6E); the positive cells seen along the sinusoids in the vicinity of the affected Glisson's sheath had more abundant cytoplasm (Fig. 6F). In both the controls (Fig. 6G) and ANIT group (Fig. 6H), the appearances of OX6-positive cells were limited mainly in the Glisson's sheath; they were spindle-shaped and dendritic in appearance, and showed the significantly increased number in the affected Glisson's sheath of the ANIT group (Fig. 6H).

The double immunofluorescence labeling for ED1/OX6 (Fig. 7A-C) or ED2/ OX6 (Fig. 7D-F) revealed that approximately 39% and 58% of the OX6-positive cells at PFI

weeks 10 and 19 reacted to ED1, respectively. The respective percentage of ED2/OX6 at PFI weeks 10 and 19 was 24 and 21.

Mesenchymal cell immunohistochemistry for vimentin, desmin and α-SMA

In control livers, a small number of vimentin-positive cells were present along the sinusoids, indicative of HSCs (Fig. 8A); however, desmin- and α-SMA-positive cells were not seen in the hepatic lobules of the controls (Fig. 8C, E). In the Glisson's sheath of controls, vascular smooth muscle cells reacted to desmin (Fig. 8C) and α-SMA (Fig. 8E); however, no mesenchymal cells reacting to desmin or α-SMA were present in the Glisson's sheath, although vimentin-positive mesenchymal cells were sporadically seen.

In ANIT-injected rats, vimentin-positive cells (Fig. 8B) began to increase at PFI week 3 (++) and retained more increased number at PFI weeks 7-16 (+++) (Table 3). At PFI week 3, a few desmin-positive cells began to be seen in the affected Glisson's sheath (±), and thereafter, the number increased slightly until PFI week 19 (+) (Fig. 8D); however, the number was much smaller as compared with that of vimentin- and α-SMA-positive cells (Table 3). α-SMA-positive cells began to increase at PFI week 7 in the affected Glisson's sheath (++), and subsequently, the increased number (+++) continued until PFH week 19 (Table 3).

Vimentin-, desmin- and α-SMA-positive cells seen in the affected Glisson's sheath were spindle-shaped or oval in shape; interestingly, vimentin-positive cells were distributed in the affected Glisson's sheath, whereas desmin and α-SMA-positive cells were located mainly around the interlobular bile ducts.

The double immunofluorescence labeling was carried out for samples at PFI weeks 10 and 19; mesenchymal cells reacting to both desmin and vimentin were often seen (Fig. 9A-C), whereas mesenchymal cells reacting to both α-SMA and desmin (Fig. 9D-F) were

small in number. Mesenchymal cells reacting to both α-SMA and vimentin (Fig. 9G-I) were not seen.

Expression of MCP-1, TGF-β1 and CSF-1 mRNAs

The level of MCP-1 mRNA expression was significantly increased at PFI weeks 10-16, showing maximum at PFI week 10; the level was gradually decreased at PFI weeks 13 and 16 (Fig. 10A). TGF-β1 mRNA expression level was significantly increased at PFI weeks 10, 16, and 19, and that at PFI week 13 tended to increase (Fig. 10B). CSF-1 mRNA level was increased significantly only at PFI week 19 (Fig. 10C).

Discussion

ANIT-induced lesions in the Glisson's sheath as an animal model

Cholangiofibrosis caused by bile duct injury is characterized by inflammatory cell reaction and subsequent fibrogenesis (Golbar et al. 2011). Repeated and continuous injuries to bile ducts may be responsible for the induction of the cholangiopathy. On the other hand, severe and acute damage of bile ducts gives rise to both bile duct necrosis/desquamation and hepatocyte injury. The administration of ANIT into rats injuries interlobular bile duct epithelial cells, and its LD50 is 240 mg/kg for rats (Dietrich et al. 2001). Therefore, the author used a low dose (30 mg/kg) of ANIT for PFI weeks 1-5 (to induce extremely minor injury which may not be detected under the light microscopy), and then the ANIT dose was increased to 75 mg/kg at subsequent PFI weeks 7-19. In the present rat model by ANIT injection, histopathological lesions in the Glisson's sheath, consisting of inflammation, fibrosis and bile duct proliferation (demonstrable by the Ki-67 immunohistochemistry), began to be seen at PFI week 7 and the lesions were gradually increased with more proliferating bile ducts until PFI week 19. The body weight was significantly decreased at PFI week 9 and subsequent PFI weeks, and the level of T. Bil was significantly increased from PFI week 7 suggestive of cholestasis. Because AST, ALT and ALP levels did not show any significant change, it was considered that the present lesions seen in the Glisson's sheath of the ANIT group progressed slowly without any hepatocyte damage. In humans, cholangiofibrosis is developed exclusively in the damaged Glisson's sheath at the early stages of cirrhosis due to cholangiopathy such as obstructive cholestasis (Geraghty and Goldin 1994). Therefore, the dosages used in the present study would be useful for the induction of cholangiofibrosis; the present rat model was considered to be beneficial to investigate the pathogenesis of progressive cholangiofibrosis.

Macrophages

In the present study, neutrophils were not found in the affected Glisson's sheath at any examination point, although some investigators have reported the appearance of neutrophils and their important roles in ANIT-induced hepatic lesions (Dietrich et al. 2001). In the present study, rather, mononuclear cells, identified as macrophages by the immunohistochemistry, were seen as the major inflammatory cell component. The possible functions of macrophages could be evaluated by the immunohistochemical approaches with antibodies (ED1, ED2, SRA-E5 and OX6).

ED1 recognizes CD68, of which the antigen is located on lysosomes, especially phagosomes of blood monocyte-derived infiltrating macrophages and resident macrophages. The increased expression implies enhanced phagocytosis (Damoiseaux et al. 1994, Suda et al. 1998). The number of ED1-positive cells significantly increased at PFI week 7 and the increased level was maintained until PFI week 19 except at PFI week 10. Because the histopathological lesions in the Glisson's sheath began to be seen at PFI week 7, ED1-positive cells are likely to have phagocytic activity for cell debris injured by ANIT. ED2 labels resident macrophages (Kupffer cells) in normal livers (Golbar et al. 2012). Recently, it has been reported that CD163, the antigen recognized by ED2, functions as a scavenger receptor for hemoglobin-haptoglobin complexes, and that the engagement of CD163 might reflect the production of inflammatory mediators such as interleukin-6 (IL-6) and tumor necrosis factor-α (TNF-α) (Polfliet et al. 2006). The mechanism behind ANIT-induced bile duct injury has not yet been fully characterized (Jean et al. 1998). In addition to direct injury of bile ducts in the Glisson's sheath by ANIT excreted in bile, inflammatory cells in response to the damage may contribute to the progress. Macrophages can produce inflammatory mediators and oxidative factors (oxidants) (Dietrich et al. 2001, Kodali et al. 2006). The ED2-positive cell number was significantly increased on PFI weeks 13-19. Since ED1- and ED2-positive cells were seen exclusively in the affected

Glisson's sheath, they might have important roles in enhancing ANIT-induced hepatic lesions.

The SRA-E5 antibody was generated by immunizing scavenger receptor knockout mice with recombinant human type I scavenger receptor protein (CD204) (Tomokiyo et al. 2002). CD204 expression may be related to lipid metabolism in macrophages via the scavenger receptor (Greaves 1998). The SRA-E5-positive cells showed an increased number on PFI weeks 7-19. Unlike ED1- and ED2-positive cells, interestingly, the SRA-E5-positive cells were located exclusively along the sinusoids of hepatic lobules in the vicinity of the affected Glisson's sheath, suggestive of different functions between ED1-/ED2-positive cells and SRA-E5-positive cells. The increased number of SRA-E5-positive cells with enlarged cytoplasm might mean the abnormal metabolism of lipid in the ANIT hepatotoxicity.

The significantly increased number of OX6-positive cells was seen as early as at PFI week 3, and retained until PFI week 19, indicating that OX6-positive cells already appeared at the early stages in the Glisson's sheath, despite noticeable histopathological lesions were not present. The MHC class II molecule recognized by OX6 is expressed in activated macrophages and dendritic cells (Moghaddami et al. 2005, Zhao et al. 2006). Dendritic cells are major antigen-presenting cells, consisting of the interstitial dendritic cells, interdigitating follicular cells of the spleen and lymph nodes, and Langerhans cells of the epidermis (Gao et al. 2007, Zimmerli and Hauser 2007). Interstitial dendritic cells are widely distributed in connective tissues, including the Glisson's sheath (Mori et al. 2009). MHC class II expression may be related to the activation of CD4+ T cells and subsequent induction of macrophages (Perrigoue et al. 2009). Because these macrophage populations were present mainly in the affected Glisson's sheath, the early and consistently increased number of OX6-positive cells might have attributed to induction of ED1-/ED2-positive macrophages. More intriguingly, the present double immunofluorescence labeling demonstrated that 21-58% of OX6-positive cells reacted to ED1 or ED2 at PFI weeks 10 and 19. These findings suggest that OX6-positive cells might be generated partly from

ED1- and ED2-positive cells. Recently, MHC class II-expressing cells have been suggested to modulate cytokine production in macrophages and collagen depositions by myofibroblasts (Connolly et al. 2009, Karlmark et al. 2009). Collectively, OX6-positive cells consistently seen in the present study might be responsible for induction of macrophages and development of peribiliary fibrosis.

The CCR2 ligand, MCP-1, is a member of C-C chemokine family which act as a chemotactic agent for recruitment of monocytes/macrophages in the injured tissue (Marra et al. 1998, Zamara et al. 2007, Harada et al. 2011). In the current study, significantly increased MCP-1 mRNA at PFI weeks 10-16 might be related to macrophage increment at the mid stage. TGF-β1, secreted mainly by macrophages, is a well-known fibrogenic factor capable of inducing transdifferentiation into myofibroblasts (Yang et al. 2003, Bataller and Brenner 2005, Li et al. 2007). The mRNA level of TGF-β1 increased significantly at PFI weeks 10-19 suggested that the factor participated into progressive peribiliary fibrosis. CSF-1, a multi-functional protein released by HSCs, stimulates proliferation, differentiation, and survival of mononuclear phagocytes (Wynn et al. 2001, Abboud et al. 2003). Increment of CSF-1 mRNA level at PFI week 19 suggests its roles in maintenance of macrophages participating in advanced stage of fibrogenesis.

Mesenchymal cells in the Glisson's sheath

Myofibroblasts, which contribute to a great part of collagen deposition in fibrosis, express heterogeneously mesenchymal cytoskeletons such as vimentin, desmin and α-SMA; out of them, α-SMA is the canonical marker of myofibroblasts and most sensitive indicator of fibrogenesis (Magness et al. 2004, Yamate et al. 2004, Wynn 2008). In the current study, the increase of vimentin-positive cells (starting at PFI week 3) in the affected Glisson's sheath preceded α-SMA-positive cells (starting at PFI week 7), and the increased numbers of these positive cells were retained until the PFI week 19. This study

also showed that desmin-positive cells appeared in the Glisson's sheath on PFI week 3 and subsequent weeks, although the number was smaller than vimentin- and α-SMA-positive cells. Based on expression patterns of mesenchymal cytoskeletons, myofibroblasts are categorized largely into cells expressing vimentin and desmin (VD type), cells expressing vimentin and α-SMA (VA type), and cells expressing vimentin, α-SMA and desmin (VAD type), and the expression level changes depending on stages of myofibroblastic differentiation (Chaurasia et al. 2009). The double immunolabeling revealed that there were cells expressing both desmin/vimentin or both desmin/α-SMA in the affected Glisson's sheath; however, cells expressing vimentin/α-SMA were not detected at the late stages. These findings indicated that myofibroblasts seen in progressive cholangiofibrosis could express vimentin and desmin at the early or mid stages, and thereafter came to have α-SMA cytoskeleton as well-developed type by losing vimentin. Taken these findings together, vimentin-positive pre-existing portal fibroblasts might be the origin for myofibroblasts in the cholangiofibrosis (Kruglov et al. 2006). Interestingly, α-SMA-expressing cells were located exclusively around the proliferating bile ducts at the late stages. Some investigators have proposed that cholangiocytes in cholestatic liver injury serve as another source of myofibroblasts via epithelial-mesenchymal transition (EMT) (Rygiel et al. 2008). It is interesting to investigate the possible mechanisms of EMT in this rat cholangiofibrosis model.

In conclusion, in this study, the author succeeded in establishing cholangiofibrosis model in rats by using ANIT (a hepatotoxicant causing bile duct injury). The lesions were characterized by macrophage infiltration, fibrogenesis and bile duct proliferation in the Glisson's sheath. MHC class II-expressing macrophages, recognized by OX6 antibody, appeared consistently in the affected Glisson's sheath; in addition to such a function, macrophages with phagocytic activity (CD68), inflammatory factor production (CD163) and lipid metabolism (CD204) were increased with development of the lesion. Myofibroblasts seen in cholangiofibrosis expressed variously vimentin, desmin and α-SMA; apparently, myofibroblasts reacting to α-SMA, the major marker of well-

developed myofibroblasts, were developed at the late stages and located exclusively around the proliferating bile ducts. Because the pathogenesis of cholangiofibrosis is very complicated, further investigations, particularly on relationship between macrophages and myofibroblasts, should be needed to explore possible therapeutic strategies for peribiliary fibrosis-related cirrhosis.

Summary

A progressive cholangiofibrosis was developed as an animal model in 6-week-old male F344 rats by repeated intraperitoneal injections of α-naphthylisothiocyanate (ANIT) for 19 weeks; liver samples were examined at post-first-injection (PFI) weeks 3, 7, 10, 13, 16 and 19, focusing on characteristics of macrophages and myofibroblasts by immunohistochemical analyses. In the affected Glisson's sheath consisting of inflammatory cell infiltrates, bile duct proliferation and advancing fibrosis, the number of macrophages reacting to OX6 (recognizing MHC class II) increased consistently (PFI weeks 3-19); macrophages reacting to ED1 (CD68, reflecting phagocytic activity) and ED2 (CD163, relating to proinflammatory factor production) showed a significantly increased number at PFI weeks 7-19 and PFI weeks 13-19, respectively. Interestingly, macrophages positive for SRA-E5 (CD204, reflecting lipid metabolism) increased at PFI weeks 7-19, and the appearance was limited in the sinusoids around the affected Glisson's sheath. Myofibroblasts appearing in the affected Glisson's sheath reacted to vimentin and desmin at early (PFI weeks 3-7) and mid (PFI weeks 10-13) stages, and then they came to strongly express α-smooth muscle actin at late stage (PFI weeks 16-19). This study shows that macrophages exhibit heterogeneous properties depending on stages and locations; in association with such macrophage populations, myofibroblasts expressing various cytoskeletons participate in cholangiofibrosis.

Table 1. Primary antibodies used for immunohistochemistry

Antibody	Dilution	Preteatment	Source	Specificity
Anti-ED1	1:100	Proteinase K	Millipore, Billerica, MA, USA	Exudate macrophages (monocytes)
Anti-ED2	1:100	Proteinase K	AbD Serotec, Oxford, UK	Resident macrophages (Kupffer cells)
Anti-OX6	1:100	Proteinase K	AbD Serotec	Dendritic cells, activated macrophages
Anti-SRA-E5	1:100	Heat	TransGenic Inc., Kumamoto, Japan	Macrophages, Kupffer cells
Anti-Vimentin	1:400	Heat	DakoCytomation, Glostrup, Denmark	Cells of mesenchymal origin
Anti-Desmin	1:200	Heat	Dako	Smooth muscle cells, myofibroblasts
Anti-α-SMA	1:100	Proteinase K	Dako	Smooth muscle cells, myofibroblasts
Anti-CK19	1:100	Trypsin	Novocastra Laboratories Ltd., Newcastle, UK	Cholangiocytes
Anti-Ki-67*	1:200	Heat	Abcam, Kendall Square, Cambridge, MA, USA	Proliferating cells

*; Rabbit polyclonal antibody; the rest are mouse monoclonal antibodies. **α-SMA**: α-smooth muscle actin, **CK19**: cytokeratin 19. ED1 for CD68, ED2 for CD163, OX6 for MHC class II, SRA-E5 for CD204.

Table 2. Oligonucleotide sequences of primers used in the real-time PCR

Gene	Primers	Oligonucleotide sequences	Size of amplicon (bp)
MCP-1	Sense	5’-GCTTCTGGGCCTGTTGTTC-3’	156
	Anti-sense	5’-CTGCTGCTGGTGATTCTCTTGT-3’	
TGF-β1	Sense	5’-CTTCAGCTCCACAGAGAAGAACTGC- 3’	298
	Anti-sense	5’-CACGATCATGTTGGACAACTGCTCC- 3’	
CSF-1	Sense	5’-ACAGGTGGAACTGCCAGTGTAGAA-3’	89
	Anti-sense	5’-GGTGGACGTTGCCATAATGTCTC-3’	
Rps18	Sense	5’-AAGTTTCAGCACATCCTGCGAGTA-3’	140
	Anti-sense	5’-TTGGTGAGGTCAATGTCTGCTTTC-3’	

MCP-1: monocyte chemoattractant protein-1, **TGF-β1**: transforming growth factor-β1, **CSF-1**: colony stimulating factor-1, **Rps18**: ribosomal protein s18 (an internal control gene).

Table 3. Semi-quantitative analyses for mesenchymal cell markers

	PFI weeks	Mesenchymal cell markers		
		Vimentin	**Desmin**	**α-SMA**
	Control	+	−	−
Early stage	3	++	±	−
	7	+++	±	++
Mid stage	10	+++	+	+++
	13	+++	+	+++
Late stage	16	+++	+	+++
	19	++	+	+++

PFI: post-first injection weeks of α-naphthylisothiocyanate (ANIT), **α-SMA**: α-smooth muscle actin.

Semi-quantitative grades: –; no positive cells (for α-SMA and desmin, reactivity confined to blood vessels only), ±; a few positive cells, +; occasional positive cells, ++; moderate number of positive cells, +++; many positive cells.

Figure Legends

Fig. 1. Body weight changes in rats weekly injected intraperitoneally with α-naphthylisothiocyanate (ANIT) for 19 weeks. **Cont**: control. Student's *t*-test. *; $P< 0.05$, significantly different from controls.

Fig. 2. Biochemical analyses on the levels of total bilirubin (T. Bil) (A), aspartate transaminase (AST) (B), alanine transaminase (ALT) (B) and alkaline phosphatase (ALP) (D) in ANIT-injected rats examined at post-first-injection (PFI) weeks 3, 7, 10, 13, 16, and 19. **Cont**: control. Student's *t*-test. *; $P< 0.05$.

Fig. 3. Histopathology in control (A) and ANIT-injected rats (B, C). The Glisson's sheath in a control (PFI week 19) consists of interlobular arteriole (IA), interlobular vein (IV) and interlobular bile ducts (IBs), as well as fibroblastic cells (A). In ANIT-injected rats on PFI week 7, mononuclear infiltrate, slight fibrosis (arrows) and proliferating IBs (arrowheads) are seen in the affected Glisson's sheath (B); on PFI week 19, more prominent fibrosis (arrow) and a larger number of newly-formed ductular structures (arrowheads), as well as increase in mononuclear infiltrate are present in the affected Glisson's sheath (C). HE.

Fig. 4. Immunohistochemical staining for CK19 (A, B), specific for cholangiocytes, and Ki-67 (C, D), a proliferating cell marker, in control rats (A, C) and ANIT-injected rats at PFI week 19 (B, D). Cholangiocytes in the Glisson's sheath react to CK19, although the intensity is greater in the control (A) than ANIT-induced lesion (B). Ki-67-positive proliferating cells are sporadically seen in mesenchymal cells (arrowheads) in the Glisson's sheath and hepatocytes (arrows) in the control; no cholangiocytes reacting to CK19 are seen (C). On the contrary, in the Glisson's sheath of ANIT-injected rats at PFI 19, Ki-67-labeling is seen in cholangiocytes (arrows) of proliferating bile ducts and mesenchymal cells (apparently

myofibroblasts; arrowheads) (D). **IA**: interlobular arteriole, **IV**: interlobular vein. Immunohistochemistry, counterstained with hematoxylin.

Fig. 5. The kinetics of macrophages in the Glisson's sheath and hepatic lobules around the Glisson's sheath in control (cont) and ANIT-injected rats at PFI weeks 3-19. Macrophages were identified using an antibody of ED1 (CD68) (A), ED2 (CD163) (B), SRA-E5 (CD204) (C) or OX6 (MHC class II) (D). Tukey's test. *; $P<0.05$, significantly different from controls.

Fig. 6. Distribution of macrophages in the Glisson's sheath and the periportal parenchyma at PFI week 19 in control (A, C, E, G) and ANIT-injected rats (B, D, F, H). ED2 (C)- and SRA-E5 (E)-positive cells in controls are located along the sinusoids, indicating Kupffer cells, whereas OX6-positive cells are seen exclusively in the Glisson's sheath of control (G) and ANIT-injected rats (H). As compared with controls (A for ED1, C for ED2, E for SRA-E5, G for OX6), macrophages reacting to ED1 (B)-, ED2 (D)-, SRA-E5 (F)-, and OX6 (H) show increased numbers in the affected Glisson's sheath of ANIT-injected rats. Arrows indicate representative immunopositive cells in each staining. **IA**: interlobular arteriole, **IB**: interlobular bile duct, **IV**: interlobular vein.

Fig. 7. Double immunofluorescence labeling for OX6 and ED1 or OX6 and ED2 in the affected Glisson's sheath of ANIT-injected rats at PFI week 19. Photomicrographs show macrophages positive for OX6 (green, A and D; arrows) and ED1 (red, B; arrows) or ED2 (red, E; arrows); double positive cells are shown by the digital merges (yellow, C for OX6/ED1 or F for OX6/ED2; arrows). **IV**: interlobular vein. Immunofluorescence, DAPI for nuclear staining.

Fig. 8. Distribution of mesenchymal cells for vimentin (A, B), desmin (C, D) and α-smooth muscle actin (α-SMA) (E, F) in the Glisson's sheath in control rats and ANIT-injected rats at PFI week 19. In the Glisson's sheath of controls, a few

vimentin-positive mesenchymal cells (arrows) are seen (A), whereas no cells positive for desmin (C) or α-SMA (E) are seen. In ANIT-injected rats, vimentin (B)-, desmin (D)- and α-SMA (F)-positive mesenchymal cells (apparently myofibroblasts) (arrows) are seen in the fibrotic lesions in the affected Glisson's sheath; particularly, α-SMA-positive myofibroblasts are present exclusively around the proliferating bile ducts (F, arrows). Desmin- and α-SMA-positive vascular smooth muscles (arrowheads) were excluded from the evaluation. **IA**: interlobular arteriole, **IB**: interlobular bile duct, **IV**: interlobular vein. Immunohistochemistry, counterstained with hematoxylin.

Fig. 9. Double immunofluorescence labeling for myofibroblast markers (desmin/vimentin, α-SMA/vimentin, and α-SMA/desmin) in the affected Glisson's sheath of ANIT-injected rats at PFI week 19. Photomicrographs show myofibroblasts labeled with desmin (green, A; arrows) and vimentin (red, B; arrows), α-SMA (green, D; arrows) and desmin (red, E; arrows), or α-SMA (green, G; arrows) and vimentin (red, H; arrows). Digital merges show the double labeling for both desmin and vimentin (yellow, C; arrows) or α-SMA and desmin (yellow, F; arrows), whereas no cells reacting to both α-SMA and vimentin are seen (I; an arrow indicates α-SMA-positive myofibroblasts surrounding IB). Desmin- and α-SMA-positive vascular smooth muscles (arrowheads) were excluded from the evaluation. **IV**: interlobular vein. Immunofluorescence, DAPI for nuclear staining.

Fig. 10. mRNA expressions of monocyte chemoattractant protein-1 (MCP-1) (A), transforming growth factor-β1 (TGF-β1) (B), and colony stimulating factor-1 (CSF-1) (C) by the real-time PCR in control and ANIT-injected rats. **Cont**: control. Student's *t*-test. *; $P<0.05$.

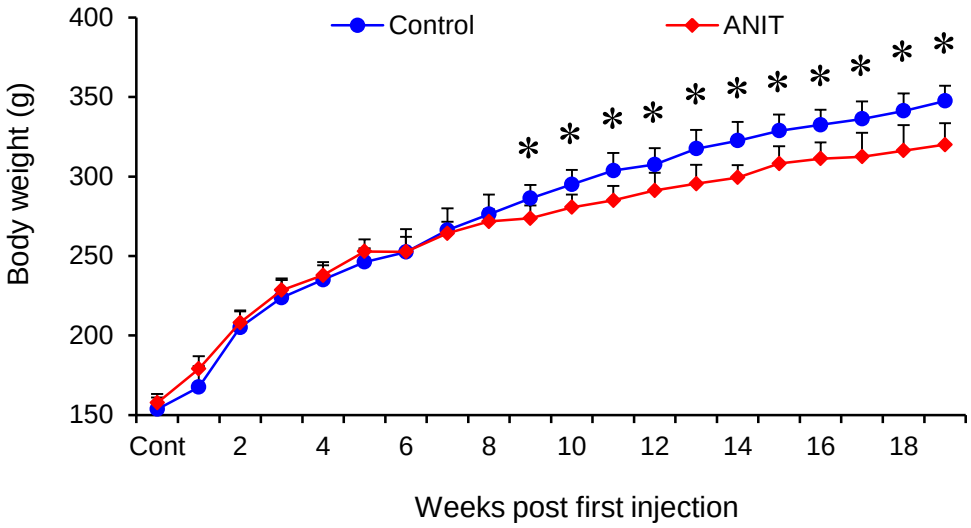
Control
ANIT
Body weight (g)
400
350
300
250
200
150
Cont
2
4
6
8
10
12
14
16
18
Weeks post first injection
*
*
*
*
*
*
*
*
*
*

Fig. 1

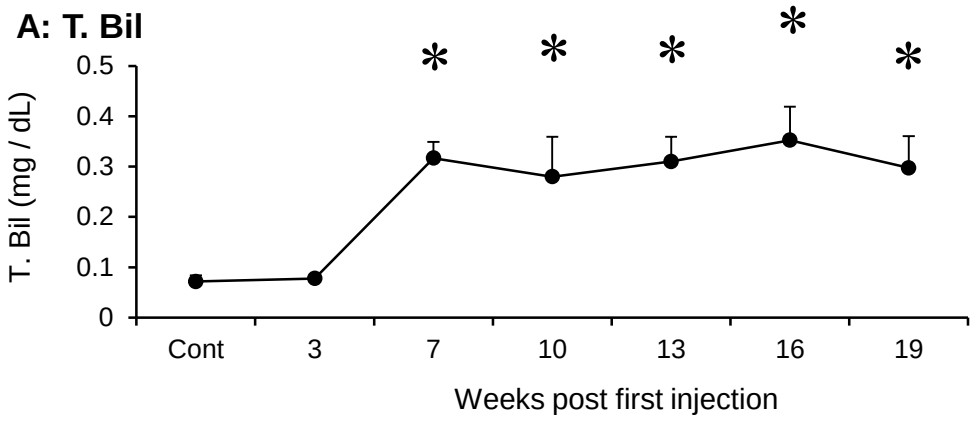
A: T. Bil
T. Bil (mg / dL)
0.5
0.4
0.3
0.2
0.1
0
Cont
3
7
10
13
16
19
Weeks post first injection

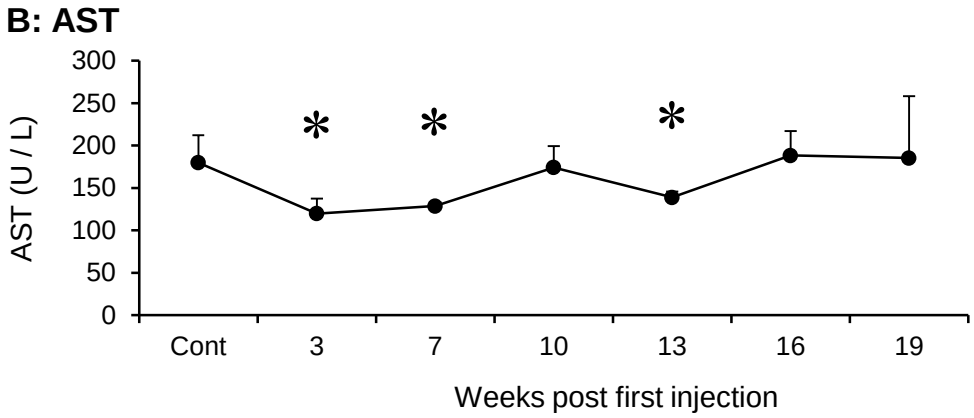
B: AST
AST (U / L)
300
250
200
150
100
50
0
Cont
3
7
10
13
16
19
Weeks post first injection

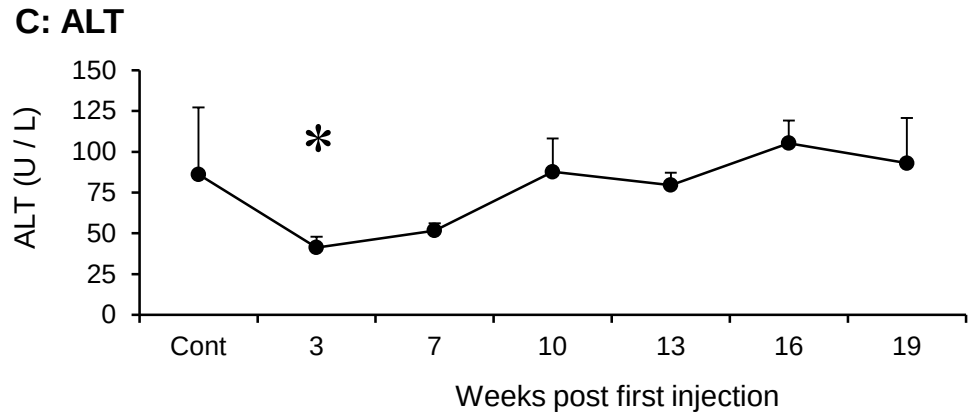
C: ALT
ALT (U / L)
150
125
100
75
50
25
0
Cont
3
7
10
13
16
19
Weeks post first injection

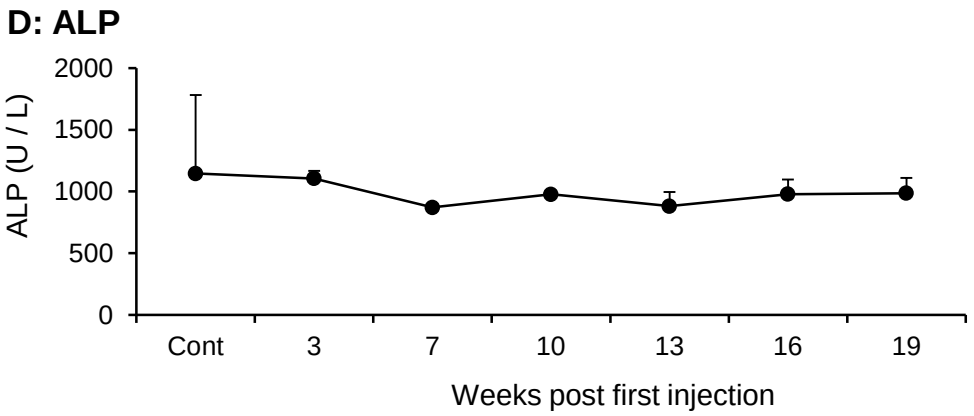
D: ALP
ALP (U / L)
2000
1500
1000
500
0
Cont
3
7
10
13
16
19
Weeks post first injection

Fig. 2

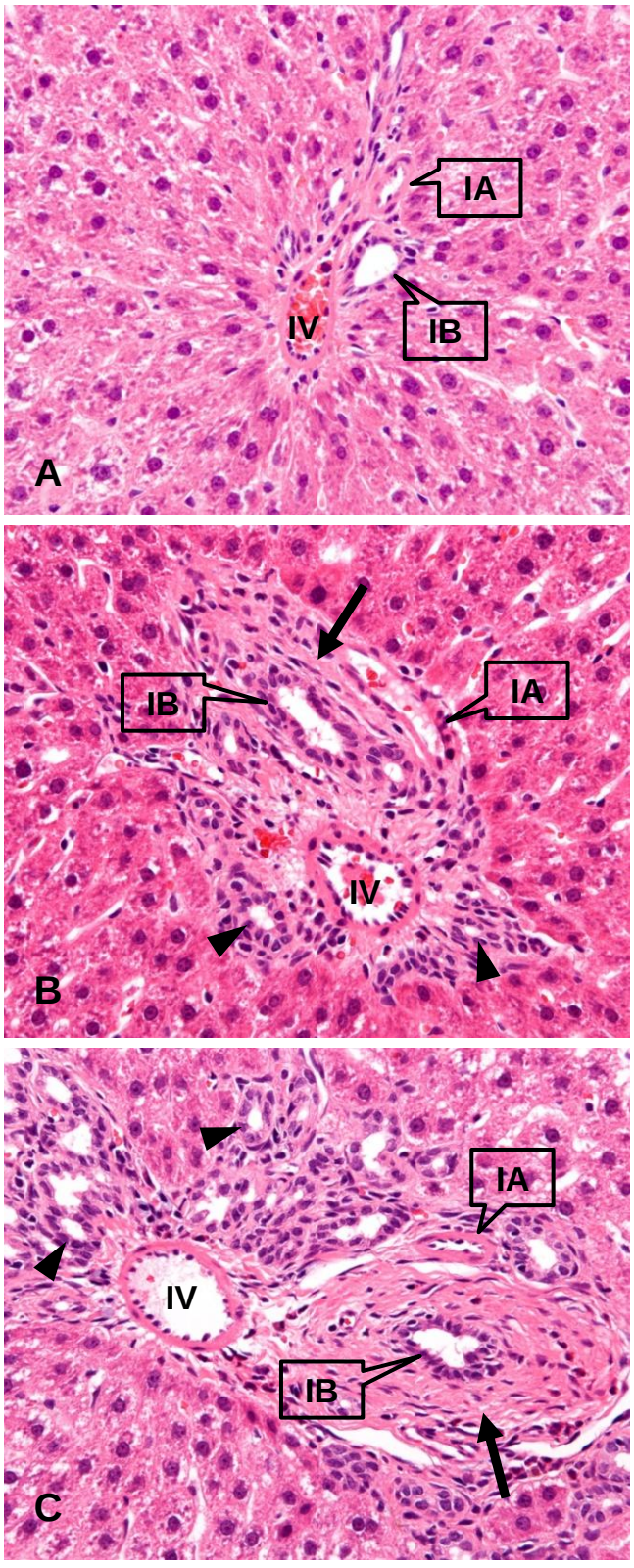

Fig. 3

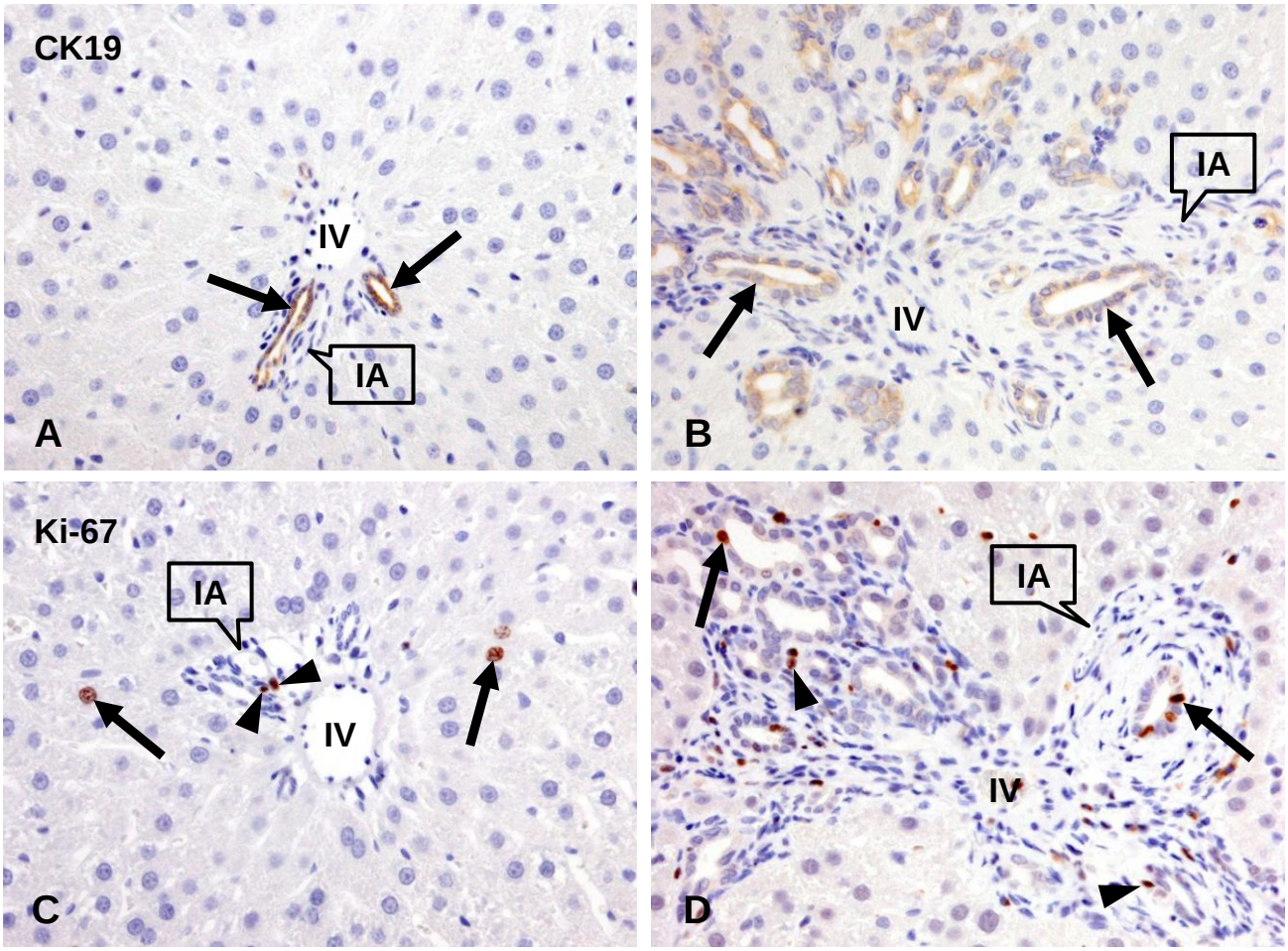

Fig. 4

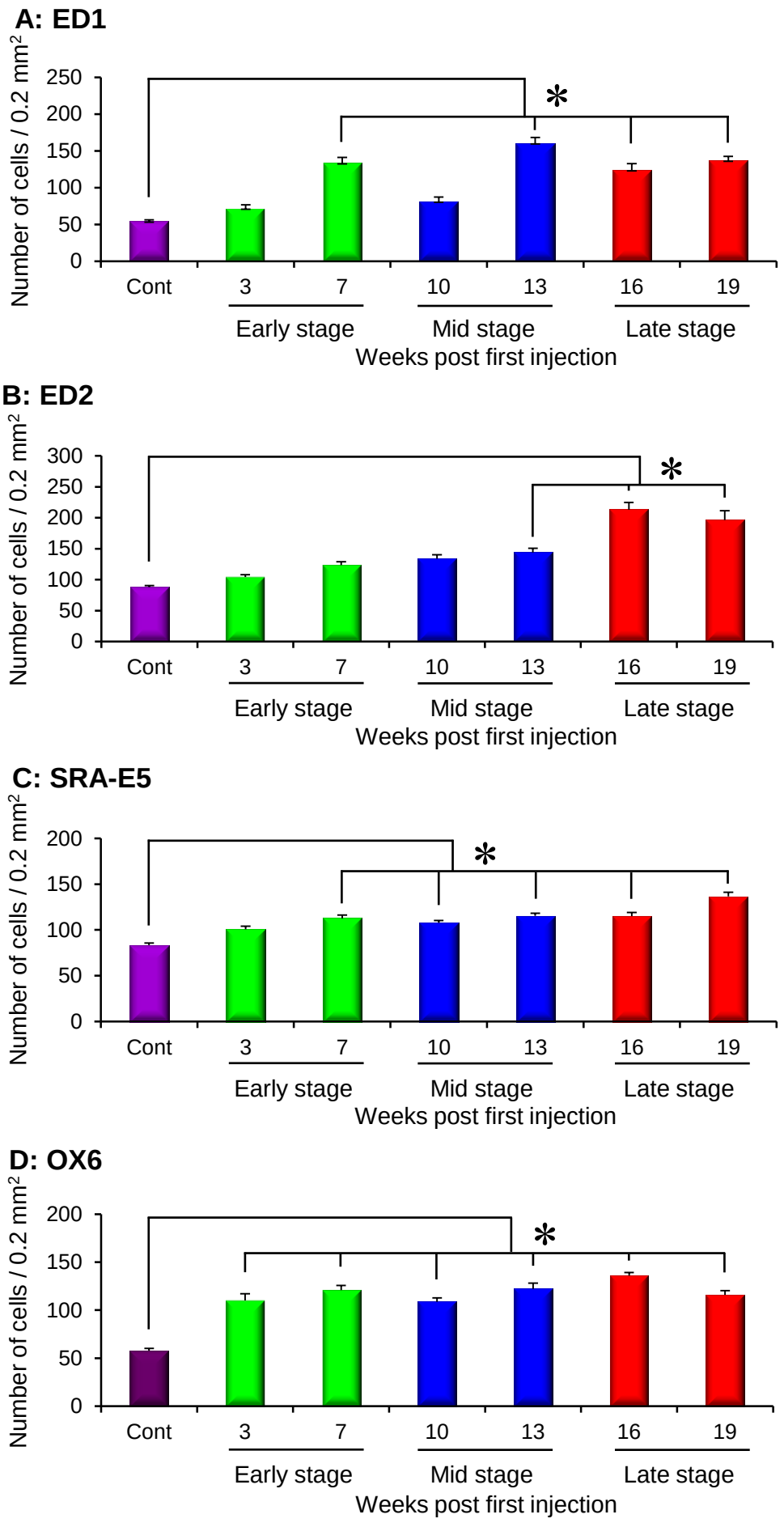
A: ED1
Number of cells / 0.2 mm2
250
200
150
100
50
0
*
Cont
3
7
10
13
16
19
Early stage
Mid stage
Late stage
Weeks post first injection
B: ED2
Number of cells / 0.2 mm2
300
250
200
150
100
50
0
*
Cont
3
7
10
13
16
19
Early stage
Mid stage
Late stage
Weeks post first injection
C: SRA-E5
Number of cells / 0.2 mm2
200
150
100
50
0
*
Cont
3
7
10
13
16
19
Early stage
Mid stage
Late stage
Weeks post first injection
D: OX6
Number of cells / 0.2 mm2
200
150
100
50
0
*
Cont
3
7
10
13
16
19
Early stage
Mid stage
Late stage
Weeks post first injection

Fig. 5

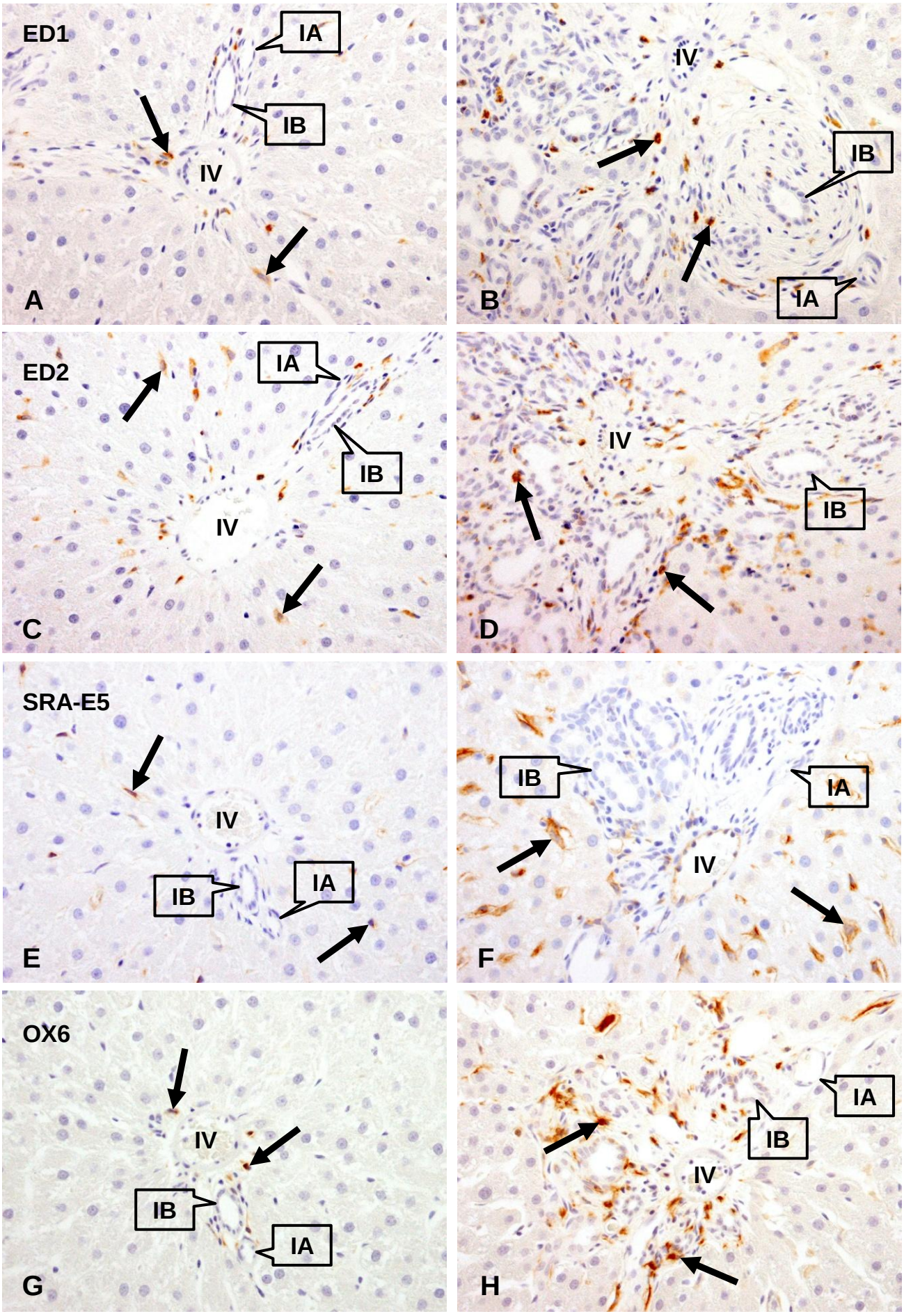
ED1
IA
IB
IV
A
IV
IB
IA
B
ED2
IA
IB
IV
C
IV
IB
D
SRA-E5
IV
IB
IA
E
IB
IA
IV
F
OX6
IV
IB
IA
G
IA
IB
IV
H

Fig. 6

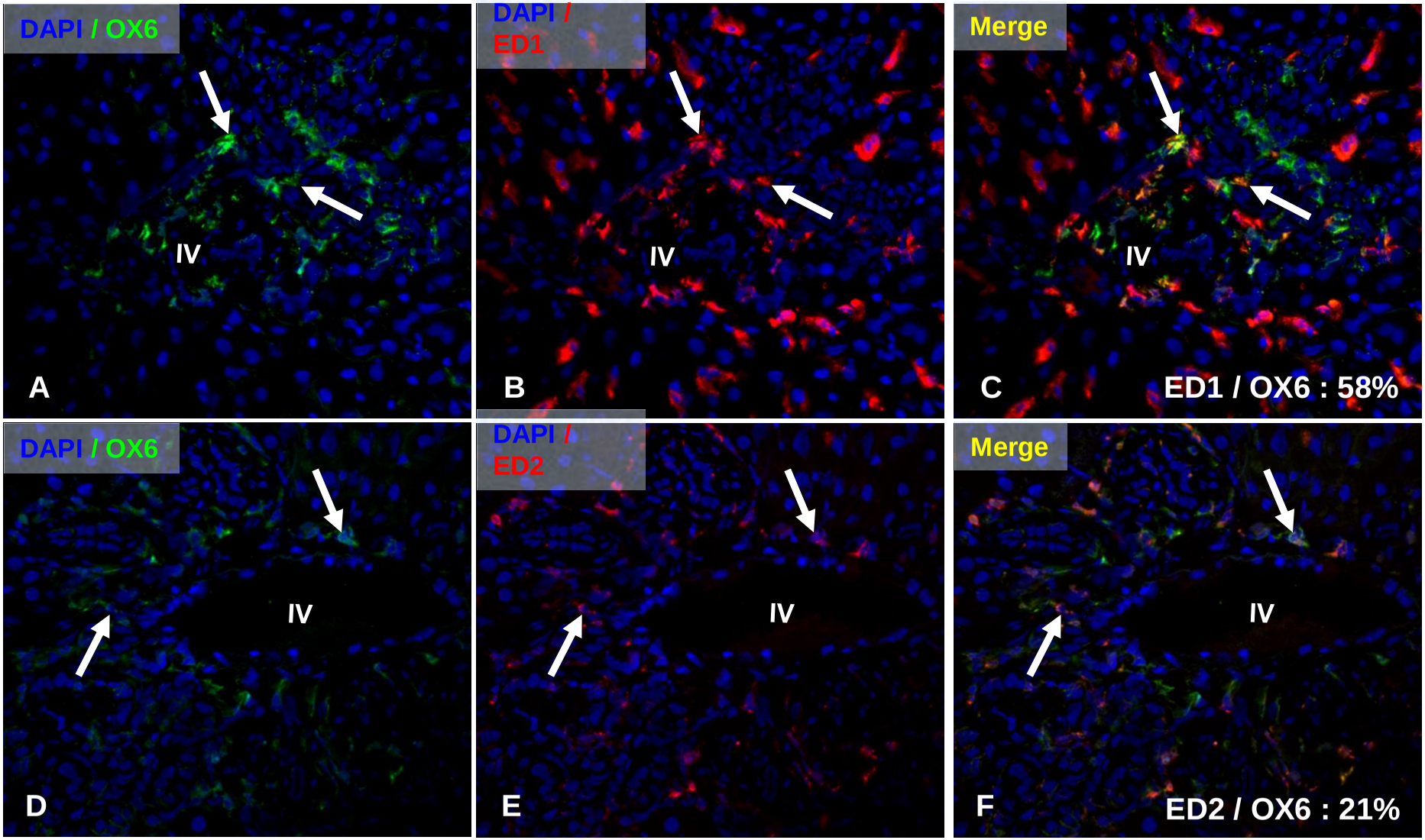
DAPI / OX6
IV
A
DAPI / ED1
IV
B
Merge
IV
C
ED1 / OX6 : 58%
DAPI / OX6
IV
D
DAPI / ED2
IV
E
Merge
IV
F
ED2 / OX6 : 21%

Fig. 7

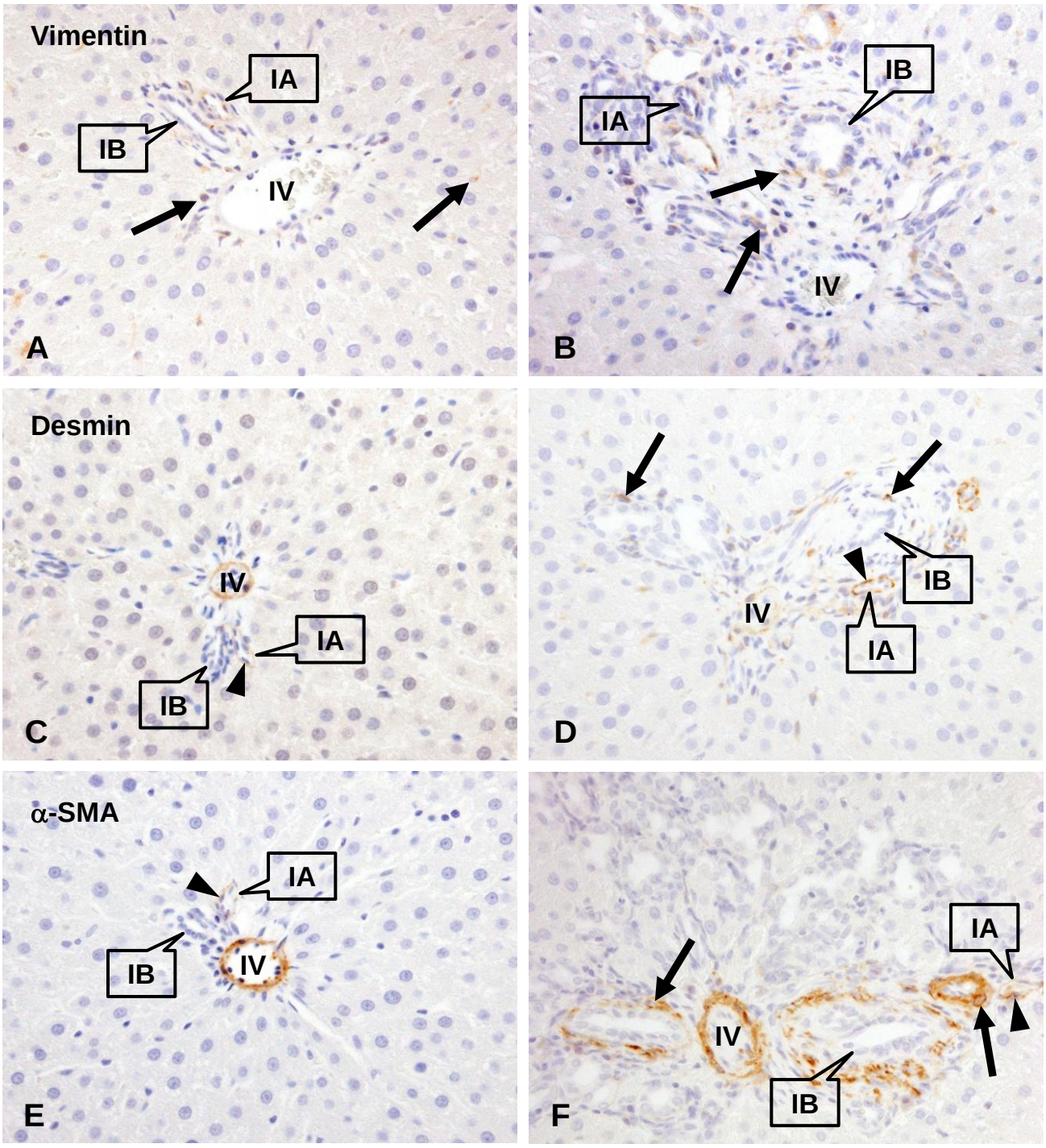
Vimentin
IA
IB
IV
A
IB
IA
IV
B
Desmin
IV
IA
IB
C
IV
IB
IA
D
α-SMA
IA
IB
IV
E
IA
IV
IB
F

Fig. 8

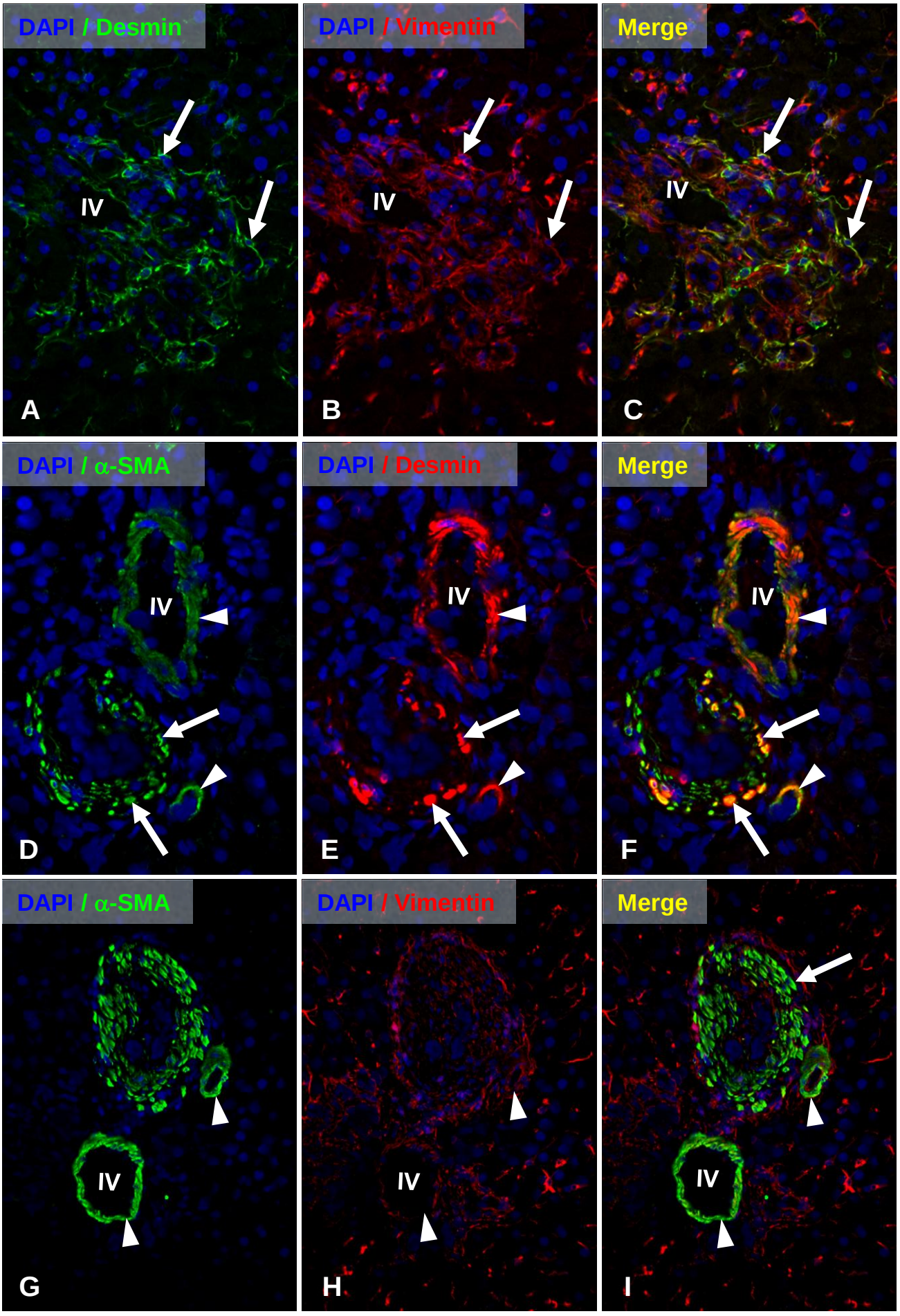
DAPI / Desmin
DAPI / Vimentin
Merge
IV
A
B
C
DAPI / α-SMA
DAPI / Desmin
Merge
D
E
F
DAPI / α-SMA
DAPI / Vimentin
Merge
G
H
I

Fig. 9

A: MCP-1

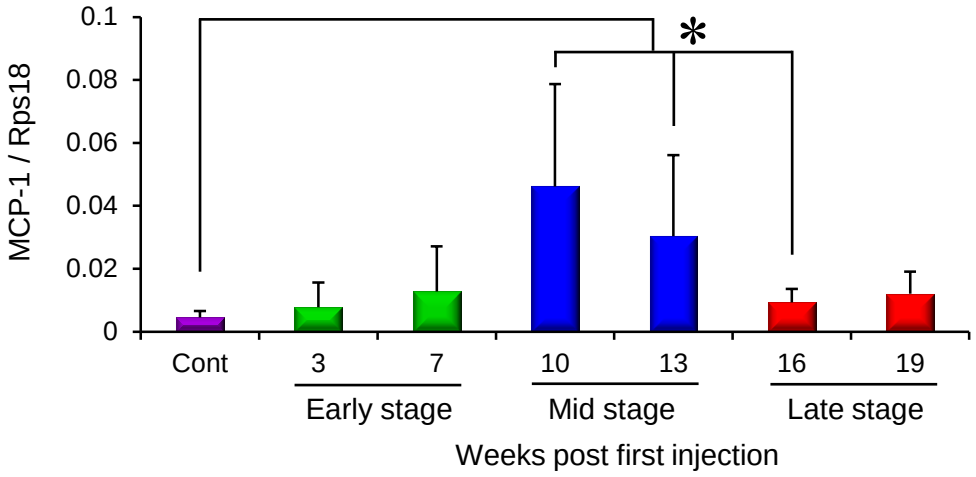

B: TGF-β1

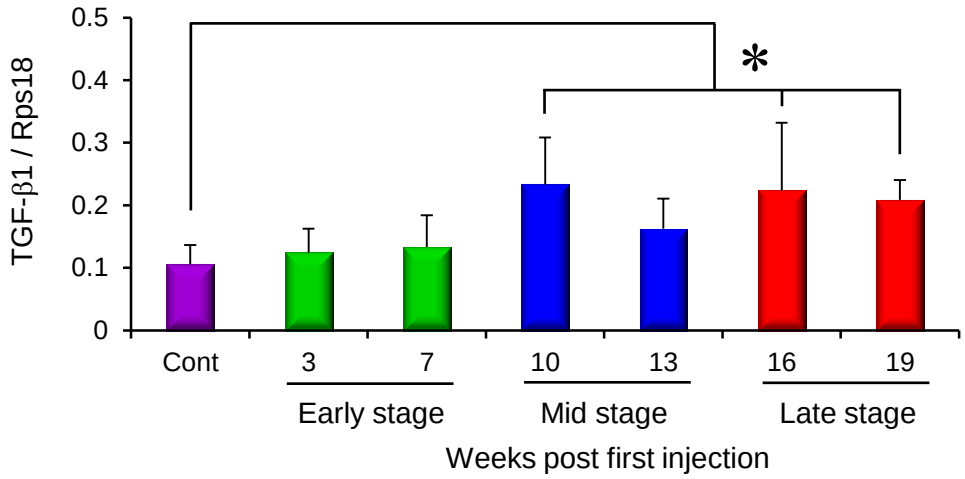

C: CSF-1

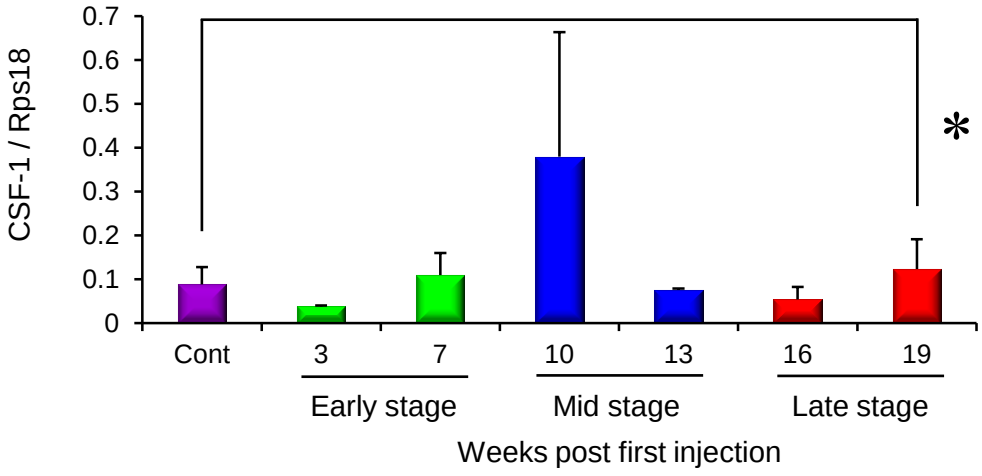

Fig. 10

Chapter 5

Comparisons of Macrophage and Myofibroblast Properties between Acute and Chronic Rat Biliary Fibrosis Models

In this thesis, the author has focused on the properties of macrophages and myofibroblasts in biliary fibrosis. Particularly, in chapters 3 and 4, the author investigated the characteristics of these cell populations in acute and chronic biliary injury fibrosis models induced in rats by single or repeated injections of α-naphthylisothiocyanate (ANIT), respectively. In order to shed comprehensively some insight on the mechanisms behind the biliary fibrosis, in chapter 5, comparisons were made in the properties of macrophages and myofibroblasts between the acute and chronic biliary fibrosis models; additionally, a comparison is made between acute biliary fibrosis in chapter 3 and acute perivenular fibrosis induced in rats by thioacetamide (TAA; a toxicant causing hepatocyte injury in the centrivenular area) which had been previously performed in the author's laboratory (Mori et al. 2009). ANIT-induced acute and chronic biliary fibrosis are designated as acute ANIT and chronic ANIT models, respectively. Acute perivenular fibrosis by TAA was named as acute TAA model.

Comparisons of macrophage immunophenotypes between the acute and chronic ANIT models (Table 1, Fig. 1)

In acute and chronic ANIT models, macrophage immunophenotypes for ED1 (CD68, reflecting phagocytosis), ED2 (CD163, reflecting proinflammatory cytokine production), SRA-E5 (CD204, reflecting lipid metabolism) and OX6 (MHC class II, reflecting antigen presentation capacity) were evaluated. In both the models, characteristically, OX6-expressing macrophages consistently increased almost throughout the entire experiment period, followed by increments of SRA-E5- and ED1-positive macrophages. These findings indicate that OX6-positive macrophages are the first responder in both the models. In chapter 1, the author demonstrated that OX6-positive macrophages existed in the Glisson's sheath as the interstitial dendritic cells in normal livers. OX6-positive macrophages, which may be stimulated by cholangiocytes injured by ANIT, can induce macrophages reacting to SRA-E5 and ED1 in the affected Glisson's

sheath. More interestingly, ED2-positive macrophages were only transiently increased in the acute model, whereas macrophages reacting to ED2 showed an increase at the late stages in the chronic model. In chapter 1, it was shown that ED2-positive macrophages in normal liver are regarded as Kupffer cells. Based on these findings, it is considered that the participation of Kupffer cells may be slight in the acute ANIT model, and delay in the chronic ANIT model. In addition, the kinetics of ED2-positive macrophages is different between the acute and chronic ANIT models.

Comparisons of myofibroblast properties between the acute and chronic ANIT models (Table 1, Fig. 2)

In the acute and chronic ANIT models, expressions of vimentin, desmin and α-smooth muscle actin (α-SMA) were investigated to know characteristics of myofibroblasts and their origin. In the acute ANIT model, vimentin- and desmin-expressions were increased at the early and mid stages, whereas α-SMA was increased at the mid and late stages. In the chronic ANIT model, vimentin-expressing cells relatively consistently increased at the early to late stages, and α-SMA-expressing cells showed an increase at the mid and late stages. However, the desmin-positive cells were rarely seen in the chronic ANIT models. In chapter 2, in *Fasciola* infection-induced chronic biliary cirrhosis in cattle as spontaneous lesion, desmin-positive cells were fewer, and vimentin- and α-SMA-positive cells were more predominant, indicating that vimentin and α-SMA may be expressed in advanced fibrotic lesions. On the basis of these findings, because α-SMA expression is the major marker of development of myofibroblasts, it is considered that well-differentiated myofibroblasts at the mid and late stages (advanced stages) in both the acute and chronic ANIT models can come to express α-SMA. Desmin and vimentin have been considered to express mainly in hepatic stellate cells (HSCs) and pre-existing fibroblasts in the Glisson's sheath, respectively, in normal livers. The portal fibroblasts are characterized by positivity for vimentin but no reactivity for desmin, and HSCs in normal

rat livers are identified by positivity both for vimentin and desmin (Penz-Österreicher et al. 2011). Therefore, the origin of myofibroblasts in the acute and chronic ANIT models may be portal fibroblasts/HSCs and portal fibroblasts, respectively, based on the expression patterns of cytoskeletons.

In both the models, TGF-β1 expression is related to the appearance of α-SMA-positive myofibroblasts at the mid and late stages. TGF-β1 may be able to induce α-SMA cytoskeletons in developing myofibroblasts.

Comparisons of macrophage immunophenotypes between the acute ANIT and TAA models (Table 2, Fig. 3)

The author investigated the properties of macrophages appearing in the affected Glisson's sheath in the acute ANIT models in chapter 3. Previously, the author's laboratory had investigated the macrophage properties in the perivenular fibrosis after TAA-induced hepatocyte injury. Therefore, the author compared the properties of macrophages between the acute ANIT and TAA models.

In the acute ANIT model, the most predominant cell type was OX6-positive macrophages showing almost consistently increased number, followed by ED1-positive macrophages. The participation of ED2-positive macrophage was simply transient. On the other hand, in the acute TAA model, ED1- and ED2-positive macrophages are major cells, with more early and consistent appearance of ED1-positive cells; OX6-positive cells were small in the number. These findings indicate that there are clearly differences in macrophage properties between the acute ANIT and TAA models (biliary vs. perivenular fibrosis); the predominant cell for the acute ANIT model is OX6-positive cells, whereas ED1-positive cells are the most important cell type for the acute TAA model. It is considered that antigen presenting cells (OX6-positive cells) in the Glisson's sheath may regulate the biliary fibrosis, and that resident (Kupffer cells) and blood monocyte-derived

macrophages (these macrophage can react to ED1) may play important roles in perivenular fibrosis. It is interesting to pursue the characteristics of these macrophages in more detail.

Table 1. Comparisons of macrophage and myofibroblast properties between the acute and chronic ANIT models

	Acute ANIT model	Chronic ANIT model
Macrophages		
OX6+ cells	Almost consistently increased during the entire experiment	Consistently increased during the entire experiment
SRA-E5+ cells	Increased with OX6+ cells increment; remained increased until the end	Increased after OX6+ cells increment; remained increased until the end
ED2+ cells	Transiently increased at the early stages	Significantly increased at the late stages
ED1+ cells	Increased at the early and mid stages	Increased at the early to late stages after OX6+ cells increment
Myofibroblasts		
Cytoskeleton expression	Expressed mainly vimentin and desmin at the early stages and α-SMA at the late stages	Expressed consistently vimentin and α-SMA at the mid and late stages; less expression of desmin
TGF-β1 expression	Transiently increased at the late stage, corresponding to α-SMA expression	Increased at the mid and late stages, corresponding to α-SMA expression
Pathogenesis of fibrosis	Interplay of macrophages with portal fibroblasts and HSCs	Interplay of macrophages mainly with portal fibroblasts

ANIT: α-naphthylisothiocyanate, **TAA**: thioacetamide, **TGF**-β1: transforming growth factor-β1 (a fibrogenic factor), **α-SMA**: α-smooth muscle actin, **HSCs**: hepatic stellate cells. OX6 for MHC class II, SRA-E5 for CD204, ED2 for CD163, ED1 for CD68.

Table 2. Comparisons of macrophage properties between acute ANIT and TAA models

Macrophages	Acute ANIT model	Acute TAA model
OX6+ cells	Most predominant almost throughout the experiment	Transiently increased at the early stages
ED2+ cells	Transiently increased at the early stages	Transiently increased at the early stage with predominance
ED1+ cells	Increased at the early and mid stages	Most predominant cells throughout the experiment

ANIT: α-naphthylisothiocyanate, **TAA**: thioacetamide. OX6 for MHC class II, ED2 for CD163, ED1 for CD68.

A: Acute ANIT model

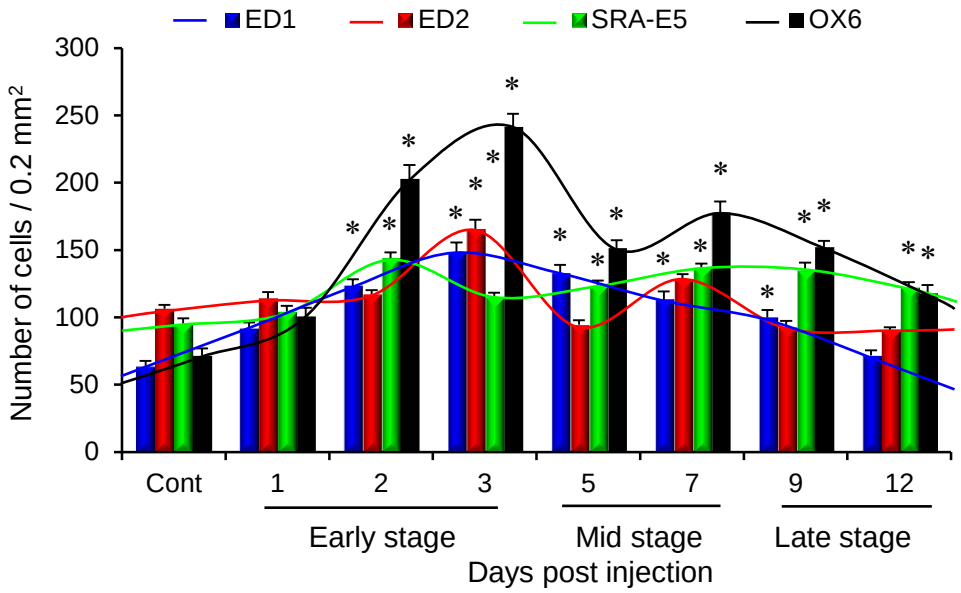

B: Chronic ANIT model

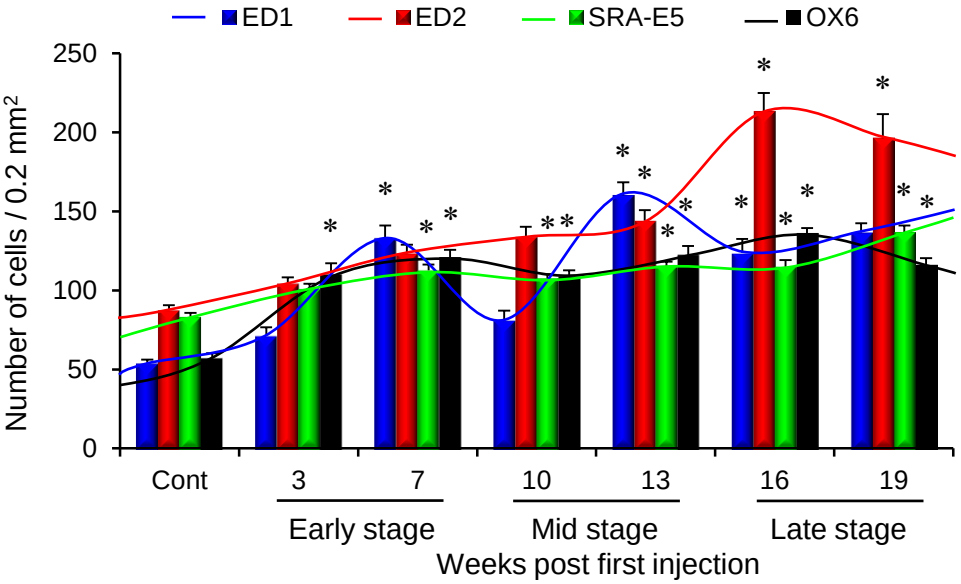

Fig. 1. Comparisons of macrophage properties between acute and chronic biliary fibrosis models (acute and chronic ANIT models). Details are described in the text. **Cont**: control. *; $P<0.05$.

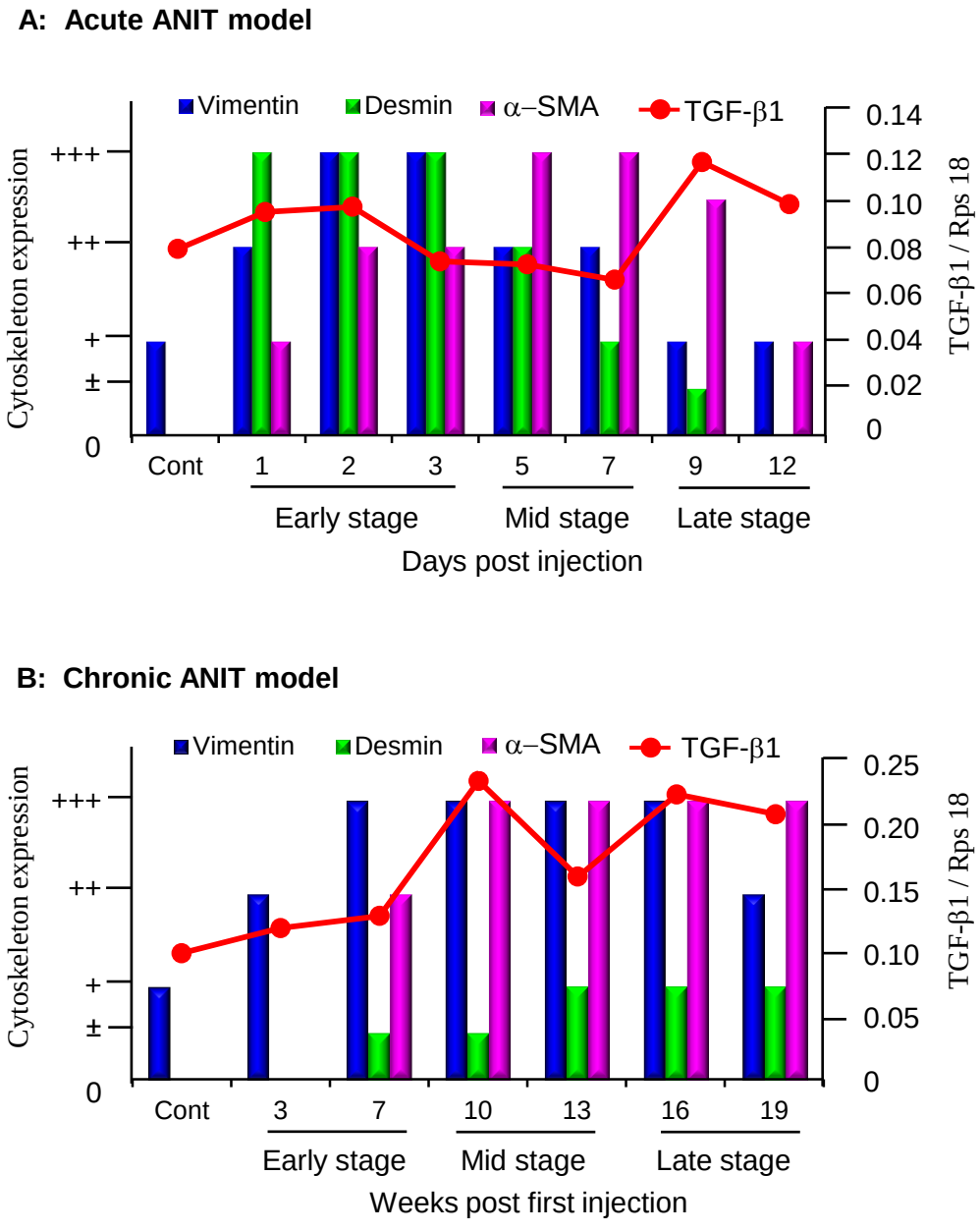

Fig. 2. Comparisons of myofibroblast properties between acute and chronic biliary fibrosis models (acute and chronic ANIT models). Details are described in the text. **Cont**: control. *; $P<0.05$.

A: Acute ANIT model

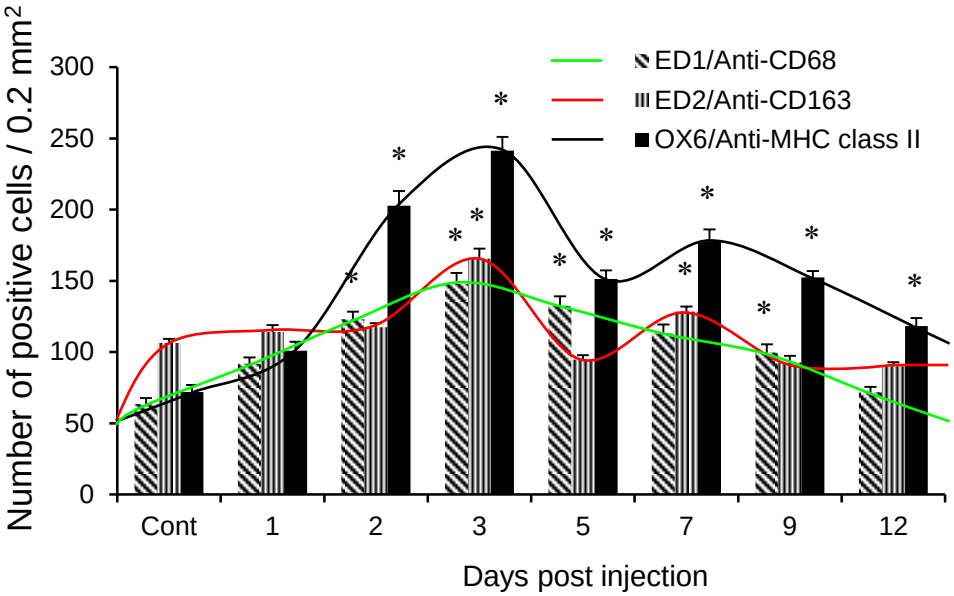

B: Acute TAA model

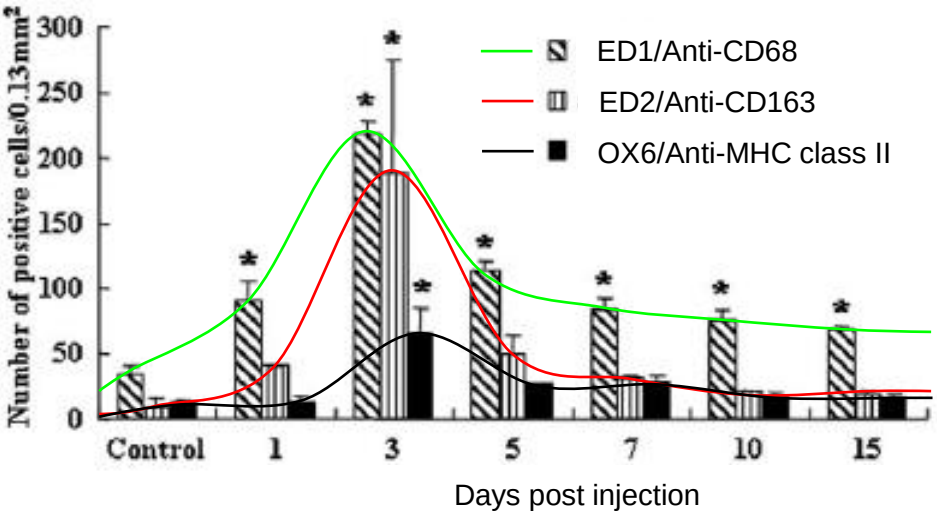

Fig. 3. Comparisons of macrophage properties between acute hepatocyte injury model induced by α-naphthylisothiocyanate (acute ANIT model) in the current study (A) and acute hepatocyte injury model induced by thioacetamide (acute TAA model) investigated previously by Mori et al. 2009 in the author's laboratory (B). Details are described in the text. **Cont**: control. *; $P<0.05$.

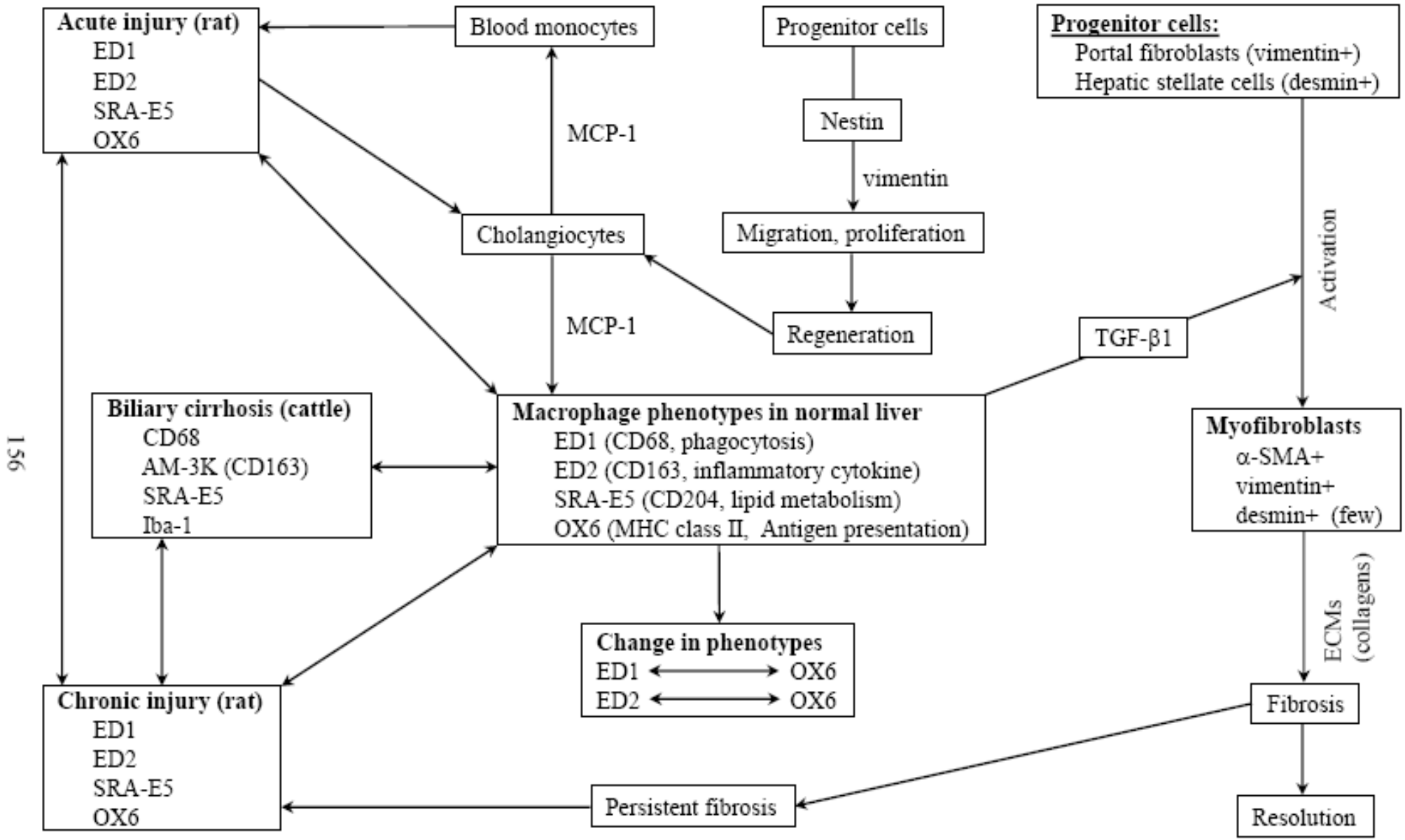

Scheme 1: Pathogenesis of biliary fibrosis based on macrophage phenotypes and myofibroblast properties in acute and chronic ANIT biliary fibrosis and *Fasciola*-infected biliary cirrhosis (detailed explanations are in chapters 1-5).

Conclusions

To clarify the pathogenesis of biliary fibrosis, the author investigated the properties of macrophages and myofibroblasts at the cellular and molecular levels using developing rat livers, *Fasciola* infection-induced biliary cirrhosis in cattle, and α-naphthylisothiocyanate (ANIT)-induced acute and chronic biliary fibrosis in rats. Based on the findings, the following conclusions are drawn:

1. Heterogeneous macrophage populations participate in rat liver formation; they show different distributions and functions, depending on age.
2. In *Fasciola*-infected cattle livers with cirrhosis as spontaneous lesions, CD68+ (phagocytosis) and CD163+ (proinflammatory factor production) macrophages are more predominant in fibrotic lesions; myofibroblasts variously express cytoskeletons, mainly α-smooth muscle actin (α-SMA) and vimentin.
3. In ANIT-induced acute and chronic biliary fibrosis, macrophages exhibit heterogeneous properties (phagocytosis, proinflammatory factor production, lipid metabolism, and MHC class II expression), demonstrable with immunohistochemistry, depending on stages of lesion progress in the damaged Glisson's sheath. Of them, MHC class II+ macrophages may have central roles in the lesion development as the predominant cell.
4. Additionally, myofibroblasts in ANIT-induced lesions in the Glisson's sheath display various cytoskeletons such as vimentin, desmin and α-SMA; in biliary fibrosis, desmin (although the reactivity is faint) tends to be expressed at early stages, and vimentin and α-SMA at mid and late stages.
5. Nestin expression would be used as an indicator for regeneration in injured cells in the Glisson's sheath.
6. Because ANIT-induced lesions in the Glisson's sheath resemble human biliary fibrosis, these lesions would be beneficial to clarify the underlying mechanisms of biliary fibrosis, as well as to test efficacy of anti-fibrotic agents as animal models.

References

Abboud SL, Bunegin M, Choudhury NG and Woodruff K. Analysis of the mouse CSF-1 gene promoter in a transgenic mouse model. Journal Histochemistry and Cytochemistry **51**: 941–949, 2003.

Abdel-Aziz G, Rescan PY, Clement B, Lebeau G, Rissel M, Grimaud JA, Campion JP and Guillouzo A. Cellular sources of matrix proteins in experimentally induced cholestatic rat liver. Journal of Pathology **164**: 167–174, 1991.

Abraham EJ, Kodama S, Lin JC, Ubeda M, Faustman DL and Habener JF. Human pancreatic islet-derived progenitor cell engraftment in immunocompetent mice. The American Journal of Pathology **164**: 817–830, 2004.

Akiyoshi H and Terada T. Centrilobular and perisinusoidal fibrosis in experimental congestive liver in the rat. Journal of Hepatology **30**: 433–439, 1999.

Andrews SJ. The life-cycle of *Fasciola hepatica*. In: Dalton JP(ed). Fasciolosis. CAB International, Oxford. pp. 1–29, 1999.

Armbrust T and Ramadori G. Functional characterization of two different Kupffer cell populations of normal rat liver. Journal of Hepatology **25**: 518–528, 1996.

Asahina K, Tsai SY, Li P, Ishii M, Maxson RE Jr, Sucov HM and Tsukamoto H. Mesenchymal origin of hepatic stellate cells, submesothelial cells, and perivascular mesenchymal cells during mouse liver development. Hepatology **49**: 998-1011, 2009.

Azumi N and Battifora H. The distribution of vimentin and keratin in epithelial and nonepithelial neoplasms. A comprehensive immunohistochemical study on formalin-

and alcohol-fixed tumors. American Journal of Clinical Pathology **88**: 286–296, 1987.

Baba S, Fujii H, Hirose T, Yasuchika1 K, Azuma H, Hoppo T, Naito M, Machimoto T and Ikai I. Commitment of bone marrow cells to hepatic stellate cells in mouse. Journal of Hepatology **40**: 255–260, 2004.

Bataller R and Brenner DA. Liver fibrosis. The Journal of Clinical Investigation **115**: 209–218, 2005.

Beaussier M, Wendum D, Schiffer E, Dumont S, Rey C, Lienhart A and Housset C. Prominent contribution of portal mesenchymal cells to liver fibrosis in ischemic and obstructive cholestatic injuries. Laboratory Investigation **87**: 292–303, 2007.

Bouhlel MA, Derudas B, Rigamonti E, Dievart R, Brozek J, Haulon S, Zawadzki C, Jude B, Torpier G, Marx N, Staels B and Chinetti-Gbaguidi G. PPARgamma activation primes human monocytes into alternative M2 macrophages with anti-inflammatory properties. Cell Metabolism **6**: 137–143, 2007.

Bouwens L. Proliferation and phenotypic expression of non-parenchymal liver cells. Scandinavian Journal of Gastroenterology **23**: 46–51, 1988.

Brancato SK and Albina JE. Wound macrophage as key regulators of repair: origin, phenotype, and function. The American Journal of Pathology **178**: 19–25, 2011.

Burt AD. Pathobiology of hepatic stellate cells. Journal of Gastroenterology **34**: 299–304, 1999.

Calvo JR, Reiter RJ, Garcia JJ, Ortiz GG, Tan DX and Karbownik M. Characterization of the protective effects of melatonin and related indoles against α-naphthylisothiocyanate-induced liver injury in rats. Journal of Cellular Biochemistry **80**: 461–470, 2001.

Carotti S, Morini S, Corradini SG, Burza MA, Molinaro A, Carpino G, Merli M, De Santis A, Muda AO, Rossi M, Attili AF and Gaudio E. Glial fibrillary acidic protein as an early marker of hepatic stellate cell activation in chronic and posttransplant recurrent hepatitis C. Liver Transplantation **14**: 806–814, 2008.

Chaurasia SS, Kaur H, de Medeiros FW, Smith SD and Wilson SE. Reprint of "Dynamics of the expression of intermediate filaments vimentin and desmin during myofibroblast differentiation after corneal injury". Experimental Eye Research **89**: 590–596, 2009.

Clouston AD, Powell EE, Walsh MJ, Richardson MM, Demetris AJ and Jonsson JR. Fibrosis correlates with a ductular reaction in hepatitis C: roles of impaired replication, progenitor cells and steatosis. Hepatology **41**: 809–818, 2005.

Connolly MK, Bedrosian AS, Clair JM, Mitchell AP, Ibrahim J, Stroud A, Pachter HL, Bar-Sagi D, Frey AB and Miller G. In liver fibrosis, dendritic cells govern hepatic inflammation in mice via TNF-α. Journal of Clinical Investigation **119**: 3213–3225, 2009.

Coulombe PA and Wong P. Cytoplasmic intermediate filaments revealed as dynamic and multipurpose scaffolds. Nature Cell Biology **6**: 699–706, 2004.

Damoiseaux JG, Dopp EA, Calame W, Chao D, MacPherson GG and Dijkstra CD. Rat macrophage lysosomal membrane antigen recognized by monoclonal antibody ED1. Immunology **83**: 140–147, 1994.

Diegelmann RF, Guzelian PS, Gay R and Gay S. Collagen formation by the hepatocyte in primary monolayer culture and in vivo. Science **219**: 1343–1345, 1983.

Dietrich CG, Ottenhoff R, de Waart DR and Oude Elferink RP. Role of MRP2 and GSH in intrahepatic cycling of toxins. Toxicology **167**: 73–81, 2001.

Dijkstra CD, Dopp EA, Joling P and Kraal G. The heterogeneity of mononuclear phagocytes in lymphoid organs: distinct macrophage subpopulations in the rats recognized by monoclonal antibody ED1, ED2 and ED3. Immunology **54**: 589–599, 1985.

Dooley S, Hamzavi J, Ciuclan L, Godoy P, Ilkavets I, Ehnert S, Ueberham E, Gebhardt R, Kanzler S, Geier A, Breitkopf K, Weng H and Mertens PR. Hepatocyte-specific Smad7 expression attenuates TGF-beta-mediated fibrogenesis and protects against liver damage. Gastroenterology **135**: 642–659, 2008.

Dranoff JA and Wells RG. Portal fibroblasts: unappreciated mediators of biliary fibrosis. Hepatology **51**: 1438–1444, 2010.

Fabriek BO, Dijkstra CD and van den Berg TK. The macrophage scavenger receptor CD163. Immunobiology **210**: 153–160, 2005.

Forbes SJ, Russo FP, Rey V, Burra P, Rugge M, Wright NA and Alison MR. A significant proportion of myofibroblasts are of bone marrow origin in human liver fibrosis. Gastroenterology **126**: 955–963, 2004.

Friedman S. Molecular regulation of hepatic fibrosis, an integrated cellular response to tissue injury. The Journal of Biological Chemistry **275**: 2247–2250, 2000.

Friedman SL, Roll FJ, Boyles J and Bissell DM. Hepatic lipocytes: the principal collagen-producing cells of normal rat liver. Proceedings of the National Academy of Sciences, USA **82**: 8681–8685, 1985.

Friedman SL. Liver fibrosis-from bench to bedside. Journal of Hepatology **38**: S38–53, 2003.

Friedman SL. Mechanism of hepatic fibrogenesis. Gastroenterology **134**: 1655–1669, 2008.

Gao D, Mondal TK and Lawrence DA. Lead effects on development and function of bone marrow-derived dendritic cells promote Th2 immune responses. Toxicology and Applied Pharmacology **222**: 69–79, 2007.

Gard AL, White FP and Dutton GR. Extraneural glial fibrillary acidic protein (GFAP) immunoreactivity in perisinusoidal stellate cells of rat liver. Journal of Neuroimmunology **8**: 359–375, 1985.

Geraghty JM and Goldin RD. Liver changes associated with cholecystitis. Journal of Clinical Pathology **47**: 457–460, 1994.

Gharaee-Kermani M, Denholm EM and Phan SH. Costimulation of fibroblast collagen and transforming growth factor beta1 gene expression by monocyte chemoattractant protein-1 via specific receptors. Journal of Biological Chemistry **271**: 17779–17784, 1996.

Gleiberman AS, Encinas JM, Mignone JL, Michurina T, Rosenfeld MG and Enikolopov G. Expression of nestin-GFP transgene marks oval cells in the adult liver. Developmental Dynamics **234**: 413–421, 2005.

Golbar HM, Izawa T, Murai F, Kuwamura M and Yamate J. Immunohistochemical analyses of the kinetics and distribution of macrophages, hepatic stellate cells and bile duct epithelia in the developing rat liver. Experimental and Toxicologic Pathology **64**: 1–8, 2012.

Golbar HM, Izawa T, Yano R, Ichikawa C, Sawamoto O, Kuwamura M, Lamarre J, Yamate J. Immunohistochemical characterization of macrophages and myofibroblasts in α-naphthylisothiocyanate (ANIT)-induced bile duct injury and subsequent fibrogenesis in rats. Toxicologic Pathology **39**: 795–808, 2011.

Graversen JH, Madsen M and Moestrup SK. CD163: a signal receptor scavenging haptoglobin-hemoglobin complexes from plasma. The International Journal of Biochemistry and Cell Biology **34**: 309–314, 2002.

Greaves DR, Gough PJ and Gordon S. Recent progress in defining the role of scavenger receptors in lipid transport, atherosclerosis and host defense. Current Opinion in Lipidology **9**: 425–432, 1998.

Gressner OA and Gressner AM. Connective tissue growth factor: a fibrogenic master switch in fibrotic liver diseases. Liver International **28**: 1065–1079, 2008.

Greve JWM, Gouma DJ and Buurman WA. Complications in obstructive jaundice: role of endotoxins. Scandinavian Journal of Gastroenterology **194**: 8–12, 1992.

Grozdanov PN, Yovchev MI and Dabeva MD. The oncofetal protein glypican-3 is a novel marker of hepatic progenitor/oval cells. Laboratory Investigation **86**: 1272–1284, 2006.

Guo L, Enzan H, Hayashi Y, Miyazaki E, Jin Y, Toi M, Kuroda N and Hiroi M. Increased iron deposition in rat liver fibrosis induced by a high-dose injection of dimethylnitrosamine. Experimental and Molecular Pathology **81**: 255–261, 2006.

Hall WC and Rojko JL. The use of immunohistochemistry for evaluating the liver. Toxicologic Pathology **24**: 4–12, 1996.

Harada K, Chiba M, Okamura A, Hsu M, Sato Y, Igarashi S, Ren XS, Ikeda H, Ohta H, Kasashima S, Kawashima A and Nakanuma Y. Monocyte chemoattractant protein-1 derived from biliary innate immunity contributes to hepatic fibrogenesis. Journal of Clinical Pathology **64**: 660–665, 2011.

Haralanova-Ileava B, Ramadori G and Armbrust T. Expression of osteoactivin in rat and human liver and isolated rat liver. Journal of Hepatology **42**: 565–572, 2005.

Hautekeete M and Geerts A. The hepatic stellate (Ito) cell: its role in human liver disease. Virchows Archiv **430**: 195–207, 1997.

Haworth R, Platt N, Keshav S, Hughes D, Darley E, Suzuki H, Kurihara Y, Kodama T and Gordon S. The macrophage scavenger receptor type A is expressed by activated macrophages and protects the host against lethal endotoxic shock. The Journal of Experimental Medicine **186**: 1431–1439, 1997.

Herrmann H and Aebi U. Intermediate filaments and their associates: multi-talented structural elements specifying cytoarchitecture and cytodynamics. Current Opinion in Cell Biology **12**: 79–90, 2000.

Heymann F, Trautwein C and Tacke F. Monocytes and macrophages as cellular targets in liver fibrosis. Inflammation and Allergy-Drug Targets **8**: 307–318, 2009.

Hickling KC, Hitchcock JM, Chipman JK, Hammond TG and Evans JG. Induction and progression of cholangiofibrosis in rat liver injured by oral administration of furan. Toxicologic Pathology **38**: 213–229, 2010.

Hines JE, Johnson SJ and Burt AD. In vivo response of macrophages and perisinusoidal cells to cholestatic liver injury. The American Journal of Pathology **142**: 511–518, 1993.

Hinz B, Phan SH, Thannickal VJ, Galli A, Bochaton-Piallat ML and Gabbiani G. The myofibroblast: one function, multiple origins. The American Journal of Pathology **170**: 1807–1816, 2007.

Hoffman RM. The pluripotency of hair follicle stem cells. Cell Cycle. **5**: 232–233, 2006.

Hunziker E and Stein M. Nestin-expressing cells in the pancreatic islets of Langerhans. Biochemical and Biophysical Research Communications **271**: 116–119, 2000.

Ide M, Kuwamura M, Kotani T, Sawamoto O and Yamate J. Effects of gadolinium chloride ($GdCl_3$) on the appearance of macrophage populations and fibrogenesis in the thioacetamide induced rat hepatic lesions. Journal of Comparative Pathology **133**: 92–102, 2005.

Ide M, Yamate J, Kuwamura M, Kotani T, Sakuma S and Takeya M. Immunohistochemical analysis of macrophages and myofibroblasts appearing in hepatic and renal fibrosis of dogs. Journal of Comparative Pathology **124**: 60–69, 2001.

Ide M, Yamate J, Machda Y, Nakanishi M, Kuwamura M, Kotani T and Sawamoto O. Emergence of different macrophage populations in hepatic fibrosis following thioacetamide-induced acute hepatocytes injury in rats. Journal of Comparative Pathololology **128**: 41–51, 2003.

Ide M, Yamate J, Machida Y, Sawamoto O, Nakanishi M, Kuwamura M, Kotani T and Sakuma S. Macrophage populations, myofibroblastic cells, and extracellular matrix accumulation in chronically-developing rat liver cirrhosis induced by repeated injection of thioacetamide. Journal of Toxicologic Pathology **15**: 19–29, 2002.

Inagaki Y and Okazaki I. Emerging insights into Transforming growth factor β Smad signal in hepatic fibrogenesis. Gut **56**: 284–292, 2007.

Jafri M, Donnelly B, Bondoc A, Allen S and Tiao G. Cholangiocyte secretion of chemokines in experimental biliary atresia. Journal of Pediatric Surgery **44**: 500–507, 2009.

Jean PA, Kessel SL, Hill DA and Roth RA. Cytotoxicity of naphthylisothiocyanates in rat hepatocyte–neutrophil cocultures. Toxicology Letters **95**: 155–163, 1998.

Karlmark KR, Wasmuth HE, Trautwein C and Tacke F. Chemokine-directed immune cell infiltration in acute and chronic liver disease. Expert Review of Gastroenterology and Hepatology **2**: 233–242, 2008.

Karlmark KR, Weiskirchen R, Zimmermann HW, Gassler N, Ginhoux F, Weber C, Merad M, Luedde T, Trautwein C and Tacke F. Hepatic recruitment of the inflammatory Gr1+ monocyte subset upon liver injury promotes hepatic fibrosis. Hepatology **50**: 261–274, 2009.

Kim MR, Jeon ES, Kim YM, Lee JS and Kim JH. Thromboxane a(2) induces differentiation of human mesenchymal stem cells to smooth muscle-like cells. Stem Cells **27**: 191-199, 2009.

Kim Y, Ratziu V, Choi SG, Lalazar A, Theiss G, Dang Q, Kim SJ and Friedman SL. Transcriptional activation of transforming growth factor beta1 and its receptors by the Kruppel-like factor Zf9/core promoter-binding protein and Sp1: potential mechanisms for autocrine fibrogenesis in response to injury. Journal of Biological Chemistry **273**: 33750–33758, 1998.

Kisseleva T, Uchinami H, Feirt N, Quintana-Bustamante O, Segovia JC, Schwabe RF and Brenner DA. Bone marrow-derived fibrocytes participate in pathogenesis of liver fibrosis. Journal of Hepatology **45**: 429–438, 2006.

Kleeberger W, Bova GS, Nielsen ME, Herawi M, Chuang AY, Epstein JI and Berman DM. Roles for the stem cell associated intermediate filament nestin in prostate cancer migration and metastasis. Cancer Research **67**: 9199–9206, 2007.

Knittel T, Janneck T, Müller L, Fellmer P and Ramadori G. Transforming growth factor beta 1-regulated gene expression of Ito cells. Hepatology **24**: 352–360, 1996.

Kodali P, Wu P, Lahiji PA, Brown EJ and Maher JJ. ANIT toxicity toward mouse hepatocytes in vivo is mediated primarily by neutrophils via CD18. American Journal of Physiology Gastrointestinal and Liver Physiology **291**: G355–363, 2006.

Kohler C. Allograft inflammatory factor-1/Ionized calcium-binding adapter molecule 1 is specifically expressed by most subpopulations of macrophages and spermatids in testis. Cell and Tissue Research **330**: 291–302, 2007.

Kon J, Ichinohe N, Ooe H, Chen O, Sasaki K and Mitaka T. Thy1-positive cells have bipotential ability to differentiate into hepatocytes and biliary epithelial cells in galactosamine-induced rat liver regeneration. The American Journal of Pathology **175**: 2362–2371, 2009.

Kossor DC, Meunier PC, Handler JA, Sozio RS and Goldstein RS. Temporal relationship of changes in hepatobiliary function and morphology in rats following α-naphthylisothiocyanate (ANIT) administration. Toxico1ogy and Applied Pharmacology **119**: 108–114, 1993.

Kristiansen M, Graversen JH, Jacobsen C, Sonne O, Hoffman HJ, Law SKA and Moestrup SK. Identification of hemoglobin scavenger receptor. Nature **409**: 198–201, 2001.

Kruglov EA, Nathanson RA, Nguyen T and Dranoff JA. Secretion of MCP-1/CCL2 by bile duct epithelia induces myofibroblastic transdifferentiation of portal fibroblasts. American Journal of Physiology Gastrointestinal and Liver Physiology **290**: G765–G771, 2006.

Kusiluka LJM and Kambarage DM. Diseases of small ruminants in sub-Saharan Africa: a hand book on common diseases of sheep and goats in sub-Saharan Africa, VETAID; Capital Print Ltd. pp. 110, 1996.

Laskin DL and Pilaro AM. Potential role of activated macrophages in acetaminophen hepatotoxicity: isolation and characterization of activated macrophages from rat liver. Toxicology and Applied Pharmacology **86**: 204–215, 1986.

Lazaridis KN, Strazzabosco M and LaRusso NF. The cholangiopathies: disorders of biliary epithelia. Gastroenterology **127**: 1565–1577, 2004.

Lechner A, Leech CA, Abraham EJ, Nolan AL and Habener JF. Nestin-positive progenitor cells derived from adult human pancreatic islets of Langerhans contain side population (SP) cells defined by expression of the ABCG2 (BCRP1) ATPbinding cassette transporter. Biochemical and Biophysical Research Communications **293**: 670–674, 2002.

Lendahl U, Zimmerman LB and McKay RD. CNS stem cells express a new class of intermediate filament protein. Cell **60**: 585–595, 1990.

LeSage G, Glaser S, Gubba S, Robertson WE, Phinizy JL, Lasater J, Rodgers RE and Alpini G. Regrowth of the rat biliary tree after 70% partial hepatectomy is coupled to increased secretin-induced ductal secretion. Gastroenterology **111**: 1633–1644, 1996.

Li D and Friedman SL. Liver fibrogenesis and the role of hepatic stellate cells: new insights and prospects for therapy. Journal of Gastroenterology and Hepatology **14**: 618–633, 1999.

Li L, Mignone J, Yang M, Matic M, Penman S, Enikolopov G and Hoffman RM. Nestin expression in hair follicle sheath progenitor cells. Proceedings of the National Academy of Sciences, USA **100**: 9958–9961, 2003.

Li Z, Dranoff JA, Chan EP, Uemura M, S´evigny J and Wells RG. Transforming growth factor-beta and substrate stiffness regulate portal fibroblast activation in culture. Hepatology **46**: 1246–1256, 2007.

Lin WR, Lim SN, McDonald SA, Graham T, Wright VL, Peplow CL, Humphries A, Kocher HM, Wright NA, Dhillon AP and Alison MR. The histogenesis of regenerative nodules in human liver cirrhosis. Hepatology **51**: 1017–1026, 2010.

Liu X, Hu H and Yin JQ. Therapeutic strategies against TGF-beta signaling pathway in hepatic fibrosis. Liver International **26**: 8–22, 2006.

Madsen M, Moller HJ, Nielsen MJ, Jacobsen C, Graversen JH, van den Berg TK and Moestrup SK. Molecular characterization of the haptoglobin-hemoglobin receptor CD163: ligand binding properties of the scavenger receptor cysteine-rich domain region. Journal of Biological Chemistry **279**: 51561–51567, 2004.

Magness ST, Bataller R, Yang L and Brenner DA. A dual reporter gene transgenic mouse demonstrates heterogeneity in hepatic fibrogenic cell populations. Hepatology **40**: 1151–1159, 2004.

Maher JJ, Bissell M, Friedman SL and Roll EJ. Collagen measured in primary cultures of normal rat hepatocytes derives from lipocytes within the monolayer. Journal of Clinical Investigation **82**: 450–459, 1988.

Marcos LA, Terashima A and Gotuzzo E. Update on hepatobiliary flukes: fascioliasis, opisthoschiasis and clonorchiasis. Current Opinion in Infectious Diseases **21**: 523–530, 2008.

Marcos LA, Terashima A, Yi P, Andrade R, Cubero FJ, Albanis E, Gotuzzo E, Espinoza JR and Friedman SL. Mechanisms of liver fibrosis associated with experimental Fasciola hepatica infection: roles of FAS2 proteinase and hepatic stellate cell activation. The Journal of Parasitology **97**: 82–87, 2011.

Marcos LA, Yi P, Machicado A, Andrade R, Samalvides F, Sánchez J and Terashima A. Hepatic fibrosis and Fasciola hepatica infection in cattle. Journal of Helminthology **81**: 381–386, 2007.

Marra F, DeFranco R, Grappone C, Milani S, Pastacaldi S, Pinzani M, Romanelli RG, Laffi G and Gentilini P. Increased expression of monocyte chemotactic protein-1 during active hepatic fibrogenesis: correlation with monocyte infiltration. The American Journal of Pathology **152**: 423–430, 1998.

Marvin MJ, Dahlstrand J, Lendahl U and McKay RD. A rod end deletion in the intermediate filament protein nestin alters its subcellular localization in neuroepithelial cells of transgenic mice. Journal of Cell Science **111**: 1951–1961, 1998.

Michalczyk K and Ziman M. Nestin structure and predicted function in cellular cytoskeletal organization. Histology and Histopathology **20**: 665–671, 2005.

Milani S, Herbst H, Schuppan D, Kim KY, Riecken EO and Stein H. Procollagen expression by nonparenchymal rat liver cells in experimental biliary fibrosis. Gastroenterology **98**: 175–184, 1990.

Milani S, Herbst H, Schuppan D, Niedobitek G, Kim KY and Stein H. Vimentin expression of newly formed rat bile duct epithelial cells in secondary biliary fibrosis. Virchows Archiv-A: Pathological Aanatomy and Histopathology **415**: 237–242, 1989.

Mo W, Brecklin C, Garber SL, Song RH, Pegoraro AA, Au J, Arruda J AL, Dunea G and Singh AK. Changes in collagenases and TGF-β precede structural alteration in a model of chronic renal fibrosis. Kidney International **56**: 145–153, 1999.

Moghaddami M, Mayrhofer G and Cleland LG. MHC class II compartment, endocytosis and phagocytic activity of macrophages and putative dendritic cells isolated from normal tissues rich in synovium. International Immunology **17**: 1117–1130, 2005.

Mori Y, Izawa T, Takenaka S, Kuwamura M and Yamate J. Participation of functionally different macrophage populations and monocyte chemoattractant protein-1 in early

stages of thioacetamide-induced rat hepatic injury. Toxicologic Pathology **37**: 463–473, 2009.

Muchaneta-Kubara EC and el Nahas AM. Myofibroblast phenotypes expression in experimental renal scarring. Nephrology Dialysis and Transplantation **12**: 904–915, 1997.

Naito M, Hasegawa G and Takahashi K. Development, differentiation, and maturation of Kupffer cells. Microscopy Research and Technique **39**: 350–364, 1997.

Naito M, Takahashi K, Takahashi H and Kojima M. Ontogenetic development of Kupffer cells. In: Wisse E and Knook DL (editors). Sinusoidal liver cells. Elsevier Biomedical Press, Amsterdam. p 155, 1982.

Neubauer K, Knittel T, Aurisch S, Fellmer P and Ramadori G. Glial fibrillary acidic protein: a cell type specific marker for Ito cells in vivo and in vitro. Journal of Hepatology **24**: 719–730, 1996.

Ng YY, Huang TP, Yang WC, Chen ZP, Yang AH, Mu W, Nikolic-Paterson DJ, Atkins RC and Lan HY. Tubular epithelial-myofibroblast transdifferentiation in progressive tubulointerstitial fibrosis in 5/6 nefrectomized rats. Kidney International **54**: 864–876, 1998.

Ngategize PK, Bekele T and Tilahun G. Financial losses caused by ovine fascioliasis in the Ethiopian Highlands. Tropical Animal Health and Production **25**: 155–161, 1993.

Nielsen MJ, Madsen M, Moller HJ and Moestrup SK. The macrophage scavenger receptor CD163: endocytic properties of cytoplasmic tail variants. Journal of Leukocyte Biology **79**: 837–845, 2006.

Nitta T, Kim JS, Mohuczy D and Behrns KE. Murine cirrhosis induces hepatocyte epithelial mesenchymal transition and alterations in survival signaling pathways. Hepatology **48**: 909–919, 2008.

Novo E, di Bonzo LV, Cannito S, Colombatto S and Parola M. Hepatic myofibroblasts: a heterogeneous population of multifunctional cells in liver fibrogenesis. International Journal of Biochemistry and Cell Biology **41**: 2089–2093, 2009.

Ogawa K, Suzuki H, Hirohashi T, Ishikawa T, Meier PJ, Hirose K, Akizawa T, Yoshioka M and Sugiyama Y. Characterization of inducible nature of MRP3 in rat liver. American Journal of Physiology Gastrointestinal and Liver Physiology **278**: G438–446, 2000.

Ohsawa K, Imai Y, Kanazawa H, Sasaki Y and Kohsaka S. Involvement of Iba1 in membrane ruffling and phagocytosis of macrophages/microglia. Journal of Cell Science **113**: 3073–3084, 2000.

Omenetti A, Syn WK, Jung Y, Francis H, Porrello A, Witek RP, Choi SS, Yang L, Mayo MJ, Gershwin ME, Alpini G and Diehl AM. Repair-related activation of hedgehog signaling promotes cholangiocyte chemokine production. Hepatology **50**: 518–527, 2009.

Paranthan RR, Bargagna-Mohan P, Lau DL and Mohan R. A robust model for simultaneously inducing corneal neovascularization and retinal gliosis in the mouse eye. Molecular Vision **17**: 1901–1908, 2011.

Parker GA and Picut CA. Liver Immunobiology. Toxicologic Pathology **33**: 52–62, 2005.

Parola M, Marra F and Pinzani M. Myofibroblast-like cells and liver fibrogenesis: emerging concepts in a rapidly moving scenario. Molecular Aspects of Medicine **29**: 58–66, 2008.

Patil AS, Sable RB and Kothari RM. An update on transforming growth factor-β (TGF-β): sources, types, functions and clinical applicability for cartilage/bone healing. Journal of Cellular Physiology **226**: 3094–3103, 2011.

Penz-Österreicher M, Österreicher CH and Trauner M. Fibrosis in autoimmune and cholestatic liver disease. Best Practice and Research Clinical Gastroenterology **25**: 245–258, 2011.

Perrigoue JG, Saenz SA, Siracusa MC, Allenspach EJ, Taylor BC, Giacomin PR, Nair MG, Du Y, Zaph C, van Rooijen N, Comeau MR, Pearce EJ, Laufer TM and Artis D. MHC class II–dependent basophil–$CD4^+$ T cell interactions promote T_H2 cytokine–dependent immunity. Nature Immunology **10**: 697–705, 2009.

Piera-Velazquez S, Li Z and Jimenez SA. Role of endothelial-mesenchymal transition (EndoMT) in the pathogenesis of fibrotic disorders. The American Journal of Pathology **179**: 1074–1080, 2011.

Pinzani M and Rombouts K. Liver fibrosis: from the bench to clinical targets. Digestive and Liver Disease **36**: 231–242, 2004.

Pinzani M, Vizzutti F, Arena U and Marra F. Technology insight: noninvasive assessment of liver fibrosis by biochemical scores and elastography. Nature Clinical Practice Gastroenterology and Hepatology **5**: 95–106, 2008.

Platt N, Haworth R, Darley L and Gordon S. The many roles of the class A macrophage scavenger receptor. International Review of Cytology **212**: 1–40, 2002.

Polfliet MM, Fabriek BO, Daniels WP, Dijkstra CD and van den Berg TK. The rat macrophage scavenger receptor CD163: expression, regulation and role in inflammatory mediator production. Immunobiology **211**: 419–425, 2006.

Qi Z, Atsuchi N, Ooshima A, Takeshita A and Ueno H. Blockade of type beta transforming growth factor signaling prevents liver fibrosis and dysfunction in the rat. Proceedings of the National Academy of Sciences, USA **96**: 2345–2349, 1999.

Ramadori G and Saile B. Portal tract fibrogenesis in the liver. Laboratory Investigation **84**: 153–159, 2004.

Rathinam C, Poueymirou WT, Rojas J, Murphy AJ, Valenzuela DM, Yancopoulos GD, Rongvaux A, Eynon EE, Manz MG and Flavell RA. Efficient differentiation and function of human macrophages in humanized CSF-1 mice. Blood **118**: 3119–3128, 2011.

Rees EPV, Dijkstra CD, Van Der Ende MB, Janse EM and Sminia T. The ontogenetic development of macrophage subpopulations and Ia-positive non-lymphoid cells in gut-associated lymphoid tissue of the rat. Immunology **63**: 79–85, 1988.

Richardson MM, Jonsson JR, Powell EE, Brunt EM, Neuschwander-Tetri BA, Bhathal PS, Dixon JB, Weltman MD, Tilg H, Moschen AR, Purdie DM, Demetris AJ and Clouston AD. Progressive fibrosis in nonalcoholic steatohepatitis: association with altered regeneration and a ductular reaction. Gastroenterology **133**: 80–90, 2007.

Robertson H, Kirby JA, Yip WW, Jones DE and Burt AD. Biliary epithelial-mesenchymal transition in posttransplantation recurrence of primary biliary cirrhosis. Hepatology **45**: 977–981, 2007.

Rockey DC and Chung JJ. Reduced nitric oxide production by endothelial cells in cirrhotic rat liver: Endothelial dysfunction in portal hypertension. Gastroenterology **114**: 344–351, 1998.

Rogler LE. Selective bipotential differentiation of mouse embryonic hepatoblasts in vitro. The American Journal of Pathology **150**: 591–602, 1997.

Rygiel KA, Robertson H, Marshall HL, Pekalski M, Zhao L, Booth TA, Jones DE, Burt AD and Kirby JA. Epithelial-mesenchymal transition contributes to portal tract fibrogenesis during human chronic liver disease. Laboratory Investigation **88**: 112–123, 2008.

Ryu JH and Daniels CE. Advances in the management of idiopathic pulmonary fibrosis. F1000 Medicine Reports **2**: 28, 2010.

Sakai N, Wada T, Furuichi K, Shimizu K, Kokubo S, Hara A, Yamahana J, Okumura T, Matsushima K, Yokoyama H and Kaneko S. MCP-1/CCR2-dependent loop for fibrogenesis in human peripheral CD-14 positive monocytes. Journal of Leukocyte Biology **79**: 555–563, 2006.

Sakamoto A, Kawasaki T, Kazawa T, Ohashi R, Jiang S, Maejima T, Tanaka T, Hamakubo T, Sakai J, Kodama T and Naito M. Expression of liver X receptor-α in rat fetal tissues at different developmental stages. Journal of Histochemistry and Cytochemistry **55**: 641–649, 2007.

Sappino AP, Schürch W and Gabbiani G. Differentiation repertoire of fibroblastic cells: expression of cytoskeletal proteins as marker of phenotypic modulations. Laboratory investigation **63**: 144–161, 1990.

Schecter AD, Rollins BJ, Zhang YJ, Charo IF, Fallon JT, Rossikhina M, Giesen PL, Nemerson Y and Taubman MB. Tissue factor is induced by monocyte chemoattractant protein-1 in human aortic smooth muscle and THP-1 cells. Journal of Biological Chemistry **272**: 28568–28573, 1997.

Schuppan D and Afdhal NH. Liver cirrhosis. The Lancet **371**: 838–851, 2008.

Schuppan D, Cho JJ, Jia JD and Hahn EG. Interplay of matrix and myofibroblasts during hepatic fibrogenesis. Current Topics in Pathology **93**: 205–215, 1999.

Seki E, Minicis SD, Inokuchi S, Taura K, Miyai K, Rooijen NV, Schwabe RF and Brenner DA. CCR2 promotes hepatic fibrosis in mice. Hepatology **50**: 185–197, 2009.

Shen ZJ, Esnault S, Rosenthal LA, Szakaly RJ, Sorkness RL, Westmark PR, Sandor M and Malter JS. Pin1 regulates TGF-beta1 production by activated human and murine eosinophils and contributes to allergic lung fibrosis. The Journal of Clinical Investigation **118**: 479–490, 2008.

Shiojiri N, Lemire JM and Fausto N. Cell lineages and oval cell progenitors in rat liver development. Cancer Research **51**: 2611–2620, 1991.

Sjoberg G, Jiang WQ, Ringertz NR, Lendahl U and Sejersen T. Colocalization of nestin and vimentin/desmin in skeletal muscle cells demonstrated by three-dimensional fluorescence digital imaging microscopy. Experimental Cell Research **214**: 447–458, 1994.

Song L, Lee C and Schindler C. Deletion of the murine scavenger receptor CD68. The Journal of Lipid Research **52**: 1542–1550, 2011.

Spagnoli FM, Amicone L, Tripodi M and Weiss MC. Identification of a bipotential precursor cell in hepatic cell lines derived from transgenic mice expressing cyto-met in the liver. Journal of Cell Biology **143**: 1101–1112, 1998.

Sporrer D, Weber M, Wanninger J, Weigert J, Neumeier M, Stogbauer F, Lieberer E, Bala M, Kopp A, Schaffler A and Buechler C. Adiponectin downregulates CD163 whose cellular and soluble forms are elevated in obesity. European Journal of Clinical Investigation **39**: 671–679, 2009.

Steinert PM and Liem RKH. Intermediate filament dynamics. Cell **60**: 521–523, 1990.

Strazzabosco M, Fabris L and Spirli C. Pathophysiology of cholangiopathies. Journal of Clinical Gastroenterology **39**: S90–91, 2005.

Strieter RM, Gomperts BN and Keane MP. The role of CXC chemokines in pulmonary fibrosis. The Journal of Clinical Investigation **117**: 549–556, 2007.

Suda T, McCaarthy K, Vu Q, McCormack J and Schneeberger EE. Dendritic cell precursors are enriched in the vascular compartments of lung. American Journal of Respiratory Cell and Molecular Biology **19**: 728–737, 1998.

Suzuki H, Kurihara Y, Takeya M, Kamada N, Kataoka M, Jishage K, Sakaguchi H, Kruijt JK, Higashi T, Suzuki T, van Berkel TJ, Horiuchi S, Takahashi K, Yazaki Y and Kodama T. The multiple roles of macrophage scavenger receptors (MSR) in vivo: resistance to atherosclerosis and susceptibility to infection in MSR knockout mice. Journal of Atherosclerosis and Thrombosis **4**: 1–11, 1997.

Takahashi K, Naito M and Takeya M. Development and heterogeneity of macrophages and their related cells through their differentiation pathways. Pathology International **46**: 473–485, 1996.

Tanaka M, Itoh T, Tanimizu N and Miyajima A. Liver stem/progenitor cells: their characteristics and regulatory mechanisms. The Journal of Biochemistry **149**: 231–239, 2011.

Tanaka M, Okabe M, Suzuki K, Kamiya Y, Tsukahara Y, Saito S and Miyajima A. Mouse hepatoblasts at distinct developmental stages are characterized by expression of EpCAM and DLK1: Drastic change of EpCAM expression during liver development. Mechanisms of development **126**: 665–676, 2009.

Tanimoto T, Shirota K, Ohtsuki Y and Araki K. Eosinophilic proliferative pylephlebitis in the liver of Japanese beef cattle with fascioliasis. The Journal of Veterinary Medical Science **60**: 1073–1080, 1998.

Tian YW, Smith PG and Yeoh GC. The oval-shaped cell as a candidate for a liver stem cell in embryonic, neonatal and precancerous liver: identification based on

morphology and immunohistochemical staining for albumin and pyruvate kinase isoenzyme expression. Histochemistry and Cell Biology **107**: 243–250, 1997.

Tomokiyo R, Jinnouchi K, Honda M, Wada Y, Hanada N, Hiraoka T, Suzuki H, Kodama T, Takahashi K and Takeya M. Production, characterization, and interspecies reactivities of monoclonal antibodies against human class-A macrophage scavenger receptors. Atherosclerosis **161**: 123–132, 2002.

Tsuruta S, Nakamuta M, Enjoji M, Kotoh K, Hiasa K, Egashira K and Nawata H. Anti-monocyte chemoattractant protein-1 gene therapy prevents dimethylnitrosamine-induced hepatic fibrosis in rats. International Journal of Molecular Medicine **14**: 837–842, 2004.

Tsutsumi M, Takada A and Takase S. Characterization of desmin-positive rat liver sinusoidal cells. Hepatology **7**: 277–284, 1987.

Turato C, Calabrese F, Biasiolo A, Quarta S, Ruvoletto M, Tono N, Paccagnella D, Fassina G, Merkel C, Harrison TJ, Gatta A and Pontisso P. SERPINB3 modulates TGF-β expression in chronic liver disease. Laboratory Investigation **90**: 1016–1023, 2010.

Valledor AF, Borras FE, Cullell-Young M and Celada A. Transcription factors that regulate monocyte/macrophage differentiation. Journal of Leukocyte Biology **63**: 405–417, 1998.

Verrecchia F, Tacheau C, Schorpp-Kistner M, Angel P and Mauviel A. Induction of the AP-1 members c-Jun and JunB by TGF-beta/Smad suppresses early Smad-driven gene activation. Oncogene **20**: 2205–2211, 2001.

Walczak P, Chen N, Hudson JE, Willing AE, Garbuzova-Davis SN, Song S, Sanberg PR, Sanchez-Ramos J, Bickford PC and Zigova T. Do hematopoietic cells exposed to a neurogenic environment mimic properties of endogenous neural precursors? Journal of Neuroscience Research **76**: 244–254, 2004.

Wallace K, Burt AD and Wright MC. Liver fibrosis. Biochemical Journal **411**: 1–18, 2008.

Warheit DB, Webb TR, Reeda KL, Frerichs S, Sayes CM. Pulmonary toxicity study in rats with three forms of ultrafine-TiO2 particles: Differential responses related to surface properties. Toxicology **230**: 90–104, 2007.

Watanabe T, Hasegawa G, Yamamoto T, Hatakeyama K, Suematsu M and Naito M. Expression of heme oxygenase-1 in rat ontogeny. Archives of Histology and Cytology **66**: 155–162, 2003.

Wiese C, Rolletschek A, Kania G, Blyszchuk P, Tarasov KV, Tarasova Y, Wersto RP, Boheler KR and Wobus AM. Nestin expression-a property of multilineage progenitor cells? CMLS Cellular and Molecular Life Science **61**: 2510–2522, 2004.

Wynn AA, Miyakawa K, Miyata E, Dranoff G, Takeya M and Takahashi K. Role of granulocyte/macrophage colony-stimulating factor in zymocel-induced hepatic granuloma formation. The American Journal of Pathology **158**: 131–145, 2001.

Wynn TA and Barron L. Macrophages: master regulators of inflammation and fibrosis. Seminars in Liver Disease **30**: 245–257, 2010.

Wynn TA, Thompson RW, Cheever AW and Mentink-kane MM. Immunopathogenesis of schistosomiasis. Immunolical Reviews **201**: 156–167, 2004.

Wynn TA. Cellular and molecular mechanisms of fibrosis. Journal of Pathology **214**: 199–210, 2008.

Yamanaka K, Hatano E, Narita M, Kitamura K, Yanagida A, Asechi H, Nagata H, Taura K, Nitta T and Uemoto S. Olprinone attenuates excessive shear stress through up-regulation of endothelial nitric oxide synthase in a rat excessive hepatectomy model. Liver Transplantation **17**: 60–69, 2011.

Yamashiro S, Takeya M, Nishi T, Kuratsu J, Youshimura T, Ushio Y, Takahashi K. Tumor derived monocyte chemoattractant protein-1 induces intratumoral infiltration of monocyte derived macrophage subpopulation in transplanted rat tumors. The American Journal of Pathology **145**: 856–867, 1994.

Yamate J, Kumagai D, Tsujino K, Nakatsuji S, Kuwamura M, Kotani T, Sakuma S and LaMarre J. Macrophage populations and apoptotic cells in the liver before spontaneous hepatitis in Long-Evans cinnamon (LEC) rats. Journal of Comparative Pathology **120**: 333–346, 1999.

Yamate J, Kuribayashi M, Kuwamura M, Kotani T and Ogihara K. Differential immunoexpressions of cytoskeletons in renal epithelial and interstitial cells in rat and canine fibrotic kidneys, and in kidney-related cell lines under fibrogenic stimuli. Experimental and Toxicologic Pathology **57**: 135–147, 2005.

Yamate J, Machida Y, Ide M, Kuwamura M, Sawamoto O and LaMarre J. Effects of lipopolysaccharide on the appearance of macrophage populations and fibrogenesis in cisplatin-induced renal injury. Experimental and Toxicologic Pathology **56**: 13–24, 2004.

Yamate J, Tatsumi M, Nakatsuji S, Kuwamura M, Kotani T and Sakuma S. Immunohistochemical observations on the kinetics of macrophages and myofibroblasts in rat renal interstitial fibrosis induced by cis-diamminedichloroplatinum. Journal of Comparative Pathology **112**: 27–39, 2003.

Yamate J, Yoshida H, Tsukamoto Y, Ide M, Kuwamura M, Ohashi F, Miyamoto T, Kotani T, Sakuma S and Takeya M. Distribution of cells immunopopsitive for AM-3K, a novel monoclonal antibody recognizing human macrophages, in normal and diseased tissues of dogs, cats, horses, cattle, pigs, and rabbits. Veterinary Pathology **37**: 837–847, 2000.

Yang C, Zeisberg M, Mosterman B, Sudhakar A, Yerramalla U, Holthaus K, Xu L, Eng F, Afdhal N and Kalluri R. Liver fibrosis: insights into migration of hepatic stellate cells in response to extracellular matrix and growth factors. Gastroenterology **124**: 147–159, 2003.

Yoshioka K, Enaga S, Taniguchi K, Fukushima U, Uechi M and Mutoh K. Morphological characterization of ductular reactions in canine liver disease. Journal of Comparative Pathology **130**: 92–98, 2004.

Young ND, Jex AR, Cantacessi C, Hall RS, Campbell BE, Spithill TW, Tangkawattana S, Tangkawattana P, Laha T and Gasser RB. A portrait of the transcriptome of the neglected trematode, Fasciola gigantica-biological and biotechnological implications. PLoS Neglected Tropical Diseases **5**: e1004, 2011.

Zamara E, Galastri S, Aleffi S, Petrai I, Aragno M, Mastrocola R, Novo E, Bertolani C, Milani S, Vizzutti F, Vercelli A, Pinzani M, Laffi G, LaVilla G, Parola M, Marra F. Prevention of severe toxic liver injury and oxidative stress in MCP-1-deficient mice. Journal of Hepatology **46**: 230–238, 2007.

Zeisberg M, Yang C, Martino M, Duncan MB, Rieder F, Tanjore H and Kalluri R. Fibroblasts derive from hepatocytes in liver fibrosis via epithelial to mesenchymal transition. Journal of Biological Chemistry **282**: 23337–23347, 2007.

Zhang J, Yu ZX, Fujita S, Yamaguchi ML and Ferrans VJ. Interstitial dendritic cells of the rat heart: quantitative and ultrastructural changes in experimental myocardial infarction. Circulation **87**: 909–920, 1993.

Zhang X, Yu WP, Gao L, Wei KB, Ju JL and Xu JZ. Effects of lipopolysaccharides stimulated Kupffer cells on activation of rat hepatic stellate cells. World Journal of Gastroenterology **10**: 610–613, 2004.

Zhao L, Kaneko T, Okiji T, Takagi M and Suda H. Immunoelectron microscopic analysis of CD11c-positive dendritic cells in the periapical region of the periodontal ligament of rat molars. Journal of Endodontics **32**: 1164–1167, 2006.

Zimmerli SC and Hauser C. Langerhans cells and lymph node dendritic cells express the tight junction component Claudin-1. Journal of Investigative Dermatology **127**: 2381–2390, 2007.

Zulewski H, Abraham EJ, Gerlach MJ, Daniel PB, Moritz W, Müller B, Vallejo M, Thomas MK and Habener JF. Multipotential nestin positive stem cells isolated from adult pancreatic islets differentiate ex vivo into pancreatic endocrine, exocrine, and hepatic phenotypes. Diabetes **50**: 521–533, 2001.

Acknowledgements

The author wishes to express sincere gratitude and appreciation to his supervisor, Dr. Jyoji Yamate, Professor, Laboratory of Veterinary Pathology for his scholastic guidance, constructive criticism and valuable instructions, continuous patronage in conducting the research works, and careful editing for the thesis. It would not have been possible to prepare this thesis without his kind help; the author greatly appreciates his devotion to the author and help. The author is grateful to Dr. Yoichi Nakamura, Professor, Laboratory of Integrative Physiology, and Dr. Saburo Matsuo, Professor, Laboratory of Toxicology, for their critical review of this thesis.

The author is indebted and thankful and would like to express heartfelt gratitude and regards to Dr. Mitsuru Kuwamura, Associate Professor, Laboratory of Veterinary Pathology, and Dr. Takeshi Izawa, Assistant Professor, Laboratory of Veterinary Pathology, for their valuable suggestion and generous technical support.

The author acknowledges the friendly support and co-operation of the undergraduate and graduate students, Laboratory of Veterinary Pathology, during the tenure of the study and expresses his kind thanks for their assistance.

The author appreciates the supports of his colleagues and office staff, Department of Animal Husbandry and Veterinary Science, University of Rajshahi, Bangladesh, during pursuing studies in Japan.

The author expresses special thanks to his family members, friends, relatives and well-wishers for their support. The author deeply appreciates the encouragement and loves of his wife, Seema, and accompany of his sons, Farhan, and Sabri.

At last but not the least, the author gratefully acknowledges the kind co-operation and support of the International Office and Rinku student support office, Osaka Prefecture University.

This study was carried out at the Laboratory of Veterinary Pathology, Division of Veterinary Sciences, Graduate School of Life and Environmental Sciences, Osaka Prefecture University, Osaka, Japan.

The author appreciates the sacrifice of the animals used in this study.

The author's stay in Japan during the study (October 2007 to March 2012) was supported by the Japanese Government Ministry of Education, Culture, Sports, Science and Technology (MEXT; Monbukagakusho) Scholarship (No. 072543).

This work was supported by Grant-in-Aids for Scientific Research B (Nos. 18380188 and 22380173 to Dr. J. Yamate), Japanese Society for the Promotion of Science (JSPS), and for Challenging Exploratory Research (No. 23658265 to Dr. J. Yamate), Japan Science and Technology Agency.